Olívia Carolina da Rosa

DESIGNING A THERMOELECTRIC ENERGY GENERATOR FOR WASTE HEAT RECOVERY IN HEAVY-DUTY DIESEL ENGINES

Florianópolis
2017

Ficha de identificação da obra elaborada pelo autor,
através do Programa de Geração Automática da Biblioteca Universitária da UFSC.

Olívia Carolina da Rosa

DESIGNING A THERMOELECTRIC ENERGY GENERATOR FOR WASTE HEAT RECOVERY IN HEAVY-DUTY DIESEL ENGINES

Esta Dissertação foi julgada adequada para a obtenção do título de "Mestre em Engenharia Mecânica", e aprovada em sua forma final pelo Programa de Pós-Graduação em Engenharia Mecânica.

Florianópolis, 10 de Março de 2017.

_____
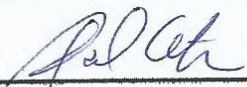
Prof. Jonny Carlos da Silva, Dr. Eng.
Coordenador do Curso
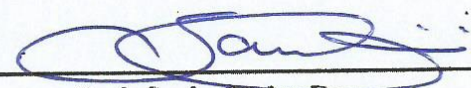
Banca Examinadora:

_____

Prof. Amir Antônio Martins de Oliveira Júnior – Orientador
Universidade Federal de Santa Catarina, Brasil

_____

Prof. Jader Riso Barbosa Júnior, Ph.D.
Universidade Federal de Santa Catarina, Brasil

_____

Prof. Marcelo Lobo Heldwein, Dr. sc. ETH.
Universidade Federal de Santa Catarina, Brasil

_____

Prof. Rafael de Camargo Catapan, Dr. Eng.
Universidade Federal de Santa Catarina, Brasil

_____

Prof. Saulo Güths, Dr.
Universidade Federal de Santa Catarina, Brasil

ACKNOWLEDGEMENTS

RESUMO

A quantidade de energia térmica rejeitada nos gases de exaustão durante a operação de um motor diesel é aproximadamente 30 % da energia fornecida a partir do combustível. Uma alternativa para recuperar essa energia é a utilização de um gerador termoelétrico, o qual pode ser usado como energia para os sistemas auxiliares ou como energia suplementar, no caso de veículos elétricos híbridos. Este estudo tem como objetivo conceber um gerador termoelétrico e um trocador de calor acoplado à exaustão de um motor diesel, limitados por critérios de mínima eficiência térmica e máxima perda de carga no tubo de escape. O motor, o trocador de calor, e o gerador termoelétrico foram simulados em regimes permanente e transiente, usando um modelo zero dimensional para o motor e um modelo de uma dimensão para o trocador de calor/ gerador termoelétrico com propriedades em função da temperatura. O modelo de regime permanente e propriedades constantes foi usado para otimização através de duas estratégias, uma buscando a máxima potência e outra a máxima eficiência de conversão. A configuração otimizada consiste de um trocador de calor de 9 tubos, com diâmetro de 0,022 m e comprimento 0,414 m, operando com o fluido de arrefecimento do motor como fluido frio, utilizando silício-germânio como material das células termoelétricas. Quando em regime transiente, a configuração para máxima potência com 562 células termoelétricas por tubo atingiu um pico de 3500 W no início da operação e potência média de 811 W durante o transiente periódico, com eficiência termoelétrica igual a 4.27 % . A configuração para máxima eficiência de conversão contou com 150 células termoelétricas por tubo e foi capaz de gerar 1100 W no início de operação e obter potência média igual a 550 W durante o transiente periódico, com eficiência termoelétrica igual a 10.4 % . O modelo em regime transiente e com propriedades variáveis revelou o potencial de obter maior potência durante transientes curtos. Quando comparados com as realizações atuais, os resultados indicam a viabilidade do projeto para veículos de tamanho médio e pesados.

Palavras-chave: Gerador Termoelétrico, Motor Diesel, Eficiência Energética, Otimização.

RESUMO EXPANDIDO

Geradores Termoelétricos para Recuperação de Calor Residual

Em 1821, Thomas Seebeck foi o primeiro a relatar a diferença de potencial eletrostático criado entre dois condutores submetidos a um gradiente de temperatura. A partir de então, o efeito termoelétrico é empregado como princípio de funcionamento em muitos equipamentos, por exemplo, pequenos refrigeradores, termopares e geradores termoelétricos.

Os geradores termoelétricos podem ser utilizados para geração de energia para baixa potência, no setor aeroespacial e para a recuperação da energia térmica perdida em veículos e em processos industriais. Em um automóvel, um gerador termoelétrico (TEG) pode ser acoplado ao radiador ou sistema de exaustão, recuperando parte da energia térmica rejeitada pelo motor e aumentando a eficiência global. Este será o foco desta dissertação.

Os geradores termoelétricos convertem diretamente um fluxo de energia térmica ao longo de uma diferença de temperatura em energia elétrica. Saidur et al.; Yu and Chau [1,2] descrevem um sistema típico que inclui: um trocador de calor, um conversor termoelétrico, uma unidade de condicionamento de energia e baterias, conforme mostrado na Figura 0.1.

O motor fornece gases de exaustão a alta temperatura. Já a fonte de fluido frio para o trocador de calor pode ser água do radiador, ar bombeado por um ventilador, ou um sistema que opera com ciclo Rankine orgânico (ORC). Por meio do acoplamento entre TEG e o sistema de exaustão, esta configuração assegura o gradiente de temperatura necessário obter a diferença de potencial e assim, converter calor em energia elétrica.

Portanto, um gerador termoelétrico tem a capacidade de recuperar diretamente o calor residual e gerar eletricidade sem aumentar as emissões e, assim, obter uma melhor economia de combustível.

Motivações

Além do comportamento mais amigável ao meio ambiente, os geradores termelétricos têm outras vantagens, tais como: não têm partes móveis, possuem operação silenciosa [4], são independentes do clima e

Figure 0.1 – Diagrama do sistema para recuperação de energia
térmica na exaustão de um motor de combustão interna usando
dispositivos termoelétricos.
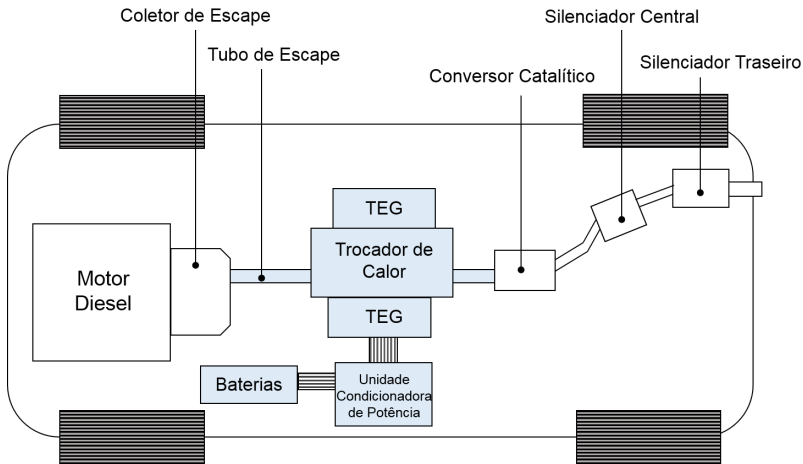
Fonte: adaptado de Zhang, Chau and Chan; Saidur et al.; Yu and Chau [1–3].

topografia [3], reduzem cargas secundárias no sistema de transmissão
do motor [5], e fornecem energia para sistemas auxiliares.

Apesar de ser uma das tecnologias mais promissoras para conver-
são de energia, os geradores termoelétricos ainda apresentam grandes
desvantagens especialmente devido à baixa eficiência de conversão calor-
eletricidade. Dificilmente esta recuperação é economicamente viável,
devido ao baixo valor associado à figura de mérito Z, um parâmetro do
material termoelétrico relacionado a eficiência de conversão de energia
térmica em energia elétrica.

Devido à baixa eficiência de conversão, o uso de um TEG acoplado
ao sistema de exaustão requereria um trocador de calor maior, a fim de
atender a potência necessária. Por conseguinte, existiria um aumento
na massa do veículo, bem como na perda de carga ao longo do sis-
tema de exaustão. Novos materiais termoelétricos (com maior figura
de mérito) poderiam ser uma solução, porém muitos deles foram testa-
dos apenas em escala de laboratório. Consequentemente, há incertezas
sobre o material e fabricação na produção em larga escala.

O mencionado acima representa apenas um exemplo das difi-
culdades em relação ao uso de geradores termoelétricos. A análise

é complexa e envolve diversas variáveis. Neste contexto, os modelos computacionais representam um meio para investigar os processos e variáveis mais importantes no projeto de um TEG, assim como uma abordagem para otimizar estes dispositivos. Infelizmente, os modelos da literatura não abrangem o comportamento do sistema em regime transiente. Consequentemente, espera-se que esta dissertação forneça uma base teórica para o desenvolvimento de novos modelos de geradores termelétricos.

Portanto, este trabalho foi motivado pela possibilidade de incorporar esta tecnologia (conversão direta de energia) em motores diesel, o que poderia gerar um impacto satisfatório no aumento da eficiência energética. Além disso, espera-se que o modelo do motor a diesel possa ser empregado em outros projetos no futuro.

Objetivos

O objetivo geral desta dissertação é projetar e otimizar um gerador termoelétrico conectado a um trocador de calor acoplado ao sistema de exaustão em um veículo com motor diesel. A fim de avaliar a energia provida pelo gerador termoelétrico, o desempenho do sistema é avaliado por simulação numérica, utilizando FORTRAN, tanto em regime permanente quanto transiente.

Para atingir este objetivo, foram definidos os seguintes objetivos específicos:

1. Revisar os conceitos fundamentais para o projeto de geradores termoelétricos e o estado-da-arte;

2. Simular o comportamento de motores diesel para avaliar a temperatura e o fluxo de massa do gases da exaustão como uma função do tempo para diferentes condições de funcionamento;

3. Projetar o trocador de calor (gases de exaustão - água), o gerador termoelétrico e integrá-los em um dispositivo termoeléctrico;

4. Avaliar por simulação numérica algumas escolhas de projeto, tais como, diferentes materiais termoelétricos, posições no sistema de exaustão e fluidos frios para o trocador de calor e o efeito do regime transiente do gerador quando acoplado ao motor diesel.

5. Otimizar o projeto do trocador de calor através da maximização da potência ou da eficiência térmica, usando uma restrição de limitação de perda de carga.

Metodologia

Esta dissertação se concentra no projeto de um gerador termoelétrico. A metodologia realizada para executar esta tarefa considera uma abordagem teórica. Esta análise foi focada no desenvolvimento do um modelo computacional, o qual foi utilizado para simular o motor diesel, o trocador de calor, e o gerador termoeléctrico.

O modelo do motor diesel de 4 tempos, naturalmente aspirado, 6 cilindros, diâmetro de cilindro 0,125 m, curso 0,14 m, taxa de compressão 16,5, potência 38 kW, torque 227 N·m na rotação nominal 1600 rpm assume: (1) escoamento unidimensional, (2) modelagem de uma única zona para a câmara de combustão, (3) transferência de calor por convecção e radiação na câmara de combustão, (4) modelagem da combustão por função de Wiebe dupla, (5) comportamento de gás ideal com propriedades constantes, (6) transferência de calor por condução transiente através das paredes da câmara de combustão.

O modelo do gerador termoelétrico composto por um trocador de calor de tubos concêntricos de fluxo paralelo formado por 25 módulos de aço AISI304 com diâmetro interno 5 cm e externo 10 cm com células termoelétricas acopladas assume: (1) escoamento plenamente desenvolvido para os gases de exaustão e fluido frio (água), (2) coeficiente global de transferência de calor constante, (3) resistência elétrica entre a interface das células termoelétricas e das paredes do trocador de calor desprezível, (4) resistência de carga ótima em função da resistência elétrica do gerador.

O modelo foi programado em linguagem FORTRAN. Através da simulação, inicialmente, foi estudado o comportamento transiente de motores diesel de modo a fornecer as variáveis de entrada para o gerador termoelétrico e para avaliar a perda de energia térmica através da exaustão. Subsequentemente, uma versão primária do gerador termoeléctrico foi concebida. Este primeiro modelo foi utilizado para identificar oportunidades para aumentar a recuperação de energia e fornecer diretrizes para a otimização do projeto do TEG.

As melhores condições de operação quanto à escolha do material termoelétrico, da posição no sistema de exaustão e do fluido frio foram identificados.

O modelo transiente foi então utilizado para a otimização dos parâmetros geométricos do gerador, quais sejam, número, diâmetro e comprimentos das tubulações do trocador de calor, visando maximizar a eficiência de conversão termoelétrica e a potência gerada, utilizando também uma restrição de perda de carga abaixo de determinado limite de operação (2 % da pressão ambiente).

Resultados

Os resultados obtidos foram:

O trocador de calor é formado por 9 tubos, com diâmetro 0,022 m e comprimento 0,414 m, operando com água como fluido frio, instalado próximo ao coletor de exaustão, com células termelétricas de SiGe, com diâmetro 0,003 m e comprimento 0,006 m.

Na situação de máxima eficiência de conversão, o gerador termoelétrico possui 150 células termoelétricas gerando 550 W com eficiência 10,4 %.

Na situação de máxima potência, o gerador termoelétrico possui 565 células termoelétricas gerando 811 W com eficiência 4,27 %

Conclusão

Através de simulações numéricas, este trabalho explorou o potencial de recuperação de energia de um gerador termoelétrico acoplado ao sistema de exaustão em um veículo com motor diesel. Os resultados indicam que o dispositivo termoelétrico pode gerar 810 W com eficiência de conversão igual a 4,27 % , o que geraria um impacto satisfatório na diminuição do consumo de combustível em veículos diesel para aplicações futuras.

As principais contribuições deste trabalho tratam do modelo computacional para simulação de motores diesel, do modelo computacional para simulação de geradores termoelétricos e da metodologia para otimização do geradores termoelétricos apresentada.

Os seguintes trabalhos futuros são recomendados: simular o comportamento do motor diesel usando CFD, com intuito de avaliar a formação de vórtices no coletor de escape; projetar o circuito elétrico e a unidade de condicionamento de energia, com intuito de investigar o acoplamento do TEG com sistema de gerenciamento de energia do veículo; e conduzir trabalho experimental, com intuito de corroborar os resultados obtidos através das simulações.

Organização da Dissertação

Esta dissertação está dividida em cinco capítulos. O Capítulo 2 trata dos conceitos mais relevantes em relação aos geradores termoelétricos, os materiais comumente utilizados, as principais vantagens e os inconvenientes. Além disso, o Capítulo 2 apresenta o estado-da-arte do uso de geração termelétrica para recuperação da energia térmica rejeitada pelo motor diesel.

O Capítulo 3 abrange os aspectos do motor diesel: uma breve revisão bibliográfica a cerca de modelos computacionais para motores, as dimensões características, os parâmetros operacionais e o modelo termodinâmico proposto. Posteriormente, os resultados são discutidos e comparados com os valores comuns na literatura, a fim de validar o modelo. Os resultados obtidos a partir do modelo termodinâmico caracterizam os gases de exaustão, um parâmetro de entrada para o gerador termoelétrico. O fluxo mássico dos gases de exaustão é necessário para manter a temperatura do lado quente do gerador termoelétrico.

No capítulo 4, o projeto do gerador termoelétrico é detalhado. Primeiramente, os conceitos fundamentais e formulação matemática de trocadores de calor são apresentados. Então, o modelo do sistema integrado (trocador de calor e gerador termoelétrico) é proposto, assim como uma metodologia para avaliar o desempenho do TEG. Desta forma, as vantagens e limitações das principais características do projeto também são discutidos neste capítulo. Além disso, é dada atenção especial ao comportamento do TEG em regime transiente. Esta análise forneceu ideias aumentar a recuperação do calor residual. Além disso, o modelo é validado por meio de comparações com modelos da literatura

Por último, as conclusões e recomendações para trabalhos futuros são apresentados no Capítulo 5.

ABSTRACT

The amount of heat energy wasted in the exhaust gas flow during operation of a diesel engine is grossly 30 % of the input energy from the fuel. An alternative to recover the heat lost through the exhaust in diesel engines is the use of thermoelectric generators, which could be used as source of power to propel auxiliary systems or as a supplement power source in case of hybrid electric vehicles. This study aims at developing and optimizing a thermoelectric generator and a heat exchanger adapted to the exhaust system, close-coupled to a diesel engine, restricted by criteria of minimum overall efficiency and maximum exhaust back-pressure. The engine, heat exchanger, and thermoelectric generator were evaluated in the steady-state and transient regime using a zero dimensional model for the engine and a one-dimensional model for the heat exchanger/thermoelectric generator with temperature dependent properties. The steady-state, constant property model was used for the optimization using two strategies, one aiming at maximum power and the other at maximum efficiency. The optimized configuration consisted of a heat exchanger with 9 tubes, with diameter of 0.022 m and length of 0.414 m, operating with engine coolant as cold fluid, using silicon germanium thermoelectric junctions. When simulated in transient regime, the configuration for maximum power with 562 thermoelectric junctions per tube was able to generate peak power at start-up of 3500 W, average power at periodic steady-state of 811 W, with 4.27 % thermoelectric efficiency. The configuration for maximum conversion efficiency had 150 thermoelectric junctions per tube, achieved peak power of 1100 W at start-up, average power at periodic steady-state of 550 W, and 10.4 % thermoelectric efficiency. The transient, variable properties simulation revealed the potential for higher power during short transients. When compared to current realizations, the results indicate the feasibility of the design for medium size and heavy-duty vehicles.

Keywords: Thermoelectric Generator, Diesel Engine, Energy Efficiency, Optimization.

LIST OF FIGURES

LIST OF TABLES

LIST OF ABBREVIATIONS AND ACRONYMS

BDC	Bottom Dead Center
BEB	Brazilian Energy Balance
CFD	Computational Fluid Dynamics
CHP	Combined Heat Power
CI	Compression-Ignition
CNG	Compressed Natural Gas
CPU	Central Processing Unit
deg	Degree
EES	Engineering Equation Solver
EPE	Empresa de Pesquisa Energética
HD	Heavy-Duty
ICE	Internal Combustion Engine
IDE	Integrated Development Environment
LDP	Light-Duty-Passenger
MPPT	Maximum Power Point Tracking
NREL	National Renewable Energy Laboratory US
NTU	Number of Transfer Units
OEM	Original Equipment Manufacturer
ORC	Organic Rankine Cycle
PV	Photovoltaic
PVG	Photovoltaic Generator
QW	Quantum Well
REE	Rare Earth Element
SUV	Sports Utility Vehicle
t CO_2-eq	Tonne of Carbon Dioxide Equivalent
TDC	Top Dead Center
TE	Thermoelectric
TEG	Thermoelectric Generator
toe	Tonne of Oil Equivalent, 1 toe= 41.85 GJ

LIST OF SYMBOLS

Roman symbols

A	Area, m^2
$A_{ku,ch}$	Surface-convection area between the flue gas and the cylinder head surface, m^2
$A_{r,ch}$	Radiation area between the flue gas and the cylinder head, m^2
A_v	Valve reference area, m^2
$\dot{C}_c$	Cold fluid heat capacity rate, W/K
$C_{D,e}$	Exhaust discharge coefficient
$C_{D,i}$	Intake discharge coefficient
$\dot{C}_{exh}$	Exhaust gas heat capacity rate, W/K
$c_{p,a}$	Air specific heat capacity, J/kg-K
$c_{p,c}$	Cold fluid specific heat capacity, J/kg-K
$c_{p,ch}$	Cylinder head specific heat capacity, J/kg-K
$c_{p,f}$	Flue gas specific heat capacity, J/kg-K
$c_{p,F}$	Fuel specific heat capacity, J/kg-K
C_R	Capacitance ratio
D	TEG module inner tube diameter,m
D_B	Bore, m
D_{out}	TEG module outer tube diameter,m
D_h	Hydraulic diamter, m
$D_{v,e}$	Exhaust valve diameter, m
$D_{v,i}$	Intake valve diameter, m
e	Surface roughness, m
f_{af}	Correction factor for choked flow equation
f_{av}	Valve lift profile in respect to valve reference area
f_d	Factor that accounts for the phase of combustion controlled by diffusion mass
f_{fd}	Friction factor
$f_{F,i}$	Fuel injection valve profile
f_p	Factor that accounts for the premixed combustion phase
$f_{r,F}$	Factor for the opening and closing of the fuel injection valve
$\overline{h}$	Average heat transfer coefficient, W/K-m^2

j_e	Current flux, A/m^2
J_e	Eletric current, A
k	Thermal conductivity, W/m-K
k_f	Flue gas thermal conductivity, W/m-K
L	Length of the conductor, m
L	Stroke, m
l_{cb}	Skin depth of the cylinder block, m
l_{ch}	Skin depth of the cylinder head, m
l_p	Skin depth of the piston, m
L_v	Maximum valve lift, m
M_f	Mass of gas, kg
$M_{F,o}$	Mass of fuel injected, kg
$M_{F,r}$	Mass of fuel burned, kg
M_F	Mass of fuel, kg
$\dot{M}_c$	Cold fluid mass flow rate, kg/s
$\dot{M}_{exh}$	Exhaust mass flow rate, kg/s
$\dot{M}_{exh}$	Exhaust mass flow rate, kg/s
$\dot{M}_{F,inj}$	Injected fuel mass flow rate, kg/s
$M_{g,a}$	Air molar mass, kg/kmol
$M_{g,f}$	Flue gas molar mass, kg/kmol
$M_{g,F}$	Fuel molar mass, kg/kmol
$(\dot{M}h)_{exh}$	Enthalpy flow of the exhaust gas, W
$(\dot{M}h)_{inj}$	Enthalpy flow of the injected fuel, W
$(\dot{M}h)_{int}$	Enthalpy flow of the intake air, W
$\dot{M}_{F,inj}$	Injected fuel mass flow rate, kg/s
$\dot{M}_{int}$	Intake mass flow rate, kg/s
$\dot{M}_{int}$	Intake mass flow rate, kg/s
$\dot{M}_{r,F}$	Fuel combustion rate, kg/s
$\dot{M}_v$	Mass flow rate, kg/s
N	Crank shaft angular speed, rpm
N_{TE}	Number of thermocouples
P	Power, W
p_{exh}	Exhaust pressure, kPa
p_f	Flue gas pressure, kPa
p_{int}	Intake pressure, kPa
p_o	Upstream stagnation pressure, kPa
Pr	Prandtl number
p_t	Downstream stagnation pressure, kPa
$\dot{Q}$	Heat transfer rate, W
$\dot{Q}_{A,ch_i}$	Net heat transfer for the volume i in the cylinder head, W

$\dot{Q}_{A,ch_o}$	Net heat transfer from the cylinder head, W
$\dot{Q}_{A,f}$	Net heat transfer from the fluid, W
$\dot{q}_{CV}$	Duty, W
$\dot{Q}_{c,w}$	The released heat from the cold side of the heat exchanger, W
$\dot{Q}_{h,w}$	The absorbed heat from the hot side of the heat exchanger, W
$\dot{Q}_{k,ch_{o1}}$	Heat flow rate by conduction from the cylinder surface to the interior of the ceramic cylinder head, W
$\dot{Q}_{k,ch-w}$	Heat transfer between the final cylinder head node and coolant water, W
$\dot{Q}_{ku,cb_{Db}}$	Surface-convection heat transfer between the gas and the cylinder block surface, W
$\dot{Q}_{ku,ch_{Db}}$	Surface-convection heat transfer between the gas and the cylinder head surface, W
$\dot{Q}_{ku,p_{Db}}$	Surface-convection heat transfer between the gas and the piston surface, W
$\dot{Q}_{max}$	Maximum heat transfer rate, W
$\dot{Q}_{r,ch-cb}$	Radiation heat transfer between the cylinder head and the cylinder block, W
$\dot{Q}_{r,ch-p}$	Radiation heat transfer between the cylinder head and the piston, W
r_c	Compression ratio
R_e	Electric resistance, Ω
Re_{D_h}	Reynolds number
$R_{e,o}$	External electrical load, Ω
$R_{k_{\Sigma,ch-w}}$	Thermal resistance for final cylinder head node and coolant water, K/W
R_k	Thermal resistance, K/W
$R_{k,ch}$	Conduction thermal resistance for the interior of the cylinder head, K/W
$R_{ku,c}$	Convection resistance between the water and the outer module surface, K/W
$R_{ku,ch}$	Surface-convection resistance between the fluid and the cylinder head surface, K/W
$R_{ku,exh}$	Convection resistance between the exhaust gas and the inner module surface, K/W
$R_{r_{\Sigma,ch-cb}}$	Overall surface-radiation resistance, K/W
R_t	Heat exchanger total thermal resistance, K/W
R_{TEG}	Conduction through the TEG module, K/W

R_u	Universal gas constant, 8.3145 J/mol-K
$\dot{S}_{cb}$	Volumetric emission and absorption of radiation for the cylinder block, W
$\dot{S}_{ch}$	Volumetric emission and absorption of radiation for the cylinder head, W
$\dot{S}_{e,J}$	Joule heating, W
$\dot{S}_{e,P}$	Peltier interfacial cooling or heating, W
$\dot{S}_{e,T}$	Thomson induced heat flow, W
$\dot{S}_f$	Energy conversion in the gas, W
sfc	Specific fuel consumption, kg/J
$\dot{S}_{F,lg}$	Heat of evaporation heat for liquid fuel, W
$\dot{S}_{m,p}$	Conversion of mechanical to thermal energy due to expansion cooling/ compression heating, W
$\dot{S}_p$	Volumetric emission and absorption of radiation for the piston, W
$\dot{S}_{r,F}$	Conversion of chemical to thermal energy due to combustion, W
T	Temperature, K
T_f	Flue gas Temperature, K
T_{c1}	Inlet temperature of cold fluid, K
T_{c2}	Outlet temperature of cold fluid, K
T_{cb_0}	Cylinder block surface temperature, K
T_{ch_0}	Cylinder head surface temperature, K
T_{ch_i}	Temperature of the i-th node for the interior of the cylinder head, K
$T_{c,w}$	Average cold wall temperature, K
T_{exh}	Exhaust Temperature, K
$T_{F,o}$	Temperature of the temperature injected, K
$T_{f,w}$	Water cooled temperature, K
T_{h1}	Inlet temperature of exhaust gas,K
T_{h2}	Outlet temperature of exhaust gas, K
$T_{h,w}$	Average hot wall temperature, K
T_{int}	Intake temperature, K
T_o	Stagnation temperature, K
t_p	Time from ignition non-dimensionalized by total time allowed for combustion
T_{rf}	Apparent radiant temperature, K
U	Overall heat transfer coefficient,W/K-m^2
UA	Heat exchanger conductance, W/K
V_c	Clearance volume, m^3
V_d	Displaced volume, m^3

V_f	Flue gas volume, m^3
$W_{c,i,n}$	Net indicated work per cycle, J
Z	Figure of merit, 1/K
ZT	Dimensionless figure of merit

Greek symbols

ΔE_h	The heat transfer rate from the exhaust gas to the thermoelectric generator, W
$\Delta \dot{E}_c$	The heat transfer rate from the water to the thermoelectric generator, W
$\Delta \theta_{r,F}$	Number of crank angles for combustion, deg
$\Delta \varphi$	Electric potential, V
Δh_{lg}	Evaporation heat, J/kg$_{fuel}$
$\Delta h_{r,F}$	Fuel heat of reaction with air, J/kg
$\Delta t_{F,i}$	Time interval during fuel injection, s
$\Delta t_{r,F}$	Time interval during combustion, s
Ψ	Power per unit area, W/m^2
α_P	Peltier coefficient, V
α_S	Seebeck coefficient, V/K
α_T	Thomson coefficient, V/K
$\alpha_{r,ch}$	Cylinder head surface absorptivity
$\alpha_{r,f}$	Flue gas absorptivity
β	Fraction of fuel burned
$\epsilon_{r,ch}$	Cylinder head surface emissivity
$\epsilon_{r,f}$	Flue gas emissivity
η_{TE}	Thermoelectric efficiency
η_f	Fuel conversion efficiency
η_{th}	Thermal efficiency
γ	Polytropic coefficient
ϕ	Fuel/air equivalence ratio
ρ_e	Electrical resistivity, Ωm
ρ_{ch}	Cylinder head density, kg/m^3
σ_{sb}	Stefan-Boltzmann constant
τ_{id}	Ignition delay interval, ms
$\theta_{F,e}$	Crank angle when injection ends, deg
$\theta_{F,s}$	Crank angle when injection begins, deg
θ_{ig}	Crank angle when ignition begins, deg
$\theta_{v,e,e}$	Crank angle when the exhaust valve closes completely, deg

$\theta_{v,e,i}$	Crank angle when the intake valve closes completely, deg
$\theta_{v,s,e}$	Crank angle when the exhaust valve begins to open, deg
$\theta_{v,s,i}$	Crank angle when the intake valve begins to open, deg
ε	Heat exchanger effectiveness

Other symbols

$(A/F)_a$	Air/Fuel mass ratio
$\langle Nu \rangle_{D_B}$	Average Nusselt number
$\langle Nu \rangle_{D_h}$	Average Nusselt number based on the hydraulic diameter

CONTENTS

1 INTRODUCTION

The Brazilian Energy Balance (BEB) [6] highlighted that, in 2015, 32.2 % of the final energy usage in Brazil was dedicated to transportation. Figure 1.1 presents the final energy consumption by sector in Brazil in 2015. Furthermore, the total anthropogenic emissions associated with the Brazilian energy matrix reached 462.3 million tons of carbon dioxide equivalent (Mt CO_2-eq), most of it (194.0 Mt CO_2-eq) generated in the transportation sector [6]. This corresponds roughly to 1.5 % of the world anthropogenic emission of CO_2 [7].

Figure 1.1 – Final energy consumption usage in Brazil in 2015 by sector.
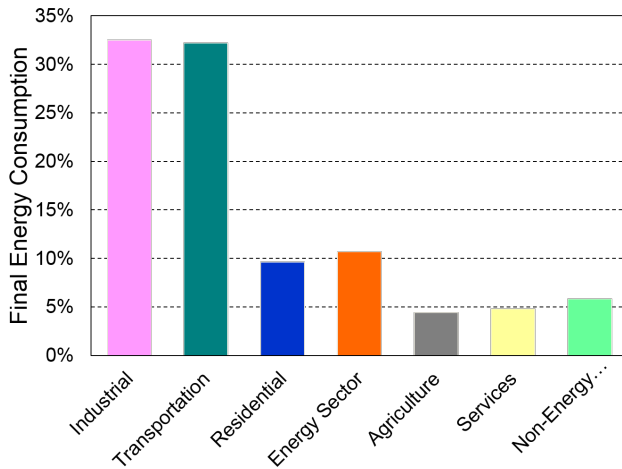
Source: adapted from *Empresa de Pesquisa Energética* (EPE [6]).

Considering only the transport sector, the consumption of diesel fuel accounted for 44.4 %, as shown in Figure 1.2. As a consequence, from of the 260.7 millions tons of oil equivalent (toe) consumed in Brazil in 2015, 14.3 % corresponded to diesel consumption; only behind electricity (17.2 %) and being the non-renewable source most consumed in Brazil. Therefore, any initiative aimed at reducing the use of this fuel has a direct impact on reducing emissions and is highly desirable.

Although new powertrains are being developed for automotive applications, for example, fuel cells, electric batteries, solar cells, hy-

Figure 1.2 – Energy consumption in transportation in Brazil in 2015.
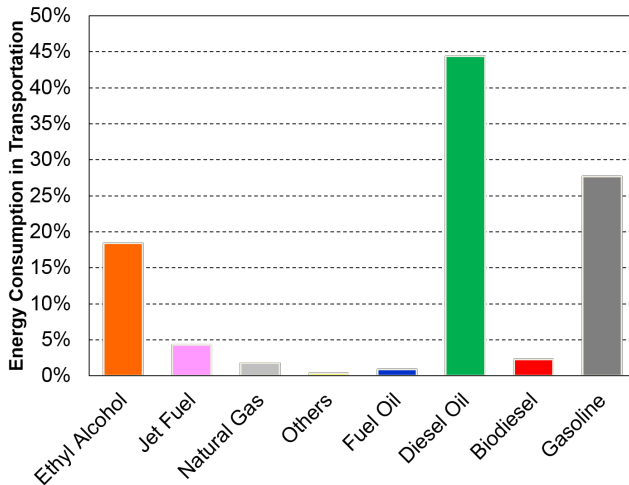
Source: adapted from EPE [6].

brid engines, etc., the internal combustion engines (ICE) are still the primary engines used in automotive, maritime, railway, and small stationary electric energy generation applications. In the current scenario, the diesel engine presents a higher efficiency than the gasoline engine, specially for high power applications [8]. Nevertheless these engines are still inefficient. Figure 1.3 shows a typical energy flow path of an ICE in which only about 25 % of the fuel internal energy is, in fact, utilized for vehicle operation, whereas 40 % is lost in the form of waste heat in the exhaust gas [3]. When added to the losses of the engine cooling system, they represent the largest opportunities for energy recovery in vehicles. For instance, Yang [5] pointed out that the fuel economy of internal combustion engine vehicles can be increased up to 20 % (e.g., from 25 % in Figure 1.3 to 30 %) simply by capturing the waste heat of exhaust gas and converting about 10 % of it to electricity. This amount of 10 % of exhaust heat corresponds to an increase of 4 % of the overall cycle efficiency, a value hardly achieved by any other means.

However, this energy available in the exhaust gas has relatively low thermodynamic availability and attempts to recover it usually affects negatively the engine performance through the increase in exhaust back pressure and lack of control of cylinder temperature. Therefore,

Figure 1.3 – Consumption of fuel combustion.

25%
Vehicle operation
Fuel combustion
5%
30% Friction
40%
Coolant
Exhaust gas
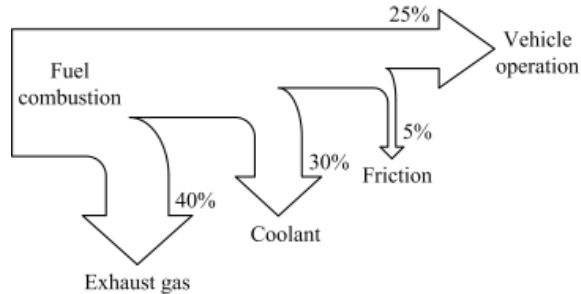
Source: adapted from Zhang, Chau and Chan [3].

the economical recovery of engine thermal energy continues to be a challenge and several systems have been proposed, such as the organic Rankine cycles (ORC) and the thermoelectric generators (TEG), which are the major focus of this work.

The organic Rankine cycles utilize an organic fluid as working fluid. These systems require a pump to circulate the organic fluid, a boiler/evaporator (usually a heat exchanger) to absorb the exhaust heat, an expander to discharge power by bringing the fluid to a lower pressure and a condenser to release the heat from the fluid before starting the cycle again. The turbines which operate with the organic fluids generally have higher efficiencies due to design considerations related to the smaller fluid molar mass [1]. Furthermore the ORC systems could be combined with a TEG for thermal energy recovery in engines and industrial and residential applications. In addition, more information concerning ORC systems can be found at [9–11].

Thermoelectric generators directly convert thermal energy flow along a temperature difference into electrical energy. TEG are based on the Seebeck effect, which is the electric potential difference created by a temperature gradient. Figure 1.4 describes a typical automotive waste heat recovery system that includes: an exhaust pipe, a heat exchanger, a thermoelectric device, a power conditioning unit and batteries Saidur et al.; Yu and Chau [1,2]. Here, this concept is extend to operate either in stand alone or in parallel to an ORC system.

The exhaust pipe provides high temperature gas. On the other hand, the source of cold fluid can be water from the radiator, air pumped by a fan or an ORC system. By coupling a thermoelectric generator in the exhaust pipe, this configuration ensures the temperature

38

Figure 1.4 – Schematic of waste heat recovery energy system
using thermoelectric devices.
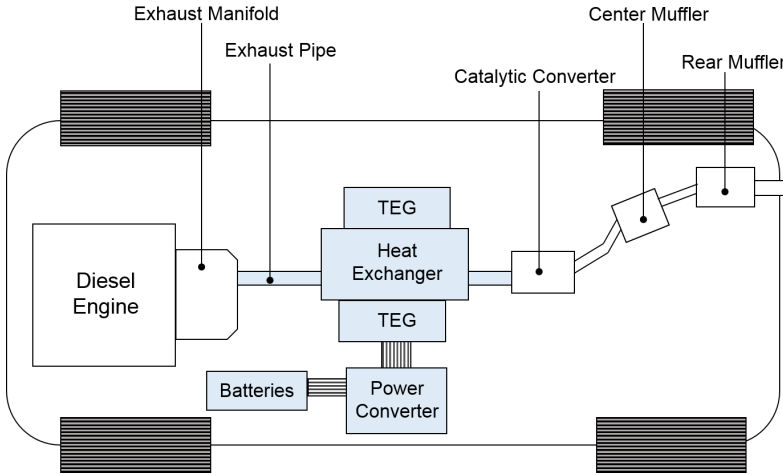
Source: adapted from Zhang, Chau and Chan; Saidur et al.; Yu and Chau [1–3].

gradient required to obtain the potential difference and thus generating energy.

Therefore, a TEG has the ability to directly recover waste heat and generate electricity without increasing harmful emissions and thus, achieving better fuel economy.

Besides the environmentally friendly behavior, thermoelectric generation has other potential advantages, such as: it has no moving parts, provides a silent operation [4], operate independently of ambient (or atmospheric) conditions [3], reduces secondary loads from the engine drive train [5], and provides electric power for new features.

In spite of being one of the most promising technologies for energy conversion, the thermoelectric generation still presents great challenges specially its low heat-to-electricity conversion efficiency. Usually, this recovery is hardly economically viable due to their small figure of merit,Z, a material characteristic of the thermoelectric pair related to the efficiency of conversion from thermal energy to electrical power.

Due to small conversion efficiency, the use of a TEG coupled to the exhaust system would require a large heat exchanger in order to meet the power required. Therefore, the vehicle mass increases, as well as, the pressure loss in the exhaust pipe. Advanced thermoelectric

materials, with dimensionless figure of merit (ZT) above 2, could be a solution, however they have been only tested on laboratory scale. Consequently, there is considerable uncertainty about materials and manufacture for large scale production.

The difficulties mentioned above represent just a sample of the difficulties regarding thermoelectric generation. The analysis is complex and involves several variables. In this context, computational models represent a means to investigate the most important processes and variables that take place in the design of a TEG and an approach to optimize these devices. The literature models (presented in the following chapter) are simplified and do not encompass the coupling of the engine and the TEG on transient phenomena. Consequently, it is expected that this master thesis can provide a basis for new models thermoelectric converters.

As mentioned previously, an increase in overall cycle efficiency of 4 % is, in principle, achievable and would request a significant improvement over today's engine performance standards. Therefore, this work was motivated by the possibility of incorporating this technology (direct energy conversion) in diesel engines, which could generate a satisfactory impact on increasing energy efficiency. Furthermore, it is expected that this model will be employed in the analysis of other opportunities in the future.

1.1   Research Objectives

The aim of this study is to design and to optimize a thermoelectric generator coupled to an exhaust pipe heat exchanger applied to heavy-duty diesel vehicles. In order to evaluate the power generated by the thermoelectric generator, the performance of the system was evaluated by numerical simulation, using FORTRAN, both in steady state and in transient regimes.

In order to achieve this objective, the following specific objectives were defined:

1. Review the fundamental concepts of thermoelectric generation and its state-of-the-art;

2. Simulate the diesel engine behavior to evaluate the exhaust gas temperature and the mass flow as a function of time for different operating conditions during periodic steady state regime;

3. Design the heat exchanger (exhaust gas - cold fluid), the thermo-

electric generator, and integrate them in a thermoelectric device;

4. Assess, by numerical simulation, few design choices, such as: different thermoelectric materials, positions in the exhaust system, and heat exchanger cold fluids; and the transient effect on the operation of the thermoelectric generator coupled to the diesel engine.

5. Optimize heat exchanger design by maximizing the power or conversion efficiency, using a pressure loss limiting constraint.

1.2 Thesis Organization

This master thesis is divided into five chapters. Chapter 2 addresses the most relevant concepts regarding the thermoelectric (TE) power generation, the materials commonly used, the advantages, and the major drawbacks. Furthermore, Chapter 2 states the latest developments and technologies on the use of thermoelectric generation for waste heat recovery of exhaust gas.

Chapter 3 encompasses the diesel engine aspects: a brief literature review concerning the engine modeling, the characteristic dimensions, the operational characteristics and the proposed thermodynamic model. Subsequently, the results are discussed and compared with common values in the literature in order to validate the model. The results obtained from the thermodynamic model characterize the exhaust gas, which is a input parameter for thermoelectric generator. The exhaust flow is necessary for maintaining the hot side temperature of the thermoelectric generator.

In Chapter 4, the design of the thermoelectric generator is presented in detail. First, the fundamental concepts and mathematical formulation of heat exchangers are reviewed. Then, the integrated system (heat exchanger and thermoelectric converter) is proposed. The primary configuration obtained provided information for a methodology to study the TEG performance. Therefore, the advantages and limitations of each design characteristic are also discussed in this chapter. In addition, special attention is given to the TEG transient behavior. This analysis provided insights for the enhancement of the wasted energy recovery. Moreover, the accuracy of the model is evaluated in comparison with other literature models

Finally, conclusions and recommendations for future works are presented in Chapter 5.

2 LITERATURE REVIEW

This chapter addresses the most relevant concepts regarding the thermoelectric generation. The discussion will begin with the description of the fundamentals of the Seebeck effect and will be followed by the design of thermoelectric generators, including the materials commonly used, the advantages, and the major drawbacks of the use of thermoelectric power generation.

In addition, the literature review will state the latest developments and technologies on waste heat recovery of exhaust gas. These includes new thermoelectric materials, heat exchanger design, control techniques to maximize the output power, hybrid systems (thermoelectric-photovoltaic) and prototyping. Finally, the specific objectives of this master thesis will be reviewed in order to verify if these still remain legitimate.

2.1 Fundamentals of the Seebeck Effect

2.1.1 Thermoelectric Phenomena

Thermoelectric effects in conductors have been known for long time. Thomas Seebeck is known to be the first to report in 1821. The Seebeck effect is the electrostatic potential difference created by a temperature gradient. Then, in 1834, Jean Peltier observed that direct current, through non-homogeneous conductor or junctions between dissimilar materials, produced a temperature difference and therefore, heat or cooling. Only in 1856, William Thomson related the Peltier and the Seebeck effects. According to Thomson, there is a (reversible) heat flux, proportional to current intensity, as long as, the material is subjected to a temperature gradient. Finally, in the beginning of 1900's, Edmund Altenkirch proposed the basic theory of the thermoelectric generator [12] and used the constant property model to derive the maximum efficiency [13].

This section attempts to address some of the mechanisms for conversion of electromagnetic energy to or from thermal energy. Three reversible phenomena — Seebeck, Peltier, and Thomson effect — and an irreversible one — Joule effect — are discussed.

2.1.1.1 Joule Effect

The Joule (or Ohmic) heating dissipates electric energy to thermal energy. From this irreversible conversion, the heat generated, by the current J_e, is $J_e^2 R_e$. Moreover, the electric resistance opposing the electric flow is given by Ohm's law:

$$R_e = \frac{\rho_e L}{A},$$ (2.1)

where ρ_e is the electrical resistivity, L the length of the conductor, and A is the cross-sectional area of the conductor.

Furthermore, the volumetric rate of energy conversion $\dot{S}_{e,J}$ can be given in terms of the change in the electrical potential $\Delta\varphi$ across the resistor as

$$\dot{S}_{e,J} = \frac{\Delta\varphi^2}{\rho_e L^2}.$$ (2.2)

2.1.1.2 Seebeck Effect

The Seebeck effect is the electrostatic potential difference created in a conductor by a temperature gradient, shown in Figure 2.1.

Figure 2.2 shows two dissimilar conductors p and n, joined at temperature T_0 while their ends are kept at temperature T_1. The magnitude of the voltage produced is proportional to the temperature difference between the ends of this device. Then, for the circuit presented, the electrostatic potential $\Delta\varphi$ is given by:

$$\Delta\varphi = \varphi_1 - \varphi_0 \equiv \pm \int_{T_0}^{T_1} \alpha_S dT,$$ (2.3)

where α_s is the Seebeck coefficient and is composed of the algebraic sum of the Seebeck coefficient of the two conductors:

$$\alpha_S = \alpha_{S,p} - \alpha_{S,n},$$ (2.4)

where, $\alpha_{S,p} > 0$ and $\alpha_{S,n} < 0$. Furthermore, the Seebeck coefficient is a function of the temperature, $\alpha_s = \alpha_s(T)$.

The appearance of this potential difference is based on the movement of free electrons. In the heated end of the conductor, the electrons in the valence shell leap from their atomic orbitals and become

Figure 2.1 – A schematic of a typical thermoelectric system configuration.
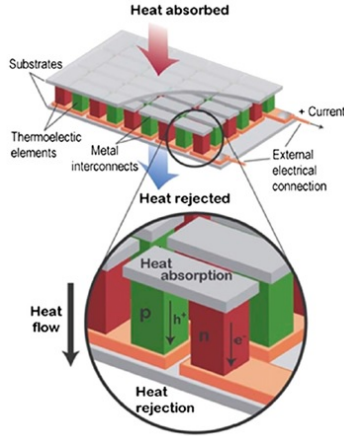
Source: Saidur, Rahim and Hasanuzzaman [14].

Figure 2.2 – Conventional representation of Seebeck thermocouple junction.
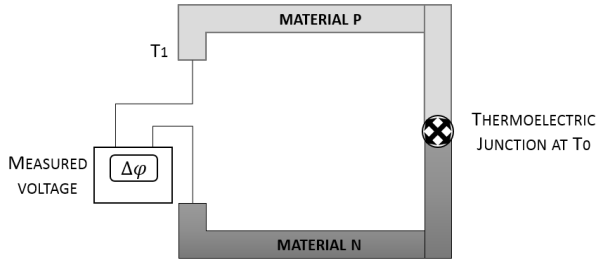
Source: adapted from Kaviany [8].

free electrons. These electrons move to the unheated area of the conductor where the energy level is lower in order to keep equilibrium. Thus, while the heated region becomes deficient in negative charges, i.e., with excess of positive charges, the unheated region acquires free electrons, i.e., excess of negative charges. This causes the appearance charge difference between the two materials, and therefore, potential difference. More information can be found in [8, 13, 15].

2.1.1.3 Peltier Effect

The Peltier effect stands for the heat absorption or release when direct current flows through a non-homogeneous conductor or a junction between two similar materials, as shown in Figure 2.3.

Although, due to the direct current, there is also heat release due to the Joule effect, the Peltier effect is reversible, which means the current can flow in both ways and the same junction can either absorb or release heat, depending on the current direction.

Figure 2.3 – Thermoelectric Peltier effect.
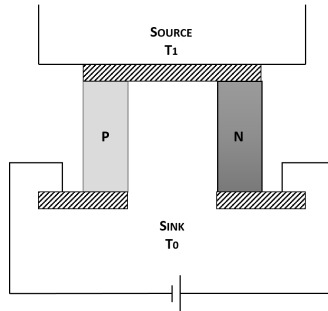
Source: adapted from Soo [12].

The heat rate absorbed or released at the junction is proportional to the direct current:

$$\dot{S}_{e,P} = \pm\alpha_P j_e A, \tag{2.5}$$

where α_p is the Peltier coefficient, j_e is the current density, and A is the cross-sectional area. Moreover, the negative sign implies the heat release and the positive, the absorption.

The Peltier coefficient is given by:

$$\alpha_P \equiv \alpha_S T, \tag{2.6}$$

where T is the absolute temperature of the junction. From this expression, it is possible to relate Peltier and Seebeck effects.

2.1.1.4 Thomson Effect

The Thomson Effect exposes that there is heat absorption or production when the current flows through a homogeneous conductor (no junction is required) submitted to temperature gradient. Figure 2.4 presents a scheme of this effect in a conductor. The heat absorbed or produced is proportional to the electric current and to the temperature difference. The proportionality constant, known as the Thomson coefficient α_T is related by thermodynamics to the Seebeck coefficient [13]. In conductors subjected to temperature variations, such as T_1 and T_0 across a conductor of length L, the heat absorbed is [8]:

$$\dot{S}_{e,T}/A = \int_0^L \alpha_T j_e \frac{dT}{dx} dx. \tag{2.7}$$

The Thomson effect arises from the Seebeck coefficient variation with temperature, since the models of the thermoelectric generator consider constant operating temperature, the Thomson effect is usually disregarded.

Figure 2.4 – Thomson effect.
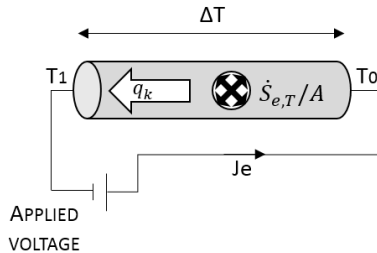
Source: adapted from Kaviany [8].

2.1.2 Applications

Thermoelectric devices use Peltier or Seebeck effect as working principle. In the following section, the main applications for these devices are presented aiming at identifying the opportunities for energy recovery.

For instance, some small refrigerators operate using Peltier effect

as working principle. These systems could be employed for example in the transportation of vaccines or organ transplants and in refrigeration systems for preservation of perishable materials in remote locations [15].

Thermocouples, used for temperature measuring, are also based on the Seebeck effect. If two wires composed of dissimilar materials are joined at both ends and one of the junctions is heated, a direct current will flow in the circuit. If this thermoelectric circuit is open, a net thermoelectric circuit potential will emerge. This open voltage is proportional to the Seebeck coefficient (thus, a material characteristic) and to the temperature gradient, which means the thermocouple could be used to measure this temperature difference.

From this principle, thermoelectric devices can be used for power generation in the form of thermoelectric generators. They have no moving parts and therefore, require less maintenance, and provide silent operation. Furthermore, since thermoelectric generators can operate in harsh environments, they emerge as flexible alternative to conventional power generation methods. In addition, thermoelectric devices can recover energy from waste heat, for example in exhaust systems, acting as a green source of electricity.

Applications may be classified in low and high power. In low power generation, for instance, it is possible to utilize waste human body heat to power a thermoelectric watch battery and to utilize any available heat source such as the surface of a hot water pipe to operate an electronic chip in a domestic gas monitoring system [16]. Another application for TEG is the use in the aerospace segment. For example, Voyager 1 — a space probe launched by NASA in 1977 programmed to explore Jupiter, Saturn, and Titan — which is still in operation, used a TEG powered by a radioactive source. Figure 2.5 presents a model of the thermoelectric device used.

For high power generation, for instance, industrial waste heat could be used to power TEGs. These are larger scale process and involve high-temperatures, therefore, are interesting opportunities for energy recovery. Hendricks and Choate [18] investigate the applicability of TEGs in three industries: glass furnaces (758 K to 1673 K), aluminium Hall-Hèroult cells (~1233 K), and reverbatory furnaces (~1033 K).

Additionally, thermoelectric generators are used in the automotive industry. In a vehicle, a TEG could be integrated to the exhaust system or to the radiator. There are few examples of companies investing in these systems. For instance, BMW presented systems that operate between 450 °C and 600 °C use the engine's cooling water.

Figure 2.5 – Model of an RTG (Radioisotope Thermoelectric Generators) unit.
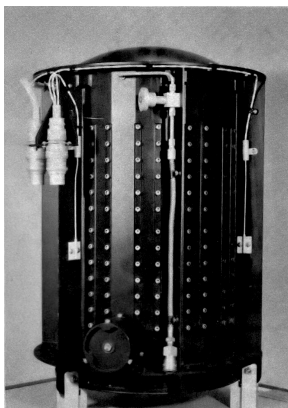
Source: Jet Propulsion Laboratory - NASA [17].

Figure 2.6 presents a TEG integrated in the exhaust manifold in a passenger vehicle. Furthermore, in 2008, the company introduced a TEG coupled to the exhaust system capable of generating 600 watts and in 2009, BMW presented a TEG coupled to the radiator. According to Mazar [19], the customers tests showed that 250 watts can be generated while CO_2 emissions and fuel consumption are reduced by 2 % at the same time.

Figure 2.6 – TEG integrated in the exhaust manifold.

Source: Mazar [19].

In a vehicle, the recovered heat converted to electric power can be used for climate control seat systems. These structures allow the

user to adjust the temperature of the passenger/driver seat in a vehicle. This strategic heating can provide a level of comfort to the occupant without heating the entire cabin of a vehicle or it can provide an extra level of comfort in addition to a standard heating system [20].

Another benefit of TEGs in vehicles is an extra energy source for hybrid vehicles. The waste heat can be converted and stored in batteries in order to improve the hybrid vehicle range or the efficiency by reducing the load on the main power source.

Finally, a thermoelectric device can be used to hold electrical loads thus reducing the load in the alternator. These loads encompass continuous (ignition, fuel injection, etc.), seasonal (air conditioners), short-time(stop lamps, electric windows, etc.), and long-time loads (lighting, heated rear window, etc.). Previous studies indicated that the fuel consumption can be reduced by 2 % to 5 % if the alternator is eliminated as the main electrical power source [21].

From the review above, a number of opportunities for TEG's deployment in vehicles have been identified. Next section focuses the design of TEG systems.

2.2 Thermoelectric Generator

2.2.1 Thermoelectric Generator Design

Thermoelectric devices are composed by many pairs of semiconductors (n and p-type). Each of these semiconductors is a called thermoelement, and a pair of thermoelements is a thermocouple. In order to predict the power converted by a thermoelectric generator, this section introduces the simplest configuration for TEG design, a single thermocouple. The following conditions were considered:

1. Any variation of the material properties with a change in temperature is neglected.

2. The Thomson heating effect is negligible.

3. The electrical resistances of the junction interfaces between the thermoelectric element and the plates are negligible.

4. The electrical resistance of the cold and hot plates between the adjacent thermoelectric elements is negligible.

5. The temperatures of the two plates are those of the source and the sink (i.e., their thermal resistances are negligible).

6. The cross-sectional area of the thermoelectric elements is assumed constant.

7. There is no heat loss from the thermoelectric elements to the surroundings [12].

A schematic diagram of the thermoelectric model is shown in Figure 2.7. The thermocouple is connected electrically in series and thermally in parallel. In addition, the generator works between a heat source (exhaust gas) providing a heat transfer rate Q_h and a heat sink removing a heat transfer rate Q_c.

Figure 2.7 – Model of a thermoelectric generator.
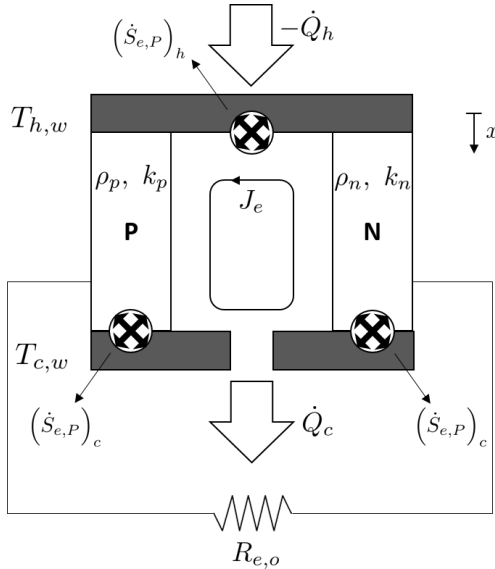
The heat is transferred to a substrate, that serves both as foundation and electric insulation for n and p-type thermoelements. Respectively, the heat is transported through conduction to cold side's substrate and then released in the heat sink, as shown in Figure 2.8.

If a resistive load is added to the circuit, as shown in the electric circuit in Figure 2.9 and the temperature difference between the substrates is maintained, a electric current flows around the circuit, due to the electric potential difference generated by Seebeck effect. As a result, the thermocouple will act as a generator.

50

Figure 2.8 – Equivalent model of a thermal circuit for a
thermoelectric generator.
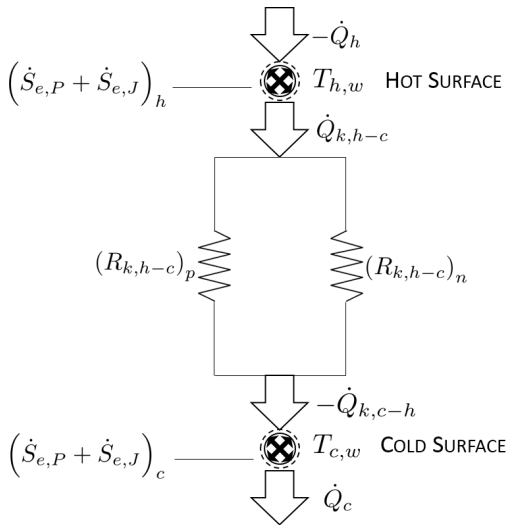
Figure 2.9 – Electric circuit diagram for a thermoelectric
generator.
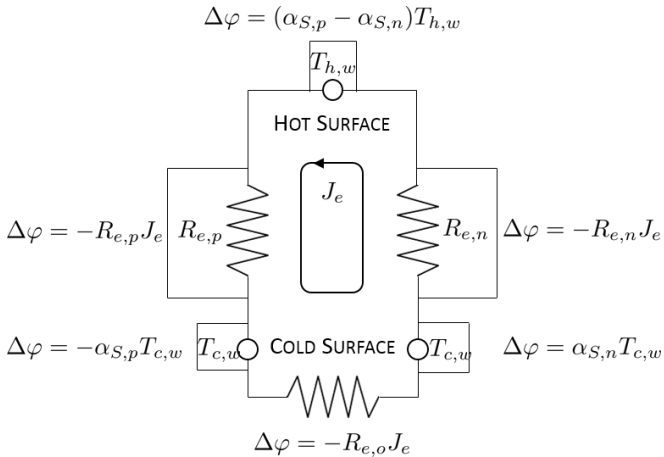
Source: adapted from Kaviany [8].

Note that part of the heat reaching the cold junction is the joule-

heating contribution. In addition, only the Seebeck effect produces a voltage across the unpaired terminals. However, the Seebeck effect is proportional to J_e, while Joule heating proportional to J_e^2. Therefore, if the current increases, the Joule heating becomes the dominating factor and the efficiency decreases.

Assuming that, $T_{h,w}$ is the average temperature of the hot side (x=0) and $T_{c,w}$ is the average temperature of the cold side ($x = L_n$ or L_p).

The power across the load is given by:

$$P = J_e^2 R_{e,o},\qquad(2.8)$$

where $R_{e,o}$ stands for the external electric load placed on the circuit.

The electric current is determined by setting the sum of the voltage potentials across the circuit in Figure 2.9 to zero, i.e.,

$$J_e = \frac{\alpha_S (T_{h,w} - T_{c,w})}{R_{e,o} + R_e},\qquad(2.9)$$

where R_e is the combined electrical resistance of the thermocouple given by:

$$R_e = \frac{\rho_p L_p}{A_p} + \frac{\rho_n L_n}{A_n}.\qquad(2.10)$$

2.2.2 Thermoelectric Efficiency

The thermoelectric efficiency for the thermocouple depends on the amount of conduction heat transfer rate along the elements. For the hot side $(x = 0)$, the heat transfer rate, in the x direction, through the p and n-type thermoelements is given by:[1]

$$\dot{Q}_{h,w} = (\alpha_{S,p} - \alpha_{S,n})J_e T_{h,w} + R_k^{-1}(T_{h,w} - T_{c,w}) - J_e^2 R_e/2,\quad(2.11)$$

where R_k is the overall thermal resistance of the thermocouple, given by:

$$\frac{1}{R_k} = \left(\frac{Ak}{L}\right)_p + \left(\frac{Ak}{L}\right)_n,\qquad(2.12)$$

and k is the thermal conductivity. Using Equations 2.8 and 2.11, the thermoelectric (conversion) efficiency can be given by the ratio of the

---

[1] The heat transfer rate equation derivation can be found in Appendix A.

electric power and the heat transfer rate from the hot side,

$$\eta_{TE} = \frac{P}{\dot{Q}_{h,w}}. \tag{2.13}$$

2.2.3 Figure of Merit

The efficiency of a thermoelectric generator can be also defined by a parameter, the figure of merit, that incorporates material properties of the two arms.

The figure of merit embodies characteristics expected to be relevant in thermoelectric materials: large Seebeck coefficient, for maximum conversion of heat into electric power; low electrical resistivity, to minimize Joule heating; and, low thermal conductivity, to minimize the irreversible effects of heat conduction.

These three properties combined lead to the figure of merit:

$$Z = \frac{\alpha_S^2}{\rho_e k}. \tag{2.14}$$

In addition, for a thermocouple, the figure of merit becomes

$$Z = \frac{(\alpha_{S,p} - \alpha_{S,n})^2 R_k}{R_e}. \tag{2.15}$$

Since the figure of merit Z has a unit $1/K$, a dimensionless parameter could be defined as ZT, where T is the average operating temperature.

There is no upper limit for ZT. However, it is hard to obtain ZT higher than 1 for most materials due to the relationship between its inherent properties. Further discussion will be deferred to Section 2.2.4.

2.2.4 Materials

Since the performance of a thermoelectric generator is limited by its dimensionless figure of merit (ZT), the ideal material for the p-n pair should have high Seebeck coefficient and average temperature of operation (T), and low thermal conductivity and electrical resistivity.

Since the ratio of the thermal conductivity to electrical conductivity for metals (Wiedemann-Franz-Lorenz law) is constant, it is not possible to reduce one while increasing the other [22]. Therefore, metals with high Seebeck coefficient tend to increase ZT.

From an application point of view, a thermoelectric material for power generation applications should also have the following characteristics: suitable chemical properties, for a low oxidation rate; adequate mechanical properties, to simplify manufacturing; and low material and fabrication costs; to high volume production.

Research conducted during the fifties and sixties led to three ideal alloy groups: bismuth telluride type materials, lead telluride and silicon germanium alloys. ZT for these materials is temperature dependent, as shown in Figure 2.10. Consequently, they reach optimum levels of heat to electricity conversion in specific temperature range: bismuth-telluride (Bi_2Te_3) is employed for temperatures below 500 K, lead telluride (PbTe) and lead tin telluride (PbSnTe) for temperatures around 770 K and operating limit up to 903 K , and silicon germanium alloys (SiGe) for temperatures around 1300 K. The lowest figure of merit belongs to the high temperature group, however there is a trade-off between high figure of merit and work under severe conditions (high temperature regime). In addition, it is possible to construct a system with a segmented structure to achieve the best average ZT over the entire operating temperature range [10]. Detailed reviews of most common used materials are provided by Rowe; Hendricks and Choate; Yang [5, 18, 22].

Although only tested in laboratory scale, integrated-circuit-type devices (skutterudites, superlattices, quantum wells, etc.) achieve higher performance. For instance, the skutterudites are materials containing rare earth element (REE), transition metals and metalloid. These compounds with crystalline structures presents good thermoelectric conversion, with ZT above 1.5.

Additionally, the super-lattices are composed by alternating layers of different material stacked periodically. The structure contributes to the movement of electrons and therefore, increases the electrical conductivity. On the other hand, the super-lattices reduce the phonon thermal conductivity, and, as a result, enhance the dimensionless figure of merit, as shown in Figure 2.11. Detailed reviews of supperlatices thermoelectric materials were carried out by Böttner, Chen and Venkatasubramanian [23].

For intermediate temperature thermoelectric power generators, Lead Telluride (PbTe) is explored , since its maximum operating tem-

Figure 2.10 – Temperature dependence of ZT for state-of-the-art materials.
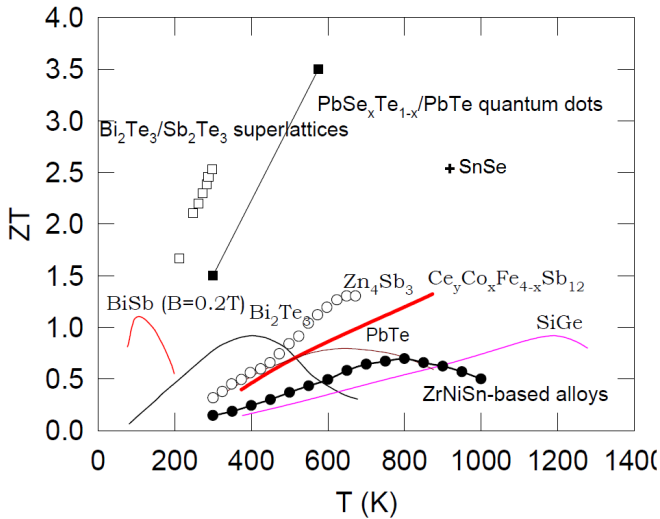
Source: adapted from Yang [5].

perature achieves 900 K. Dughaish [24] reviewed the lead telluride physical properties and the factors influencing the figure of merit. Their remarks indicated that grain size effects and lattice thermal conductivity mostly affect the figure of merit. In addition, Heremans et al. [25] explored the effects of using thallium impurity levels in lead telluride (PbTe), which enhanced the Seebeck coefficient through a distortion of the electronic density of states. As a conclusion, the authors doubled the ZT in p-type PbTe to above 1.5 at 773 K.

Lastly, Zhao et al. [26], investigated the conductivity and high figure of merit of SnSe crystals. Compared to other to other high-performance thermoelectrics, the results for SnSe presents an alternative to nanostructuring with ZT values as high as 2.6 at 923 K.

In conclusion, the selection of a suitable material for automotive waste heat recovery remains a challenge mostly due to the uncertainties on the impact on fuel economy, vehicle systems, and industrial large-scale production. Nevertheless the most advanced materials with high ZT are promising alternatives. Research on manufacturing techniques adapted to system application could increase viability and commercial interest.

Figure 2.11 – Thermoelectric figure of merit ZT for Bi_2Te_3 /Sb_2Te_3 superlattices (SL), PbSnSeTe/PbTe quantum dot superlattices (QDSL), and PbTeSe/PbTe quantum dot superlattices.
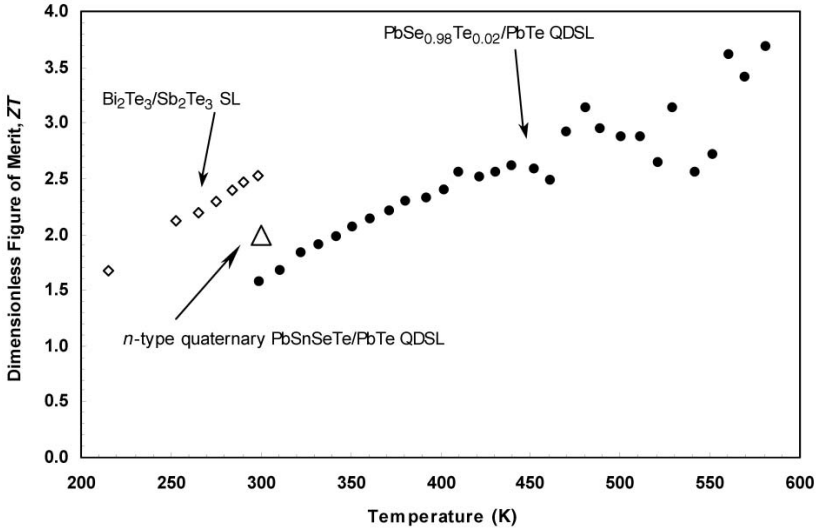
Source: Böttner, Chen and Venkatasubramanian [23].

2.2.5 Advantages and Drawbacks

The most apparent advantages of using TEGs for waste heat recovery is the higher fuel economy provided by on-board renewable energy generation. The direct production of electricity is attractive since it provides an extra energy source to propel auxiliary systems. Since with the current figure of merit, thermoelectric generators recover at most 15 % at the temperature encountered in typical diesel engine exhaust, a strategy to capture the remaining 85 % heat energy becomes interesting. [18]

In addition, thermoelectric generators takes advantage of minimizing the use of battery and reduction of vehicle battery life. As a result, TEG reduces maintenance and replacement of these equipments.

More than increasing the overall efficiency in both diesel and hybrid vehicles, thermoelectric generators have no moving parts and operate silently. Therefore, thermoelectric devices require less main-

tenance. According to Riffat and Ma [16], life testing has shown the capability of thermoelectric devices to exceed 100000 h of steady-state operation. In addition, thermoelectric devices are not positioning dependent and can work under severe or sensitive conditions.

As a conclusion, the thermoelectric generators offer several distinct advantages — from promising source of energy to low maintenance — which justify the use of such equipment in vehicles.

The primary challenge of using TEG is their low thermal efficiency (typically η_{th} 4 %) [1]. This occurs due to the low dimensionless figure of merit of the material. Commercial materials present values of ZT around 1, which does not provide a satisfactory thermal efficiency considering the system cost and industrial production. The most advanced thermoelectric pairs present ZT of the order of 2. However, these materials, e.g. super-lattices and quantum wells, have been developed and characterized only on the laboratory scale. As a result, there is a lack of on-road tests to evaluate thermal stability and to assess thermoelectric performance.

The difficulty to select a proper material for vehicle waste heat recovery leads to a problem concerning the large scale production. The uncertainty about materials and modules costs or even the OEM (Original Equipment Manufacturer) market size is crucial to reduce costs in the project. The thermoelectric device (thermocouples, heat exchanger attachment, wiring, interconnections, etc.) must be engineered in a manner that allows for low-cost large-quantity production [18].

In addition, due to the relative small efficiency, the use of TEG coupled to the engine exhaust pipe requires large under floor space for placing the system, increases vehicle mass and imposes an additional aerodynamic drag.

Another obstacle is reaching an optimum heat exchanger configuration. The hot and cold side configurations may be insufficient for satisfactory heat transfer rate. For instance, to maximize the heat transfer rate, increase the pumping power is an alternative. However, this would decrease the vehicle overall efficiency. Another alternative is working with different cold fluids, although this would require new pumps, tubing, and control systems, leading to an extra complexity. On the other hand, regarding the hot side, adding fins or adopting a radiator heat exchanger configuration would not be an option, since these would increase the backpressure.

Lastly, an additional challenge is to ensure the integration between the TEG power output and the existing vehicle power management (load matching). The TEG project should avoid modifications

to existing equipment or acquiring new components in order to meet these new requirements.

In summary, for commercial viability, it is necessary to overcome technical issues concerning the efficiency enhancement, the production scaling-up, the assembly process, and the system integration; while maintaining low costs. Nevertheless, the thermoelectric device business is still promising. Materials having figure of merit close to 2 are becoming more common and it is estimated that in the long term, it will be possible marketing materials with figure of merit close to 4. Combined with a high-performance heat exchanger, the generators may have the conversion efficiency required to make them economically attractive. According to Hendricks and Choate [18], 20 % energy conversion efficiency appears possible in advanced TEG systems operating at hot-side temperatures close to 1000 K.

Even though their industrial production still remains a challenge, the discovery of new materials, design and optimization of thermoelectric modules and heat exchangers, and integration with the vehicle may provide the overall efficiency that will turn these devices viable for vehicle applications.

2.3   State-of-the-art

This section presents some of the latest developments and technologies on waste heat recovery of exhaust gas. The discussion will begin with the latest revisions carried out, followed by state-of-the-art of thermoelectric generation in vehicles, and concluded with the presentation of other TE systems. In addition, some of the published thermoelectric generators systems are summarized in Table 2.1.

2.3.1 Reviews

In 2003, Riffat and Ma [16] presented applications for TE technologies, such as military, medicine and industrial or commercial products. The authors pointed out the development of new thermoelectric materials is the main bottleneck for the implementation thereof.

Additionally, in 2003, Crane [20] summarized potential application of thermoelectrics in diesel engines, their impacts on fuel economy and on emissions reduction. The study emphasized the user comfort in diesel vehicles, such as, the climate controlled seats. The author

acknowledged the potential of TEG technology in making significant impact in the diesel vehicle industry.

Considering only the revisions concerning the use of TE devices in vehicles, Yang [5] investigated the effect of electrical load and weight on fuel economy. The author concluded that the thermoelectric waste heat recovery technology could potentially offer fuel economy improvements, both for conventional vehicles and for hybrids. However the writer highlighted the need to develop new materials to increase thermoelectric efficiency.

Zhang, Chau and Chan [3] analyzed the latest developments of thermoelectric waste heat energy recovery for hybrid vehicles. The authors emphasized the system configurations, the materials employed, the power converter unit, and the maximum power point tracking (MPPT). The MPPT controller utilizes the battery terminal voltage and current, instead of using the TEG terminal voltage and current, to maximize the output power [2]. In addition, they suggested, in the near future, the thermoelectric technology will push the hybrid electric vehicle to a new level of fuel efficiency.

Recently, Saidur et al. [1] reviewed some the latest developments and technologies on waste heat recovery of exhaust gas. These included TEG, ORC systems, six-stroke cycle internal combustion engines and new developments on turbochargers. The study indicated, for TEG, that 4.7 % of fuel economy efficiency could be achieved and the challenges would remain related to the low thermal efficiency (<4 %).

2.3.2 Thermoelectric Generation in Vehicles

In 2001, Haidar and Ghojel [21] developed a program to evaluate the energy recovery using TEGs in medium temperature regime for a low power stationary diesel regime with rated power of 37 kW at 1800 rpm. By employing 98 bismuth telluride alloy couples, each module required a heat source capable of supplying a heat flux of about 8 W/cm^2. By keeping the temperature difference equal to 200 °C, each module converted 5 % of the thermal energy that passed through it into electricity generating 14 W of electrical power — or a total power output equal to 42.3 W.

Moreover, in 2004, Crane and Jackson [27] modeled a thermoelectric device coupled to a cross flow heat exchanger. The model was implemented in MATLAB. The results were compared with previous cross flow heat exchanger experiments as well as simple experiments

using thermocouples between counterflow hot water and cooling air flow channels. The study showed the importance of different design variables for waste heat recovery and indicated the need to assess the manufacturing process for integrating the TEG into heat exchanger design. For a heat exchanger with Bi_2Te_3 thermocouples, a net power density of 45 kW/m^3 could be achieved.

Further, Hsu et al. [28] simulated (using FloTherm software) and tested a prototype formed by eight thermoelectric generators to convert the heat from the exhaust pipe. They investigated the influence of clamp pressure on the performance of a TEG module. The results encompassed the low temperature generation, since the highest ZT value was achieved at 150 °C and the system had a very restrictive operational temperature of 20–200 °C. From the performed simulations and experiments, they obtained 44.13 W at an average temperature difference of 88.3 K and efficiency between 2 %–3 %.

Later, Hsu et al. [4] proposed a device composed by 24 TEGs. Through the simulation and experimental analysis, they evaluated the maximum power as a function of temperature difference. Results presented 12.41 W of maximum power output at average temperature difference of 30 K when engine rate boosts to 3500 rpm. Besides the low efficiency (about 0.3 %), this study and their previous work gave an overview of TEG design and provided insights on low-temperature waste heat generation.

Considering the use of different materials, Karri, Thacher and Helenbrook [29] modelled, in ADVISOR 2002, a thermoelectric generators placed in the exhaust stream of a sports utility vehicle (SUV) and a stationary, compressed-natural gas-fueled engine generator set (CNG). Both configurations used bismuth telluride and quantum-well thermoelectric materials. Results indicated - 0.2 % for relative fuel savings using Bi_2Te_3 and 1.25 % using Quantum Well (QW) generators. The negative value was caused by parasitic losses mainly due to the power required to transport the TEG weight. Assuming no parasitic losses, the power generated by the TEG using bismuth telluride was about 33 to 140 W, with relative fuel savings about 0.68 % to 0.83 %.

Considering the use of skutterudites, Hendricks and Lustbader [30] and [31] developed an integrated heat exchanger/ thermoelectric power system analysis tool in Matlab/ Simulink. They analyzed the effect of the thermoelectric system in light-duty-passenger (LDP) and heavy-duty (HD) vehicle waste heat recovery applications. The LDP was characterized by the exhaust temperature equal to 973 K and exhaust mass flow rate ranged from 0.01 kg/s to 0.03 kg/s. On the other

hand, the HD was characterized by the exhaust temperature equal to 785 K and exhaust mass flow rate ranged from 0.02 kg/s to 0.04 kg/s. The first part [30] addressed the potential electrical power available and cold side mass flow requirements in LDP vehicle exhaust heat recovery applications. The second part [31] detailed the behavior of TEG design parameters and predicted potential TE system power output for different conditions in LDP and HD. The system analysis results indicated that up to 0.9 kW of power appear possible in LDP vehicle exhaust applications, if the TEG were placed on the vehicle catalytic converter. For HD vehicles, 5-6 kW of electrical energy production was possible.

Zhang et al. [32] performed CFD simulations and bench tests of a TEG prototype. The authors investigated the effect of using high-efficiency nanostructured bulk materials with a novel direct metal brazing process to increase the device operating temperature. By using half Heusler alloy, a 1 kW TEG system operated with 2.1 % conversion efficiency under the average temperature difference of 339 °C in the TEG module and at a 550 °C exhaust temperature.

Few works aimed at increasing system efficiency through the power control unit. Yu and Chau [2] tested and simulated a thermoelectric device to recover waste heat energy, using the MPPT. A six unit experiment was designed and tested. The results indicated the system could work under different conditions and the MPPT could be employed at initial duty cycles. The most promising results suggested that power improvements could be up to 14.5 % and 22.6 % compared with the cases without using MPPT and without power conditioning, respectively. Additionally, Zhang and Chau [33] designed and tested a hybrid energy system composed by thermoelectric units and photovoltaic (PV) panels to be implemented in auto-mobiles. The proposed hybrid system used the MPPT so that the output power could be maximized. In order to verify the validity of the system, a 100 W prototype was built and tested. The power improvement varied from 7.5 % to 9.4 % for different TEG temperatures while the photovoltaic generator (PVG) irradiance was kept at its maximum point. Then the power improvement ranged from 4.8 % to 17.9 % for different PVG irradiance while TEG temperature was kept at its maximum power point.

Wang, Wang and Dai [34] modeled a TE device that uses automobile exhaust gas for power generation. They evaluated the effect of the temperature distribution along the TEG. The theoretical model proposed suggested the hot exhaust gas temperature decreases from 500 °C to 236 °C and cooling air temperature increases from 30 °C to 80 °C. In addition, the temperature of thermocouples at hot side decreased

from 366 °C to 188 °C, while at cold side from 144 °C to 124 °C. The total power output was about 13.87 W, and the overall efficiency was about 4.82 %. Since in TEG segments the efficiency could reach almost 10 %, the authors suggested that a combination of segments made of different materials might improve the overall performance.

He et al. [35] modeled a thermoelectric generator and developed a method for power deviation analysis to design the optimal TEG module area. The model was implemented using a FORTRAN routine and the results were compared with an experimental study provided in a previous paper. Based on the simulation the optimal design areas were 0.22 m^2 for the parallel flow and 0.3 m^2 for the counter flow. The authors recommended the counter-flow configuration since it maintains a smaller deviation from the peak power output with the optimal area when there is sufficient system space.

Finally Liu et al. [36] designed and performed bench tests and road tests of TEG prototype. The bench tests aimed at charactering the TEG system based on the temperature difference, open circuit voltage, and maximum power output. The test on a vehicle provided 600 W at an average temperature difference of 182 °C, while the bench test, which included independent cooling system, generated 944 W for a temperature difference up to 240 °C. In addition, the efficiency increased from 1.28 % to 1.85 %. The authors recommended improving exhaust pipe design in order to decrease the effect of thermal contact and increase the hot-side temperature.

2.3.3 Other Applications

Evaluating other applications for TE technologies employment, Fernandes [15] designed and tested a prototype for waste heat recovery in industrial process. In this application, the thermoelectric generator was coupled to a heat pump used in a cold chamber of a supermarket. As a result, the author obtained the production of 24 Wh using 80 thermocouples. However, the return of the investment was low, 0.69 %, and the payback period was 143 years.

Moreover, Qiu and Hayden [10] proposed a dual-cycle power system formed by a thermoelectric power cycle and an organic Rankine cycle. A mathematical model was established and the system was simulated under various conditions. For a system with a power capacity of 4.8 kW, the results from the model showed an electrical efficiency of 17 % for the dual-cycle system. Experiments were conducted in order

to verify the results. Their results exhibited that the TEG generated 1012 W electricity at an average module hot wall temperature of 598 °C and a cooling fluid outlet temperature of 75 °C. The results indicated that the thermoelectric power output could reach about 22 % of the overall system output, providing a significant power supplement to the micro-combined heat and power (CHP) system.

Considering the dual-cycle application, Miller, Hendricks and Peterson [9] also modeled an integrated power cycle, in order to identify the optimal performance points for both cycles. They concluded that the ORC is not greatly affected by the operation of the TEG. Moreover, only a small proportion of the power output is generated by the TEG, although this power could be used to satisfy some of the demands of the ORC system functions such as fans for the condenser and the motor for the feed pump.

Finally, to illustrate the use of high temperatures alloys, Park and Kaviany [37] simulated and performed a parametric study (geometry, flow, stoichiometry, materials) of the thermoelectric energy conversion in a matrix of tubes subjected to combustion. The direct fuel injection and reciprocation of the air flowing in the matrix combined with the solid-gas heat transfer and the conduction allow to obtain super adiabatic temperatures at the hot junctions. By placing high temperature SiGe alloys around the tubes, a conversion efficiency of about 11 % is achievable. However, the high thermal conductivities prevented high energy conversion efficiency: using materials with lower thermal conductivity, such as Bi_2Te_3, 25 % conversion efficiency would be possible.

2.4   Summary

This section presented a literature review on a series of aspects related to the thermoelectric generation. The thermoelectric phenomena, the basic design, and some efficiency parameters were explored.

In addition, it was noticed that the literature reports values of energy efficiency improvement from 0.3 % [4] to 25 % considering a theoretical analysis with the best available thermoelectric pairs [37]. Moreover, the electric power generated ranges from 12.41 W [4] to 6000 W [31].

The main advantages and challenges for potential application of TEG were also discussed. In order to overcome these limitations, some major research areas should be prioritized: new materials development,

heat exchanger optimization, and control unit design.

The proper design of the TEG requires a combined design that incorporates the TEG, the heat exchanger and the engine, since design choices in the heat exchanger may relatively affect the engine operation. None of the previous modeling efforts incorporate the engine as part of the model. Also, the performance of the TEG is heavily coupled to the temperature difference between hot and cold sides. During operation, heavy duty diesel engines experience hot excursions and start up from cold or warm conditions. All experimental work developed relied on steady-state condition. Here, transient operation is modeled and analyzed in order to assess the improvement in enegy generation and efficiency during transient operation.

Therefore, considering these areas and the state-of-the art presented, the objective described in the beginning of this Master thesis remains legitimate.

Table 2.1 – A summary of the state-of-the-art of thermoelectric generation in vehicles.

Reference	Year	Type	Cold fluid	TE Material	TEG Power (W)	η_{TE} (%)
Haidar and Ghojel [21]	2001	Simulation and experiment (bench test)	Water	Bi_2Te_3	42	5
Hendricks and Lustbader [30]	2002a	Simulation	Air	Combination 3[1]	900	8.2 (estimated)
Hendricks and Lustbader [31]	2002b	Simulation	Air	Combination 1[2]	6000	2.1 (estimated)
Crane and Jackson [27]	2004	Simulation and experiment (bench test)	Air	Bi_2Te_3	1000	2.12
Yu and Chau [2]	2009	Simulation and experiment (bench test)	Water	Bi_2Te_3	600	No information
Hsu et al. [28]	2010	Simulation and experiment (test on vehicle)	Air	Bi_2Te_3	44.13	2.1
Hsu et al. [4]	2011	Simulation and experiment (test on vehicle)	Air	Bi_2Te_3	12.41	0.3
Karri, Thacher and Helenbrook [29]	2011	Simulation	Engine coolant	QW	453	8.53
Zhang and Chau [33]	2011	Experiment	No information	Bi_2Te_3	100	No information
Wang, Wang and Dai [34]	2012	Simulation	Air	No information	13.87	4.82
Zhang et al. [32]	2015	Simulation and experiments (bench test)	Water	Half-Heusler	1000	2.1
Liu et al. [36]	2015	Simulation and experiments (bench and vehicle)	Water	Bi_2Te_3	944	1.85

[1] p-type $CeFe_4Sb_{12}$ / Zn_4Sb_3 / p-type Bi_2Te_3; n-type CoSb, / n-type Bi_2Te_3
[2] p-type $CeFe_4Sb_{12}$/ p-type Bi_2Te_3; n-type $CoSb_3$ /n-type Bi_2Te_3

3 DIESEL ENGINE

The diesel engine provides input information for the thermoelectric generator. The exhaust flow maintains the hot side temperature of the thermoelectric converter. Therefore, the objective of this chapter is to employ a thermodynamic model for the diesel engine, in order to obtain the conditions for exhaust gas (mass flow and temperature) as a function of time for different operating conditions. Furthermore, the model provides data to evaluate the TEG conversion and thermal efficiency.

The diesel engine behavior is investigated through modeling and simulation using a FORTRAN program. The model employed is based on a combination of other models already available in the literature.

This chapter is organized according to the following structure. It begins with the literature review, which describes the fundamentals of diesel engines, operating parameters and performance. After, the engine model is presented through the solution of conservation equations for mass (total and fuel) and energy. The analysis considers the diesel engine as a sequence of steady states, in order to follow variations in the engine's characteristics during the cycle (0-720). After, the results are discussed and compared with common values in the literature, the model is used to provide as input / parameter's for the thermoelectric generator design.

3.1 Literature Review

3.1.1 Diesel Engine

In 1892, Rudolf Diesel patented a new form of internal combustion engine, the compression-ignition (CI) engine. His concept of initiating combustion by injecting a liquid fuel into air heated solely by compression permitted doubling the efficiency over other internal combustion engines [38]. In CI engines, the air is compressed to a temperature higher than the autoignition temperature of the fuel, and combustion begins on contact as the fuel is injected into hot air.

In order to obtain one power stroke in a four strokes diesel engine, each ideal, four strokes, cylinder requires two revolutions of the crankshaft. Therefore, the diesel cycle encompasses the following processes:

- Intake stroke: it starts with the piston at the top dead center (TDC) —the position enclosing the smallest volume in the cylinder —and ends at bottom dead center (BDC) —the position of the largest volume in the cylinder. During the intake stroke, fresh air is drawn into the cylinder through the intake valve.

- Compression stroke: the intake and exhaust valves are closed and the piston moves upward, compressing the air charge. In the end of the compression stroke, the combustion takes place and the pressure rises rapidly.

- Combustion and power stroke: the combustion is approximated as constant-pressure heat addition process. The high-pressure gases force the piston down, which in turn propels the crankshaft to rotate, producing useful work during the expansion stroke. At the end of the power stroke (at the BDC), the cylinder is filled with combustion products and the exhaust valve opens to initiate the exhaust process.

- Exhaust stroke: the piston moves upward to purge the exhaust gases through the exhaust valve. Finally, the exhaust valve closes to start a new cycle.

The resulting ideal cycle consists of four internally reversible processes:

1 — 2 Isentropic compression;

2 — 3 Constant pressure heat addition;

3 — 4 Isentropic expansion;

4 — 1 Constant volume heat rejection;

The main characteristics of the diesel cycle process are summarized in the p-V diagram of Figure 3.1.

3.1.2 Performance Parameters

In order to evaluate the engine performance, parameters, for instance, work, specific fuel consumption, conversion and thermal efficiency, are employed. The basic concepts have been presented in classical literature on internal combustion engines, such as Heywood [38].

Figure 3.1 – p-V diagram for the ideal Diesel cycle.

1 – 2 WIN: INPUT WORK
(ISENTROPIC COMPRESSION)
2 – 3 QIN: INPUT HEAT
(FUEL INJECTION AND COMBUSTION
AT CONSTANT PRESSURE)
3 – 4 WOUT: OUTPUT WORK
(ISENTROPIC EXPANSION)
4 – 1 QOUT: OUTPUT HEAT
(EXHAUST AT CONSTANT PRESSURE)
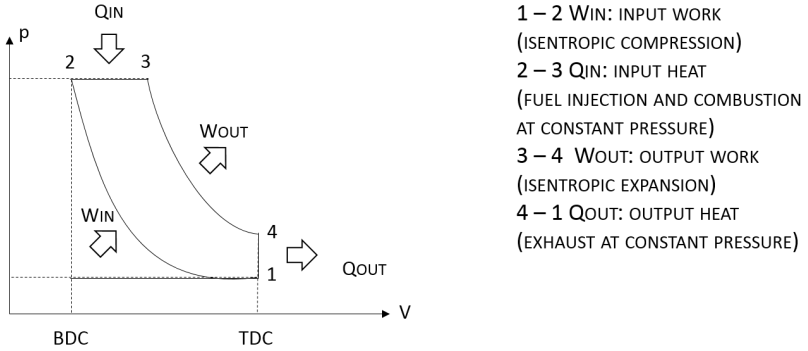
In the following, the most common performance parameters are discussed.

The net indicated work per cycle stands for the work delivered to the piston over the entire four-stroke cycle. The work is obtained by integrating the cycle in the p-V diagram:

$$W_{c,i,n} = \oint p_f \, dV_f. \tag{3.1}$$

The specific fuel consumption (sfc) is a measure of the fuel consumption per power developed by the engine:

$$sfc = \frac{\dot{M}_{F,inj}}{P}, \tag{3.2}$$

where $\dot{M}_{F,inj}$ is the injected fuel mass flow rate.

The net power per cycle (P) is given by the ratio of work produced by the crank shaft angular speed:

$$P = \frac{W_{c,i,n}N}{120}. \tag{3.3}$$

In addition, the fuel conversion efficiency (η_f) is the ratio of work produced by the engine and fuel energy:

$$\eta_f = \frac{W_{c,i,n}}{M_{F,o}\Delta h_{r,F}}, \tag{3.4}$$

where $M_{F,o}$ is the mass of fuel injected and $\Delta h_{r,F}$ stands for the heat of reaction with air. Therefore, η_f measures the engine capacity to convert the fuel energy into work.

Finally, the thermal efficiency (η_{th}) is defined by:

$$\eta_{th} = \frac{W_{c,i,n}}{M_{F,r}\Delta h_{r,F}}, \tag{3.5}$$

where $M_{F,r}$ is the mass of fuel burned. In state-of-the-art engines, η_{th} is basically equal to η_f.

3.1.3 State-of-the-art

This section presents some of the published articles on engine zero dimensional models. The aim is to recognize the basic models needed for the dynamic modeling as a sequence of steady-states.

Alegre [39] simulated the engine behavior and performed an exergetic analyses. Two models were developed: the diagnosis model was used to analyze the combustion process of a real engine, when the cylinder pressure diagram is determined experimentally; while the predictive model, allows to simulate the behavior of a real engine, when the burning rate is specified. Although the author has considered the hypothesis of chemical balance and homogeneity of mixture of gases contained in the cylinder (which limits the analysis of the formation of pollutants), the model took into account the propagation of waves in the ducts (which makes it possible to evaluate the effect of geometry characteristics of the exhaust system).

In 1998, Rakopoulos and Giakoumis [40] proposed a single-zone thermodynamic model, following the filling and emptying modeling technique. the model was used to analyze the operation of an indirect injection, naturally aspirated, diesel engine under transient conditions resulting from a rapid increase in load. The model also covered the dynamic simulation of the engine with special sub-models to model the conservation of energy in the crankshaft, the inertia forces, the governor dynamics and the fuel pump characteristics. The aim was to derive a better simulation for transient operation, since this was not treated as a series of steady state operating points. In order to validate the findings, the model was tested favorably (at steady state conditions) against results derived from detailed experimental work. Furthermore, the authors also proposed a multi-cylinder engine model, which solves separately the governing equations for each cylinder.

Chow and Wyszynski [41] provided an overview of engine systems modeling by first and second law analysis. The aim was to improve the systems modeling methods, mainly the gas composition in the catalytic exhaust converters and fuel processors, in order to meet the increasing demands of fuel efficiency and emission legislation. The authors described the engine system as a set of cylinders by using the filling and emptying (zero-dimensional) model. In contrast to the inlet and exhaust manifolds, which were also described by a gas dynamics model. Furthermore, the applicability of these gas model to chemically complex system was also discussed.

Park and Kaviany [42] investigated the effect of an in-cylinder porous regenerator on the thermal efficiency of diesel engines. For this engine, each cylinder had one intake and exhaust valves. The model included the surface-convection, surface/volume radiation and conduction heat transfer modes. Concerning the conduction through the cylinder walls, prescribed temperature of the cooling water was used for the analysis. The authors used one-dimensional energy conservation equations for solid phases of the regenerator, the piston, the cylinder head and block.

Lastly, Pereira and Oliveira [43] discussed the trapping and destruction of soot in the exhaust of a diesel engine using a porous foam as a filtration medium. The filing and emptying model included six cylinders, direct injection, compression ignition, low-heat rejection engine with no valve overlap. From the model, they obtained the crank angle variations of the volume-averaged solid and gas temperatures, the gas pressure, and the gas mass flow rate at the exhaust port.

From the review above, it is noticed that in the literature are generally employed single zone and filling and emptying models. Furthermore, information was obtained on the transient engine behavior, their multi-cylinder and exhaust features.

3.2 Methods

3.2.1 Overall Characteristics of the Diesel Engine

The engine modeled is a heavy-duty, high efficiency diesel engine that was previously employed on [42–44]. Therefore, only the overall characteristics are summarized here.

The diesel cycle is a four-stroke, naturally aspirated (admitting atmospheric air) cycle. The engine modeled is a water cooled, six-

cylinder, low-heat rejection engine with no valve overlap, and direct injection.

For this engine, each cylinder has one intake and one exhaust valve. Furthermore, the cylinder head is lined with a ceramic layer to provide thermal insulation of the combustion chamber and the cylinder block is made of cast iron, that allows the cylinder surface to remain cold enough so that the lubricant film can survive.

Figure 3.2 presents a rendering of the most important engine dimensions and emphasizes the three modeled subsystems: cylinder head, cylinder block and piston. Table 3.1 and 3.2 provides engine geometric and operation data.

Figure 3.2 – The geometric parameters and variables of the diesel engine.
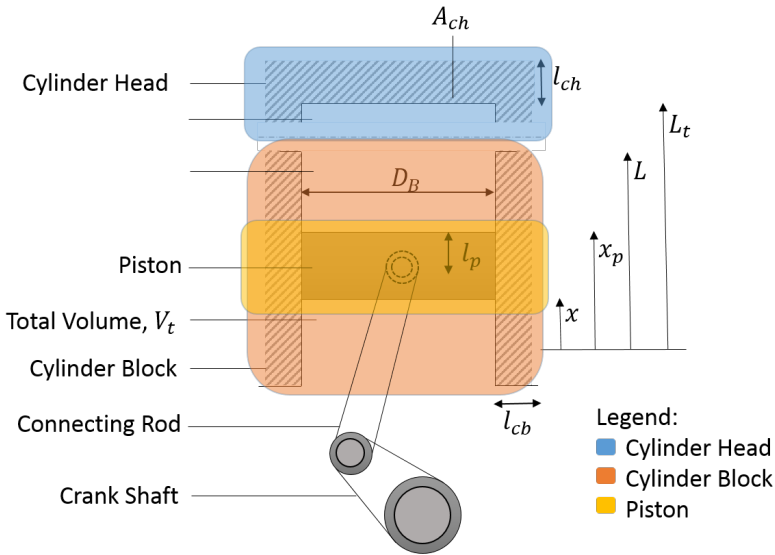
Source: adapted from Park and Kaviany [42].

3.2.2 Basic Assumptions

In order to derive a mathematical model to describe the diesel engine, this section presents the simplifying assumptions considered.

The main object of study is the instantaneous content of the

Table 3.1 – Overall operating characteristics of the diesel engine modeled.

Parameter, unit	Symbol	Magnitude
Bore, m	D_B	0.125
Stroke, m	L	0.14
Skin depth of the cylinder head, mm	l_{ch}	0.4
Skin depth of the cylinder block, mm	l_{cb}	3.0
Skin depth of the piston, mm	l_p	6.0
Clearance volume, cm^3	V_c	245.4
Displaced volume, cm^3	V_d	1,718
Compression ratio	r_c	16.5
Crank shaft angular speed, rpm	N	1600
Water cooled temperature, K	$T_{f,w}$	380
Fuel heat of reaction with air, J/kg	$\Delta h_{r,F}$	42.5E6
Air/Fuel mass ratio	$(A/F)_a$	30

cylinder, i.e. air, fuel, and combustion products. The cylinder encloses a volume open to the transfer of mass and energy in the form of work and heat. Therefore, the combustion is modeled by heat addition and the exhaust process by heat rejection. Throughout the power cycle , the cylinder is treated as variable volume plenum, spatially uniform in pressure [45].

Consequently, the gas pressure and mass flow at the exhaust valves are approximately described by a quasi-dimensional model. When reverse flow past the intake valve occurs, rapid mixing of the back flow gases within the intake manifold is assumed [45]. The gases are modeled as a one-dimensional, frozen composition, compressible flow. In addition, ideal behavior is assumed for evaluating gas properties.

Furthermore, the diesel engine combustion chamber is modeled as a thermal resistances circuit and its heat transfer is taken into account using average convection and radiation exchange coefficients.

Part of the cylinder head, block and piston are divided into small volumes to capture surface temperature variations. The remainder of the cylinder head and block and piston counts as a large volume. Figure 3.3 presents the subsystems described in Figure 3.2: these systems receive energy, due to convective heat transfer (green), from combustion gas and transfer heat by radiation (red) between themselves. Internally, for each of the subsystems, there are the conductive heat transfer (purple) and the convection exchange with the coolant (green). In addition,

Table 3.2 – Fuel injection, intake and exhaust characteristics of
the diesel engine modeled.

	Parameter, unit	Symbol	Magnitude
Injection	Mass of fuel injected, g	$M_{F,o}$	0.216
	Crank angle when injection begins, deg	$\theta_{F,s}$	348
	Crank angle when injection ends, deg	$\theta_{F,e}$	372
Intake	Discharge coefficient,	$C_{D,i}$	0.7
	Valve diameter, m	$D_{v,i}$	0.044
	Crank angle when the valve begins to open, deg	$\theta_{v,s,i}$	0
	Crank angle when the valve closes completely, deg	$\theta_{v,e,i}$	224
	Intake pressure, kPa	p_{int}	357
	Intake temperature, K	T_{int}	329
Exhaust	Discharge coefficient	$C_{D,e}$	0.7
	Valve diameter, m	$D_{v,e}$	0.044
	Crank angle when the valve begins to open, deg	$\theta_{v,s,e}$	474
	Crank angle when the valve closes completely, deg	$\theta_{v,e,e}$	720
	Exhaust pressure, kPa	p_{exh}	251

the first node (left) indicates the heat transfer in the combustion gas,
where there are components

3.2.3 Conservation Equations

This chapter presents the mathematical model of the diesel engine obtained from the formulation of the conservation equations, for the mass of fuel and energy for this open thermodynamic system. The model is based on the literature, e.g. [38, 42, 45, 46], and the contributions of each author will be indicated throughout the text.

Figure 3.3 – Thermal circuit model.
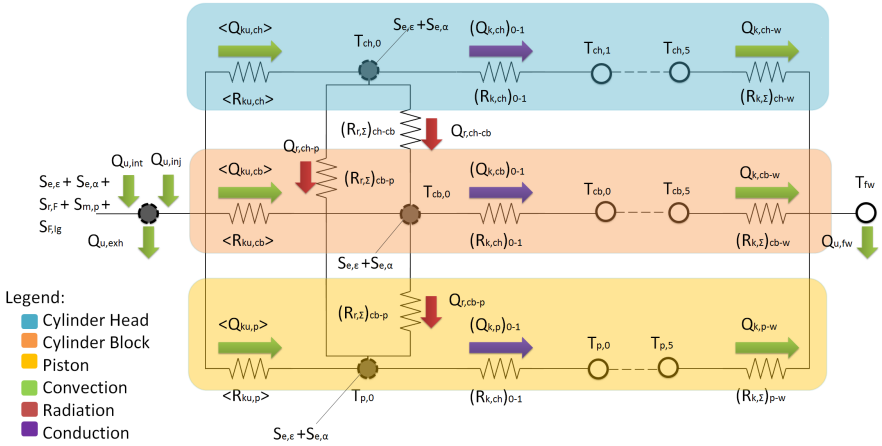
3.2.3.1 Conservation of Total Mass

The rate of change of the total mass in the combustion chamber is equal to the sum of the mass flow rates into and out of the system. Since the quantity of gas in the combustion chamber changes during the intake, injection, and exhaust; the conservation of mass of gas can be written as:

$$\frac{d\,M_f}{d\,t} = \dot{M}_{int} - \dot{M}_{exh} + \dot{M}_{F,inj}. \tag{3.6}$$

3.2.3.2 Conservation of Fuel Mass

The fuel quantity in the combustion chamber changes due to injection and combustion. Then, the conversation of mass of fuel is:

$$\frac{d\,M_F}{d\,t} = \dot{M}_{F,inj} - \dot{M}_{F,r}. \tag{3.7}$$

3.2.3.3 Conservation of Energy

The first law of thermodynamics, neglecting kinetic and potential energy changes, may be written as

$$\frac{\partial}{\partial t} \int_{VC} \rho u \, dV + \int_{SC} u(\rho \vec{v} \cdot \vec{u}) dA = \dot{Q} + \dot{W}. \tag{3.8}$$

Neglecting the work of the viscous stress, assuming uniform flow in the inlet and outlet sections, and assuming that the gas behaves as an ideal gas and that the specific heat at constant pressure c_p is constant, the energy conservation equation for gas can be re-arranged as: [1]

$$\frac{dT_f}{dt} = \frac{\dot{S}_f - \dot{Q}_{A,f}}{(Mc_p)_f}, \tag{3.9}$$

where $\dot{S}_f$ is the energy conversion in the gas. Furthermore, the net heat transfer from the fluid $(\dot{Q}_{A,f})$ is:

$$\dot{Q}_{A,f} = (\dot{M}h)_{int} + (\dot{M}h)_{exh} + (\dot{M}h)_{inj} + \dot{Q}_{ku,ch\,Db} + \dot{Q}_{ku,cb\,Db} + \dot{Q}_{ku,p\,Db}, \tag{3.10}$$

where $(\dot{M}h)_{int}$ is the enthalpy flow of the air intake, $(\dot{M}h)_{exh}$ is the enthalpy flow of the exhaust gas, $(\dot{M}h)_{inj}$ is the enthalpy flow of the fuel injected. Moreover, $\dot{Q}_{ku,ch\,Db}$, $\dot{Q}_{ku,cb\,Db}$, and $\dot{Q}_{ku,p\,Db}$ are the surface-convection heat transfer between the gas and the cylinder head, cylinder block, and piston surfaces. The energy conversion in the gas, $\dot{S}_f$, has contributions of combustion $(\dot{S}_{r,F})$, expansion cooling/compression heating $(\dot{S}_{m,p})$, fuel evaporation $(\dot{S}_{F,lg})$ and volumetric emission and absorption of radiation, i.e., [42]

$$\dot{S}_f = \dot{S}_{m,p} + \dot{S}_{F,ig} - \dot{S}_{ch} - \dot{S}_{cb} - \dot{S}_p + \dot{S}_{r,F}. \tag{3.11}$$

The following sections will be devoted to develop expressions to calculate each term of the conservation equations. First, each term from the net heat transfer in flue gas, presented in Equation 3.10, will be described. Then, each term in the energy conversion in the gas, presented in Equation 3.11, will be described.

---

[1]The mathematical proof can be found in [38, 46]

3.2.4 Gas Exchange Process

The intake and exhaust flows are approximately described by a quasi-dimensional model. Therefore, during the intake and exhaust, the cylinder is considered filled by a homogeneous mixture of non reactive ideal gases. In addition, as previously described, during exhaust, the gas mixture consists of a mixture of flue gases with frozen chemical composition.

This section attempts to present the model to evaluate the mass through the intake and exhaust valves. Furthermore, in this section, expressions to calculate the enthalpy flows of Equation 3.10 will be presented.

3.2.4.1 Flow through the Valves

The mass flow rate through the intake and exhaust valves are affected by a discharge coefficient (C_d), the upstream stagnation pressure (p_o), the stagnation temperature (T_o), and a reference area (A_v), characteristic of the valve design. The mass flow rate is described by Heywood; Assanis et al. [38, 45] (among others) and is given by:

$$\dot{M}_v = C_D A_v f_{a,f} \frac{p_o}{(R_u/M_g T_o)^{1/2}}, \tag{3.12}$$

where f_{af} indicates the appropriate equation if the mass flow is chocked $\left(\frac{p_t}{p_o} \leq \left(\frac{2}{\gamma-1}\right)^{\frac{\gamma}{\gamma-1}}\right)$ or not:

$$f_{a,f} = \begin{cases} \frac{p_t}{p_o}^{1/\gamma} \left(\frac{2\gamma}{\gamma-1}\left[1-\left(\frac{p_t}{p_o}\right)^{\frac{\gamma-1}{\gamma}}\right]\right)^{1/2} & \text{if } \frac{p_t}{p_o} > \left(\frac{2}{\gamma-1}\right)^{\frac{\gamma}{\gamma-1}}, \\ \gamma^{1/2}\left(\frac{2}{\gamma+1}\right)^{\frac{\gamma+1}{2(\gamma-1)}} & \text{if } \frac{p_t}{p_o} \leq \left(\frac{2}{\gamma-1}\right)^{\frac{\gamma}{\gamma-1}}. \end{cases} \tag{3.13}$$

For flow into the cylinder through an intake valve, p_o is the intake system pressure (p_{int}) and the static pressure just downstream (p_t) is the cylinder pressure. For flow out of the cylinder through an exhaust valve, p_o is the cylinder pressure and p_t is the exhaust pressure (p_{exh}) [38]. During solution, in order to improve convergence, the value of stagnation pressure was approximated as the fluid pressure at the start of exhaust process. The impact of this assumption will be discussed in the Results Section.

In the following, the reference area (A_v) is given by:

$$A_v = \pi D_v L_v f_{a,v}, \qquad (3.14)$$

where D_v is the valve diameter, L_v is the maximum valve lift and f_{av} is a valve lift profile given by:

$$f_{a,v} = \begin{cases} 0 & \text{if } \theta \leq \theta_{v,s}, \\ \frac{\theta}{(\theta_{v,s}-\theta_{v,e})} & \text{if } \theta_{v,s} < \theta \leq (\theta_{v,s}+\theta_{v,e})/2, \\ \frac{(\theta_{v,e}-\theta)}{(\theta_{v,s}-\theta_{v,e})} & \text{if } (\theta_{v,s}+\theta_{v,e})/2 < \theta \leq \theta_{v,e}, \\ 0 & \text{if } \theta > \theta_{v,e}. \end{cases} \qquad (3.15)$$

This linear approximation for the valve lift function is sufficient to reproduce the main intake and exhaust phenomena, as showing by Kaviany [8].

3.2.4.2 Enthalpy Flow of the Intake Air

The flow out of the intake manifold occurs due to the pressure difference between the intake manifold and the cylinder. This pressure difference could be negative causing a back flow of the intake air. Then, assuming that the intake mass flow rate $\dot{M}_{int}$ is positive when entering the cylinder, the enthalpy flow of the intake air is:

$$(\dot{M}h)_{int} = \begin{cases} 0 & \text{if } \dot{M}_{int} \leq 0, \\ \dot{M}_{int}\, c_{p,a}\, (T_f - T_{int}) & \text{if } \dot{M}_{int} > 0. \end{cases} \qquad (3.16)$$

3.2.4.3 Enthalpy Flow of the Exhaust Gas

For the exhaust gas, the back flow is also possible. Then, assuming that the exhaust mass flow rate $\dot{M}_{exh}$ is positive when leaving the cylinder, the enthalpy heat flow of the exhaust gas is:

$$(\dot{M}h)_{exh} = \begin{cases} 0 & \text{if } \dot{M}_{exh} \geq 0, \\ \dot{M}_{exh}\, c_{p,f}\, (T_f - T_{exh}) & \text{if } \dot{M}_{exh} < 0. \end{cases} \qquad (3.17)$$

3.2.5 Enthalpy of Fuel Injected

As described by Kaviany [8], in the Equation 3.10, the sensible enthalpy flow due to fuel injection is:

$$(\dot{M}h)_{inj} = M_{F,inj}\, c_{p,F}\, (T_f - T_{F,o})\,, \tag{3.18}$$

where the fuel mass flow is assumed constant during the fuel injection period and is given by:

$$\dot{M}_{F,inj} = M_{F,o}\frac{f_{F,i}}{\Delta t_{F,i}}, \tag{3.19}$$

where $\Delta t_{F,i}$ represents time interval during injection and $f_{F,i}$ is the fuel injection profile:

$$f_{Fi} = \begin{cases} 0 & \text{if } \theta < \theta_{F,s}, \\ 1 & \text{if } \theta_{F,s} \le \theta \le \theta_{F,e}, \\ 0 & \text{if } \theta > \theta_{F,e}. \end{cases} \tag{3.20}$$

The crank angle when injection begins $\theta_{F,e}$ is equal to 348 ° and when it ends $\theta_{F,s}$ is equal to 372 °. From these angles, it is possible to calculate the fuel injection period:

$$\Delta t_{Fi} = \frac{(\theta_{F,e} - \theta_{F,s})}{N\ 360/60}. \tag{3.21}$$

And therefore, determine the mass of injected fuel and predict its enthalpy flow.

3.2.6 Surface-Convection

The surface-convection heat transfer between the gas and the cylinder head, presented in Equation 3.10, is:

$$\dot{Q}_{ku,ch\,Db} = \frac{T_f - T_{ch_0}}{R_{ku,ch}}, \tag{3.22}$$

where the surface convection resistance $R_{ku_{ch}}$ is:

$$R_{ku_{ch}} = \frac{D_B}{\langle Nu \rangle_{D_B} k_f A_{ku,ch}}, \tag{3.23}$$

where k_f is the flue gas thermal conductivity, $A_{ku,ch}$, the surface-convection area and $\langle Nu \rangle_{D_B}$ the average Nusselt number, determined from the Woschni correlation (using the average cylinder gas velocity and the cylinder pressure) provided by Woschni (1967 apud Heywood [38], 1988).

Similar equation for surface-convection heat transfer can be deduced for the cylinder block and the piston.

In the following, the terms exposed in the Equation 3.11 will be discussed.

3.2.7 Evaporation Heat for Liquid fuel

The latent heat contribution in the energy conversion of flue gas, due to liquid fuel evaporation (Equation 3.11) is given by [8]:

$$\dot{S}_{F,lg} = -\dot{M}_{F,inj}\Delta h_{lg}, \tag{3.24}$$

where Δh_{lg} is equal to 116 kJ/kg$_{fuel}$ and corresponds to the enthalpy of evaporation.

3.2.8 Expansion Cooling and Compression Heating

In the Equation 3.11, the energy conversion in the gas through the expansion cooling/compression heating ($\dot{S}_{mp}$) is described by Park and Kaviany [42] and is given by:

$$\dot{S}_{mp} = V_f \frac{dp_f}{dt}, \tag{3.25}$$

where, V_f and p_f are the flue gas volume and pressure.

3.2.9 Combustion Model

The diesel combustion is an unsteady, heterogeneous and thus, a complex phenomenon. A complete mathematical combustion analysis would require accurate models of compressible viscous air motion, fuel spray penetration, droplet break-up and evaporation, air entrainment into the spray, combustion kinetics, turbulent diffusion and so on [45]. Even though, a simple but adequate model for the system (diesel engine and thermoelectric generator) is to consider the process of combustion

as a heat release.

The stages of diesel combustion can be identified in a heat release diagram, as shown in figure 3.4:

Figure 3.4 – Typical diesel engine heat-release diagram identifying different diesel combustion phases.
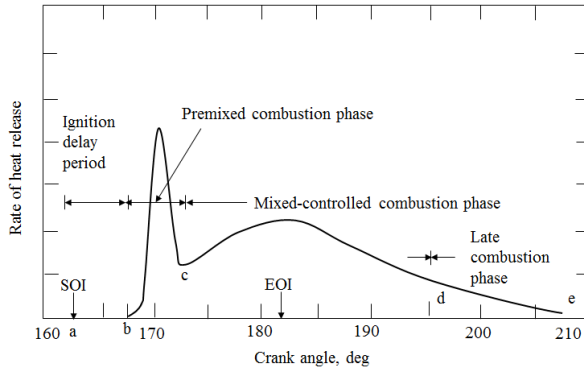
Source: adapted from Heywood [38].

- Ignition delay period: the period between the start of injection and ignition (the start of positive heat release due to combustion [45]).

- Premixed combustion phase: during this short period, the combustion of the fuel, which has mixed previously (during the ignition delay period), with air occurs. This premixed combustion leads to a rapid initial release of energy that increases the temperature and pressure in the cylinder. This increase, in turn, results in reduction in ignition delay for the remainder of the injected fuel which is burned at a controlled rate by mixing between fuel and air (stability of the flame front) [48–50].

- Mixed controlled combustion phase: during this stage, once the fuel and air premixed during the ignition delay have been consumed, the heat release is limited by the rate that the mixture becomes available for burning. The heat release rate may or may not reach a second (usually lower) peak in this phase [45].

- Late combustion phase: Heat release continues at a lower rate into the expansion stroke. A small fraction of unburned fuel (present

in the soot or in fuel rich combustion products) could remain from
the combustion during this phase.

In order to evaluate the heat release, Watson, Pilley and Mar-
zouk (1980 apud Oliveira [46], 2014) proposed that the fuel burning
rate could be expressed as the sum of two components. Each function
is set to reproduce each combustion stage: the premixed combustion
phase and the combustion phase controlled by mass diffusion.

Taking this into account, the contribution due to combustion in
gas energy conversion is given by [42]:

$$\dot{S}_{r,F} = \dot{M}_{r,F}\Delta h_{r,F}, \tag{3.26}$$

where $\dot{M}_{r,F}$ is the combustion rate of the fuel and is given by

$$\dot{M}_{r,F} = M_{F,o}\frac{f_{r,F}}{\Delta t_{r,F}}. \tag{3.27}$$

The time interval during combustion $(\Delta t_{r,F})$ is given by:

$$\Delta t_{r,F} = \Delta\theta_{r,F}\frac{60}{N\ 360}, \tag{3.28}$$

where $\Delta\theta_{r,F} = 125$ ° is the number of crank angles for combustion.

Then, $f_{r,F}$ is the factor that represents the beginning and ending
of fuel combustion. It is equal to a nonzero number during combustion
and zero in the other periods, as described by Heywood; Oliveira [38,46]

$$f_{rF} = \begin{cases} 0 & \text{if } \theta < \theta_{ig}, \\ \beta f_p + (1+\beta)f_d & \text{if } \theta_{ig} \le \theta \le \theta_{ig} + \Delta\theta_{Fr}, \\ 0 & \text{if } \theta > \theta_{ig} + \Delta\theta_{Fr}, \end{cases} \tag{3.29}$$

The fraction of the fuel β which burns in the premixed phase has
been correlated by Watson, Pilley and Marzouk (1980 apud Heywood
[38], 1988) by the relation:

$$\beta = 1 - \frac{a\phi^b}{\tau_{id}^c}, \tag{3.30}$$

where ϕ is the fuel/air equivalence ratio, τ_{id} the ignition delay
(in milliseconds) and $a = 0.9$, $b = 0.3$, and $c = 0.9$ are constants
depending on engine design — diesel engine, supercharged with single

direct injection.

The factor that accounts for the premixed combustion phase is described by [38] and is given by:

$$f_p = C_{p,1}C_{p,2}t_p^{C_{p,1}-1}(1-t_p^{C_{p,1}})^{C_{p,2}-1}, \qquad (3.31)$$

where t_p is the time from ignition non-dimensionalized by total time allowed for combustion [$= (t-t_{ig})/\Delta t_{comb}$] [38]. In addition, the factor that accounts for the phase of combustion controlled by diffusion of mass is described by Heywood [38] and is given by:

$$f_d = C_{d,1}C_{d,2}t_p^{C_{d,2}-1}exp(-C_{d,1}t_p^{C_{d,2}}), \qquad (3.32)$$

The other constants are very specific to the type of engine and fuel. Watson, Pilley and Marzouk (1980 apud Heywood [38], 1988) suggested the following correlations for diesel oil, supercharged with single direct injection:

$$C_{p,1} = 2 + 1.25 \cdot 10^{-8}(\tau_{id} \ N)^{2,4}, \qquad (3.33)$$

$$C_{p,2} = 5000, \qquad (3.34)$$

$$C_{d,1} = 14, 2/\phi^{0,664}, \qquad (3.35)$$

$$C_{d,2} = 0, 79C_{d,1}^{0,25}. \qquad (3.36)$$

Further, detailed information regarding the combustion and fuel burning rate can be found in [38, 39, 45, 46, 48–50, 52, 53].

3.2.10 Volume Radiation

In the energy conversion in the gas, Equation 3.11, the volumetric radiation encompasses the emission and absorption radiation between the gas and the cylinder head, the cylinder block, and the piston. This section attempts to model the volumetric emission and absorption between the gas and cylinder head. A similar analysis can be done for the cylinder block and the piston.

In the diesel engine, the primary sources of heat transfer within the cylinder are the high temperature burned gases and the soot particles, formed at an intermediate step in the combustion process, in the flame.

In the compression-ignition engines, most of the fuel burns in a turbulent diffusion flame as fuel and air mix together [38]. However,

82

since the particle size distribution, density, temperature, and flame geometry are not well defined, experiments are needed to determine the flame emissivity.

Flynn et al. (1972 apud Assanis et al. [45], 1985) measured the instantaneous radiant heat transfer in a direct-injection diesel engine under a wide range of engine operating conditions and obtained an apparent radiant temperature $(T_{r,f})$, an apparent gray-body emissivity, and a total radiant heat transfer rate at each crank angle during the cycle. Their results indicated that during the time of peak heat release, the apparent radiant temperature was close to the flame temperature. Furthermore, during the period of maximum radiation, the apparent emissivity was 0.8 to 0.9, and it dropped almost linearly to zero by the end of the combustion process [45].

Therefore, the volumetric emission and absorption of radiation for the cylinder head is Park and Kaviany [42]:

$$\dot{S}_{ch} = +\epsilon_{r,f}\alpha_{r,ch}\sigma_{sb}T_{r,f}^4 A_{r,ch} - \epsilon_{r,ch}\alpha_{r,f}\sigma_{sb}T_{ch_o}^4 A_{r,ch}, \qquad (3.37)$$

where, $\epsilon_{r,f}$ and $\alpha_{r,f}$ are the gas emissivity and absorptivity; $\epsilon_{r,ch}$ and $\alpha_{r,ch}$ are the cylinder head surface emissivity and absorptivity respectively.

Furthermore, the energy conversion due to radiation absorption and emission can also be found through energy conservation equation for the cylinder head:

$$\dot{S}_{ch} = \dot{Q}_{A,ch_o}, \qquad (3.38)$$

where $\dot{Q}_{A,ch_o}$ is the net heat transfer from the cylinder head, which will be explained in the following sections.

3.2.11 Surfaces

In this section, the energy conservation equation applied to the cylinder head surface will be used in order to assess the net heat transfer from the cylinder head surface. As mentioned before, in Equation 3.38, from the net heat transfer is possible to obtain the energy conversion due to radiation absorption and emission. Therefore, by evaluating the heat transfer in the cylinder head surface, we clarify one more term $(\dot{S}_{ch})$ in the energy conversion equation for the flue gas (Equation 3.11). Furthermore, similar analysis could be performed for the cylinder block $(\dot{S}_{cb})$ and piston surfaces $(\dot{S}_p)$.

As previously stated,

$$\dot{S}_{ch} = \dot{Q}_{A,ch_o}. \tag{3.39}$$

The net heat transfer in the cylinder head surface is given by [8]:

$$\dot{Q}_{A,ch_o} = -\dot{Q}_{ku,ch\,Db} + \dot{Q}_{r,ch-cb} + \dot{Q}_{r,ch-p} + \dot{Q}_{k,ch_{o1}}. \tag{3.40}$$

The surface convection heat transfer between the flue gas and the cylinder head surface $\dot{Q}_{ku,ch\,Db}$ was previously discussed in Section 3.2.6.

Then, $\dot{Q}_{r,ch-cb}$ represents the heat transfer by surface radiation between the cylinder head and the cylinder block and is given by:

$$\dot{Q}_{r,ch-cb} = \sigma_{sb} \frac{T_{ch_o}^4 - T_{cb_o}^4}{R_{r_{\Sigma,ch-cb}}}, \tag{3.41}$$

where the overall surface-radiation resistance $(R_{r_{\Sigma,chcb}})$ is modeled by Heywood; Kaviany [8, 38] considering the cylinder head and block and piston as a three-surface enclosure. In addition, they have also considered the surfaces opaque, diffuse, and gray. The heat transfer by surface radiation between the cylinder head and the piston $(\dot{Q}_{r,ch-p})$ follows similar procedure.

Finally, the last term in Equation 3.40, the heat transfer by conduction from the cylinder head surface to the interior of the cylinder head is:

$$\dot{Q}_{k,ch_{o1}} = \frac{T_{ch_0} - T_{ch_1}}{R_{k,ch_{o1}}}, \tag{3.42}$$

where T_{ch_1} stands for the temperature of the first node into the cylinder's head interior and $R_{k,ch_{o1}}$ the conduction resistance between the cylinder head surface and the interior of the cylinder head.

Nevertheless, it is necessary to determine the temperature of the first node T_{ch_1} to compute the heat transfer through conduction in the surface. Therefore, it is necessary to evaluate the heat transfer within the cylinder head to determine the temperature T_{ch_1}.

3.2.12 Wall Conduction Model

This section attempts to evaluate the heat transfer within the cylinder head. The temperatures within the wall are determined through a heat balance between the heat transfer rate through conduction from

cylinder head surface and heat transfer to the coolant water. Since the heat transfer rate from the gas to the cylinder head surface is a harmonic function of time, with a period of one engine cycle, this time-boundary condition sets up temperature waves that propagates into the wall structure.

In order to assess the variation of temperature in the cylinder head during cyclic transients, the cylinder head, with skin depth (l_{ch}) was divided into four volumes with uniform thickness Δl_{ch_i} and a large one with thickness $\Delta l_{ch_{Nch}}$. The energy equation for an arbitrary volume i is:

$$\frac{dT_{ch_i}}{dt} = \frac{\dot{Q}_{A,ch_i}}{-\rho_{ch}\Delta l_{ch_i}c_{p,ch}}. \tag{3.43}$$

The net transfer is

$$\dot{Q}_{A,ch_i} = -\frac{T_{ch_{i-1}} - T_{ch_i}}{R_{k,ch_{i-1,i}}} + \frac{T_{ch_i} - T_{ch_{i+1}}}{R_{k,ch_{i,i+1}}}. \tag{3.44}$$

For the first small volume, $i = 1$:

$$\dot{Q}_{A,ch_1} = -\dot{Q}_{k,ch_{o1}} + \dot{Q}_{k,ch_{12}}, \tag{3.45}$$

where $\dot{Q}_{k,ch_{12}}$ is the heat transfer by conduction from the cylinder head first node to the second,

$$\dot{Q}_{k,ch_{12}} = \frac{T_{ch_1} - T_{ch_2}}{R_{k,ch_{1,2}}}. \tag{3.46}$$

For the last large volume, $N_{ch} = 5$:

$$\dot{Q}_{A,ch_{Nch}} = -\dot{Q}_{k,ch_{Nch-1,Nch}} + \dot{Q}_{k,ch-w}, \tag{3.47}$$

where

$$\dot{Q}_{k,ch-w} = \frac{T_{ch,Nch} - T_{fw}}{R_{k_{\Sigma,ch-w}}}, \tag{3.48}$$

and $R_{k_{\Sigma,ch-w}}$ is the thermal resistance between the final cylinder head node and the coolant water kept at temperature T_{fw} equal to 380 K. Further information to determine the conduction resistance are provided by Kaviany [8].

To determine this last heat transfer rate term $\dot{Q}_{k,ch-w}$, it is necessary to calculate the temperature $T_{ch,Nch}$ for the last arbitrary volume, that involves an iterative procedure which will be described later.

3.2.13 Single-Cylinder Model

The differential and algebraic equations above mentioned are solved separately for each cylinder of an internal combustion engine — a single cylinder model.

At steady-state operation, the performance of each cylinder is essentially the same [40]. By evaluating the mass and energy flows between individual components throughout the engine's operating cycle, the total system performance can be estimated. Therefore, it is possible to employ this model to examine steady-state engine operation at constant load and speed.

However, it is still necessary to model the interaction between the cylinders in the exhaust manifold. Then, the exhaust manifold will be treated as a global open system.

3.2.14 Numerical Solution

This section presents the concepts necessary to the numerical model adopted.

The code was written in Fortran language and the simulation was performed using Codeblocks (a free C, C++ and Fortran Integrated Development Environment, IDE).

In the model, the conservation equations, for an open thermodynamic system, are applied in the cylinder. In addition, individual sub-models (described on previously sections) are brought together, in the form of sub-routines, to structure a complete model. These sub-routines encompasses the mass flow rate through the valves, the average Nusselt number for flue gas, the apparent adiabatic temperature, etc.

The main program includes routines corresponding to the intake, compression, combustion and exhaust processes. The complete model results in a set of simultaneous first order differential equations. A flow scheme showing the complete model is shown in Figure 3.5.

In the model, the initial state of fluid in the cylinder is characterized by approximate estimates of property values. Therefore, in order to predict the fluid's initial state, more than one iteration is necessary. The engine operating cycle simulation should end with the system reaching a quasi-steady condition, in other words, the working fluid at the same state that it started.

The cylinder model is applied for each cylinder separately. Their exhaust gases mix in the exhaust manifold, as shown in the scheme pre-

Figure 3.5 – Single cylinder model scheme.
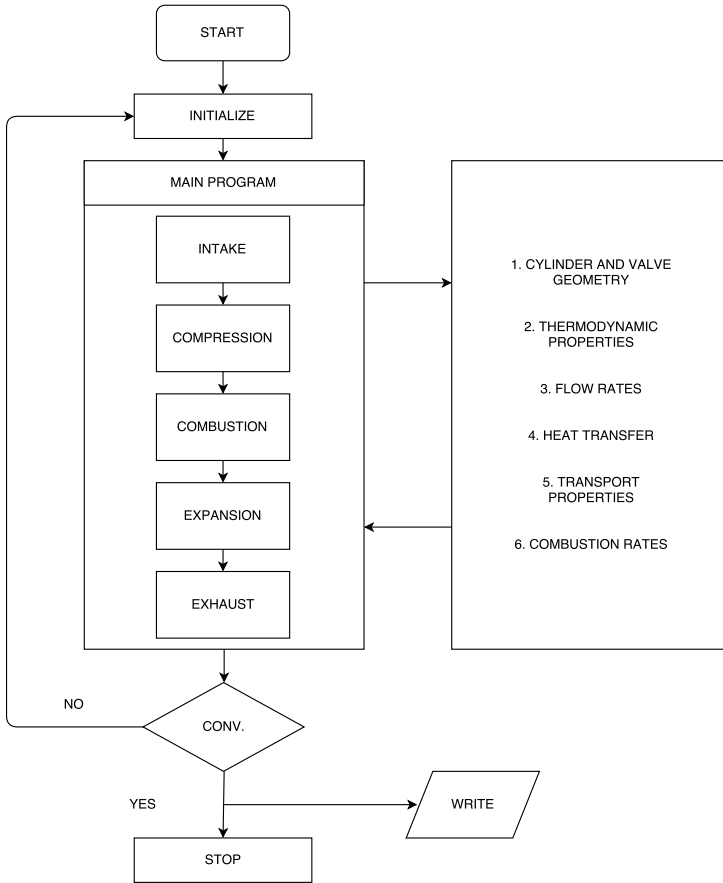
sented in figure 3.6. The exhaust manifold is treated as an open thermo-dynamic system. Thus, the conservation of mass and energy equations are applied in order to determine the exhaust manifold outputs. Since these outputs (mass flow and temperature) are time dependent, it is necessary to include the 120 ° ignition delay between each cylinder. For a typical case, the computation time in a Intel Pentium T4400 CPU is about 2 min for four crankshaft's rotations.

Figure 3.6 – Exhaust manifold model scheme.
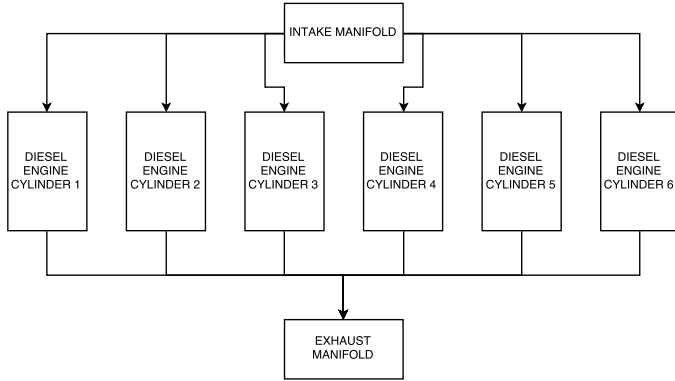
3.3 Results

This section presents the main results of the diesel engine's model developed. The single cylinder model results are compared with the literature in order to test the proposed model and to guarantee reasonable conditions for the exhaust manifold's flow properties. The exhaust manifold provides the flow necessary to heat the hot side of the thermoelectric generator.

For the single cylinder model, Figure 3.7 presents the indicated p-V diagram covering the complete engine cycle ($\theta = 0$ ° corresponds to the intake valve opening) obtained after the engine periodic steady-state regime is achieved. The net indicated work is given by the area inside the loop. The shape of this area is in agreement with the literature [42]. However, the power per cylinder per cycle, when compared to Park and Kaviany [42], was lower: 38 kW versus 41.5 kW. This difference may occur due to use of distinct constants in the Woschni correlation (Woschni [47], 1967 apud Heywood [38], 1988) to evaluate the average Nusselt number. Park and Kaviany [42] obtained the constants by the calibration of their simulation against previous measurements. On the contrary, this analysis employed the values suggested by Heywood [38].

In addition, Figure 3.8 shows the variations of the dimensionless cylinder-space volume, fluid pressure and temperature. The peak of pressure and temperature occurred immediately after $\theta = 360$ ° (during

Figure 3.7 – Predicted p-V diagram cycle.
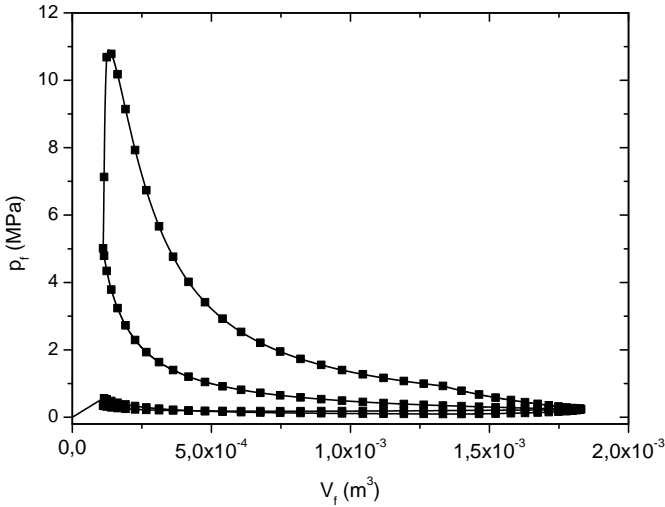
the pre-mixed flame regime in the combustion). Once more, the shape of the pressure and volume curves are consistent with previous studies [42, 43], as shown in figure 3.9.

The gases from the exhaust manifold provided the conditions necessary to maintain the TEG hot temperature. In this analysis, only the average exhaust manifold temperature and mass flow are required. The results for both quantities, for an engine in steady state operation, are shown in Figure 3.10. In addition, Figure 3.11 presents the enthalpy flow in the exhaust gas available for recovery, Q_h. Here, the hypothesis made to calculate the mass flow through the exhaust valve can be tested. There is a peak in the beginning of the exhaust process, which is a consequence of the high pressure within the combustion chamber. In order to verify the accuracy of these results, they were compared with Park and Kaviany [42]. Despite the difference in some of the constants, both presented two peaks in the exhaust mass flow. Furthermore, both maximum values, for a single cylinder, are close: 0.55 kg/s versus 0.4 kg/s (approximately) from [42]. Therefore, the model was considered acceptable and the results were employed in the thermoelectric generator analysis.

Figure 3.8 – Predicted dimensionless cylinder-space volume, fluid pressure and temperature for a cycle. (T_{max}= 2002 K, P_{max}= 11 MPa, V_{max}= 1830 cm^3)
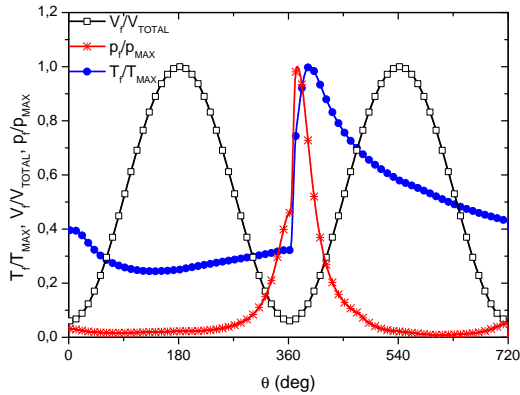
Figure 3.9 – Predicted dimensionless cylinder-space volume, fluid pressure and temperature for a cycle.
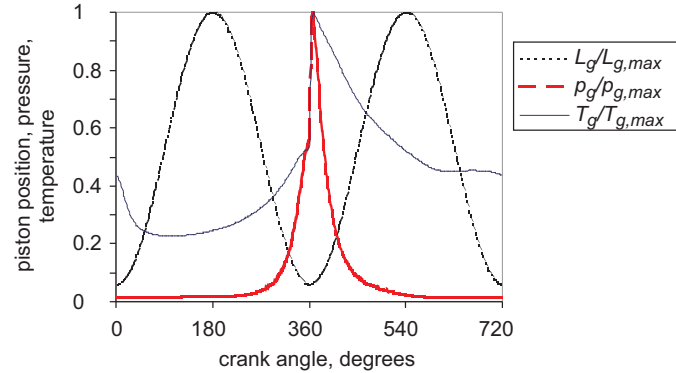
Source: Pereira and Oliveira [43].

Figure 3.10 – Exhaust manifold average temperature and mass flow.
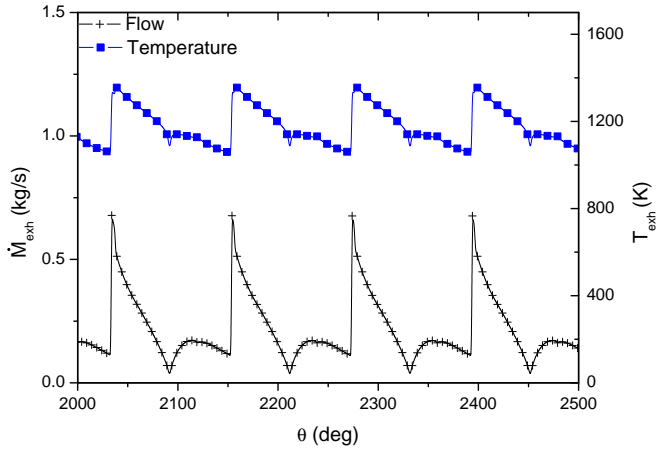
Figure 3.11 – Enthalpy flow lost through exhaust gas.
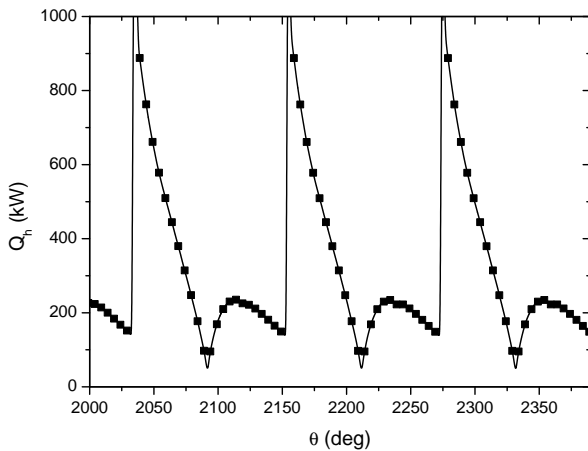
3.4 Summary

Modeling of the diesel engine provides a way of analyzing the coupling of TEG and engine. Different operation conditions can be analyzed and the effect of the transient can be assessed. From the results, we noted that the transient variation observed in the exhaust gas flow rate and energy have two basic time constants. The cycle variations have a time constant of the order of a fraction of the elapsed time for one revolution, roughly $\tau_c \approx 60/N$ (s). However, changes in engine operation parameter, such as, fuel injection and load, have a time constant of the order of several elapsed time of one revolution, depending on engine load during operation. The effects of these two time constants on the TEG performance will be evaluated next.

The diesel engine model employed was based on the mass and energy conservation equations for an open thermodynamic system. Additionally, the exhaust manifold model considered a superposition of single cylinder behavior; this imposed a limitation regarding the model's use: fixed load and steady state operation.

From the model, other outputs could be obtained: average flue gas velocity, heat transfer in the surfaces, conduction through the wall, etc. Therefore, the diesel engine model could be incorporated in other projects in the future.

The solution of the thermal model was validated by comparison with the literature. In summary, the model was considered adequate and therefore, able to characterize the hot fluid in the thermoelectric converter and to evaluate the TEG's performance.

4 THERMOELECTRIC GENERATOR

The thermoelectric system encompasses two subsystems: a heat exchanger, to provide a temperature difference in the thermoelectric junctions; and a thermoelectric generator, to convert this temperature gradient into electric potential difference. This chapter aims to present the design methodology for this arrangement and to assess their integration with the diesel engine.

This chapter is organized according to the following structure. First, the basic methodology for heat exchanger and thermoelectric generator design will be presented. From this, a simple configuration will be obtained.

Thereafter, the results will be discussed and in order to validate the analysis carried out, this chapter will present a comparison with other models described in the literature.

Furthermore, this chapter will provide guidelines for the system's optimization design. Then, a optimized arrangement will be presented. The procedure will evaluate different design decisions, like the choice of the thermoelectric junctions material, the heat exchanger cold fluid, and the TEG position. The material for thermoelectric cells encompasses relevant characteristics in thermoelectric generators, such as, high operating temperature, large conversion of heat into electric power, low thermal conductivity, and low electrical resistivity. The cold fluid must guarantee a high heat transfer rate, so that the generator presents a high temperature gradient, which would increase the power generated. Furthermore, the TEG position along the exhaust pipe influences the energy recovered and the equipment operating temperature.

An optimization analysis will be conducted in order to obtain the hot-side surface of the heat exchanger based on the pressure loss, minimum thermoelectric conversion efficiency, and minimum output power.

Finally, it will be investigated opportunities to increase the energy recovery during the thermoelectric generator transient period.

4.1 Methods

4.1.1 Heat Exchanger

A heat exchanger is designed to transfer thermal energy from a hot to a cold fluid. However, in the configuration of a TEG, the heat exchanger is used to provide a temperature difference in the thermocouples, since working under a higher temperature gradient would increase Carnot efficiency of the generator and the power output (as described on Section 2.2.1).

In this section, the basic design methods are reviewed. Although a complete heat exchanger design would require manufacturing and economical aspects also, for thermal analysis, the two most common procedures for heat exchanger designs are rating and sizing. The rating problem concerns the determination of the heat transfer rate, pressure losses, and outlet temperatures when the heat exchanger is available. On the other hand, the sizing problem concerns the determination of the heat transfer surface area, i.e., select the dimensions of a heat exchanger in order to meet previously defined temperature, flow rates and pressure losses requirements. In this study, the rating strategy is employed initially, since it is suggested a heat exchanger configuration, which coupled to a TEG provides the heat transfer rates and outlet temperatures. However, the maximum allowed pressure loss is an initial parameter, as well as, the flow of hot gases. Therefore, in this study the two analyzes are used, in order to optimize the suggested settings.

In order to perform the analysis, it is required to estimate the thermal resistance between the fluids. Furthermore it will be discussed the effect of this resistance on the overall heat transfer coefficient.

4.1.1.1 Overall Heat Exchanger Characteristics and Basic Assumptions

Initially, the simplest configuration for the heat exchanger was considered for the base design: a concentric tube heat exchanger with thermoelectric modules installed on its walls. The heat exchanger operated in a parallel-flow arrangement and was composed by modules organized in parallel, as shown in Figure 4.1.

The initial design assigned that the heat exchanger is formed by 25 tubes made of stainless steel AISI 304. The thermoelectric junctions are made of $Si_{0.3}Ge_{0.7}$ alloy. The entire set weights 7.3 kg (estimated

without considering the weight of the power electronics) and operated using water as cold and the exhaust gas as hot fluid. The electrical power conditioning unit is not modeled. Table 4.1 presents HE/TEG geometric and operation data.
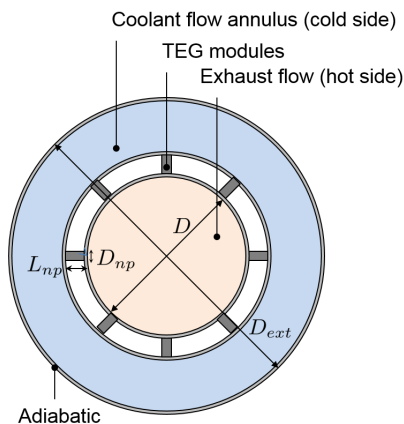
Figure 4.1 – A schematic of a module of the concentric tube heat exchanger with the thermoelectric junctions coupled.

In order to derive a mathematical model to describe the heat exchanger, in this study, it was assumed:

1. Negligible heat loss to the module surroundings;

2. Negligible kinetic and potential energy changes;

3. Negligible fouling factors;

4. Pressure loss restriction in the hot stream pipes;

5. No phase change;

6. Fully developed conditions for cold fluid (water) and exhaust gas;

7. Constant specific heat of each fluid;

8. Even distribution of both fluids over both the local and the total transfer area.

Table 4.1 – Overall geometric and operating characteristics of the heat exchanger and thermoelectric generator modeled.

Parameter, unit	Symbol	Magnitude
Number of tubes	N	25
Thickness of tubes, m	e	0.001
Tube length, m	L	0.1
Inner Diameter, m	D	0.05
Outer Diameter, m	D_{out}	0.1
Cold fluid mass flow rate, kg/s	$\dot{M}_c$	0.37
Cold fluid initial temperature, K	T_{c1}	351
Average hot fluid mass flow rate, kg/s	$\dot{M}_{exh}$	0.22
Average hot fluid initial temperature, K	T_{h1}	1118
Number of TE junctions per tube	N_{TE}	24
Conductor length, m	L_{np}	0.06
Conductor diameter, m	D_{np}	0.03

4.1.1.2 Heat Transfer Rates

The inlet of the hot side heat exchanger $(\dot{E}_{h,i})$ is connected to the engine exhaust flow $(Q_{u,exh})$. The difference between the inlet and outlet $(\dot{E}_{h,o})$ of the hot side gives the heat transfer rate in the hot fluid calculated as follows:

$$\Delta \dot{E}_h = \dot{E}_{h,i} - \dot{E}_{h,o} = (\dot{M}c_p)_{exh}(T_{h1} - T_{h2}), \tag{4.1}$$

which is the heat transfer rate from the exhaust gas to the thermoelectric generator:

$$\Delta \dot{E}_h = \dot{Q}_{h,w}. \tag{4.2}$$

Similarly for the cold side,

$$\Delta \dot{E}_c = \dot{E}_{c,o} - \dot{E}_{c,i} = (\dot{M}c_p)_c(T_{c2} - T_{c1}), \tag{4.3}$$

which is the heat transfer rate from the water to the thermoelectric generator:

$$\Delta \dot{E}_c = \dot{Q}_{c,w}. \tag{4.4}$$

The absorbed heat at hot wall $Q_{h,w,i}$ can be also addressed by

Wang, Wang and Dai [34]:

$$Q_{h,w,i} = (\bar{h}A)_{exh,i} \left(\frac{T_{h,i+1} + T_{hi}}{2} - T_{h,w,i} \right).$$ (4.5)

Similarly, for the released heat:

$$Q_{c,w,i} = (\bar{h}A)_{c,i} \left(T_{c,w,i} - \frac{T_{c,i+1} - T_{c,i}}{2} \right),$$ (4.6)

where $\bar{h}$ is the average heat transfer coefficient, which be correlated with the fluid thermal conductivity k and with the average Nusselt number based on the hydraulic diameter:

$$\langle Nu \rangle_{D_h} = \frac{\bar{h} D_h}{k}.$$ (4.7)

Calculating the average Nusselt number requires different correlations for exhaust and for water streams. In this scenario, the heat transfer between the module surfaces and the streams can be modeled as a problem of internal forced convection, which is widely discussed in the literature [55–59]. Correlations for tube with circular cross-sectional area are applied to estimate the heat transfer rates between the exhaust gas and the inner module surface; correlations for annular ducts are applied to water and outer surface.

Calculating the average Nusselt number requires different correlations for exhaust and water streams. For the exhaust flow, the Reynolds number Re_{D_h} is near 8000 and Prandtl number Pr is around 0.7. Therefore, considering fully developed turbulent flow conditions, the Nusselt number is provided by Gnielinski (1976 apud Nellis and Klein [59], 2009) correlation:

$$\langle Nu \rangle_{D_h} = \frac{\left(\frac{f_{fd}}{8} \right) (Re_{D_h} - 1000) \, Pr}{1 + 12.7 \left(Pr^{2/3} - 1 \right) \sqrt{\frac{f_{fd}}{8}}}.$$ (4.8)

The expression suggests that the Nusselt number is also sensitive to variations on the friction factor f_{fd}. For fully developed turbulent flow conditions, Zigrang and Sylvester (1982 apud Nellis and Klein [59], 2009) present an explicit correlation for the friction factor in a rough

duct:

$$f_{fd} = \left\{ -2.0 \, log_{10} \left[\frac{2e}{7.54 D_h} - \frac{5.02}{Re_{D_h}} log_{10} \left(\frac{2e}{7.54 D_h} + \frac{13}{Re_{D_h}} \right) \right] \right\}^{-2},$$
(4.9)

where e is the surface roughness, in this case, stainless steel AISI 304.

Furthermore, for the cold stream, the Reynolds number is near 300. Therefore, laminar forced convection regime was assumed. Rohsenow et al. (1998 apud Nellis and Klein [59], 2009) provide an expression for the Nusselt number for an annular duct with an adiabatic external surface and with an internal surface subjected to a constant temperature and a constant heat flux.

4.1.2 Thermoelectric Generator

In oder to predict the power output and the efficiency of a thermoelectric module, the arrangement composed of heat exchanger and thermoelectric generator is presented. This system, introduced in Figure 4.1, is divided into a series of finite volumes as shown in Figure 4.2. For each element, the electric circuit was presented in Figure 2.9 and the equivalent model of the thermal circuit engages the internal circuit of the TEG (presented in the Figure 2.8) and the circuit of the heat exchanger.

Figure 4.2 – A schematic of the thermoelectric junctions coupled to the concentric tube heat exchanger.
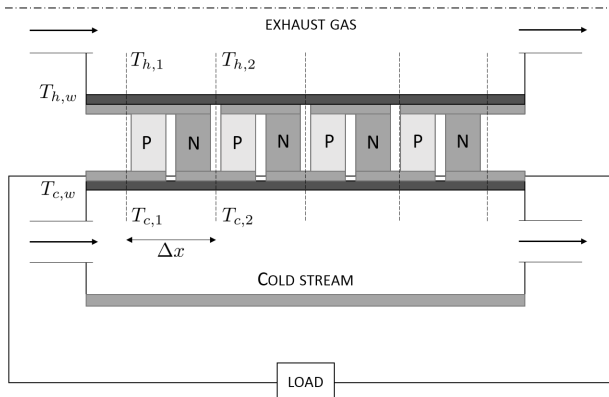
The absorbed and released heat expressions for the thermoelec-

tric generator were developed previously in Section 2.2.2 and Appendix A. Nevertheless, the first model disregarded the Thomson effect by assuming material properties constant over temperature (the Thomson effect arises only from the temperature-dependence of the Seebeck coefficient). However, in order to provide a more accurate model, this study contemplates the model presented by Angrist (1982 apud Sandoz-Rosado, Weinstein and Stevens [64], 2013), which stated the Seebeck coefficient as

$$\alpha_S = \frac{1}{T_{h,w} - T_{c,w}} \int_{T_{c,w}}^{T_{h,w}} \alpha_S(T) dT. \qquad (4.10)$$

By adopting this hypothesis, the model described in Section 2.2.2 incorporates the Thomson effect as demonstrated by Sandoz-Rosado, Weinstein and Stevens [64].

The temperature dependent thermoelectric material properties, i.e., the Seebeck coefficient, electrical resistivity, and thermal conductivity were considered. Properties measured by Tang et al.; Rowe; Heremans et al. [22, 25, 65] were curve fitted as a function of temperature. The curve fitted functions are presented in Appendix B.

In this analysis, the transient effect is considered. Therefore, the absorbed heat expression for a Δx element could be rewritten as:

$$\dot{Q}_{h,w,i} = \alpha_S J_e T_{h,w,i} + \frac{(T_{h,w,i} - T_{c,w,i})}{R_k} - \frac{J_e^2 R_e}{2} + \left(\rho c_p V \frac{dT}{dt} \right)_{h,w,i}. \qquad (4.11)$$

Similarly, for the released heat:

$$\dot{Q}_{c,w,i} = \alpha_S J_e T_{c,w,i} + \frac{(T_{h,w,i} - T_{c,w,i})}{R_k} + \frac{J_e^2 R_e}{2} - \left(\rho c_p V \frac{dT}{dt} \right)_{c,w,i}. \qquad (4.12)$$

In order to evaluate the heat transfer rates and outlet temperatures, it is necessary to determine the electric current. Equation 2.9 developed on Section 2.2.1 presents the electric current for a single thermocouple. For a series of thermocouples (thermoelectric module), the electric current is given by:

$$J_e = \frac{\alpha_S (T_{h,w,i} - T_{c,w,i})}{R_{e,o}/N_{TE} + R_e}, \qquad (4.13)$$

where N_{TE} is the number of thermocouples.

As a result, the overall power can be expressed as:

$$P = \sum_{1}^{N_{TE}} (Q_{h,w,i} - Q_{c,w,i}). \tag{4.14}$$

In summary, Figure 4.3 shows a simplified algorithm for thermodynamic modeling of the thermoelectric generator.

4.1.3 Performance Parameters

For the optimization of the heat exchanger (HE)/ thermoelectric generator (TEG) module, objective function and restriction must be stated. The performance parameters allow to quantify system performance.

4.1.3.1 Specific Power

A large power per unit of TEG area is desirable. In order to determine the maximum power per unit area, it is necessary to obtain the maximum power that the TEG is able to provide. The expression that defines the power through the load resistance is given by:

$$P = J_e^2 R_{e,o}. \tag{4.15}$$

By taking the derivation of the power with respect to the load resistance and setting equal to zero, it can be shown[1] that for optimum power output, the load resistance should be equal to the electrical resistance [8]. As follows, the maximum power is given by:

$$P = \frac{(\Delta\varphi)^2}{4R_{e,o}}, \tag{4.16}$$

where $\Delta\varphi$ is the electric potential, given by:

$$\Delta\varphi = \alpha_S(T_{h,w} - T_{c,w}). \tag{4.17}$$

---

[1]The mathematical proof can be found in Rowe [22].

Figure 4.3 – Simplified algorithm for thermodynamic modeling of the thermoelectric generator.
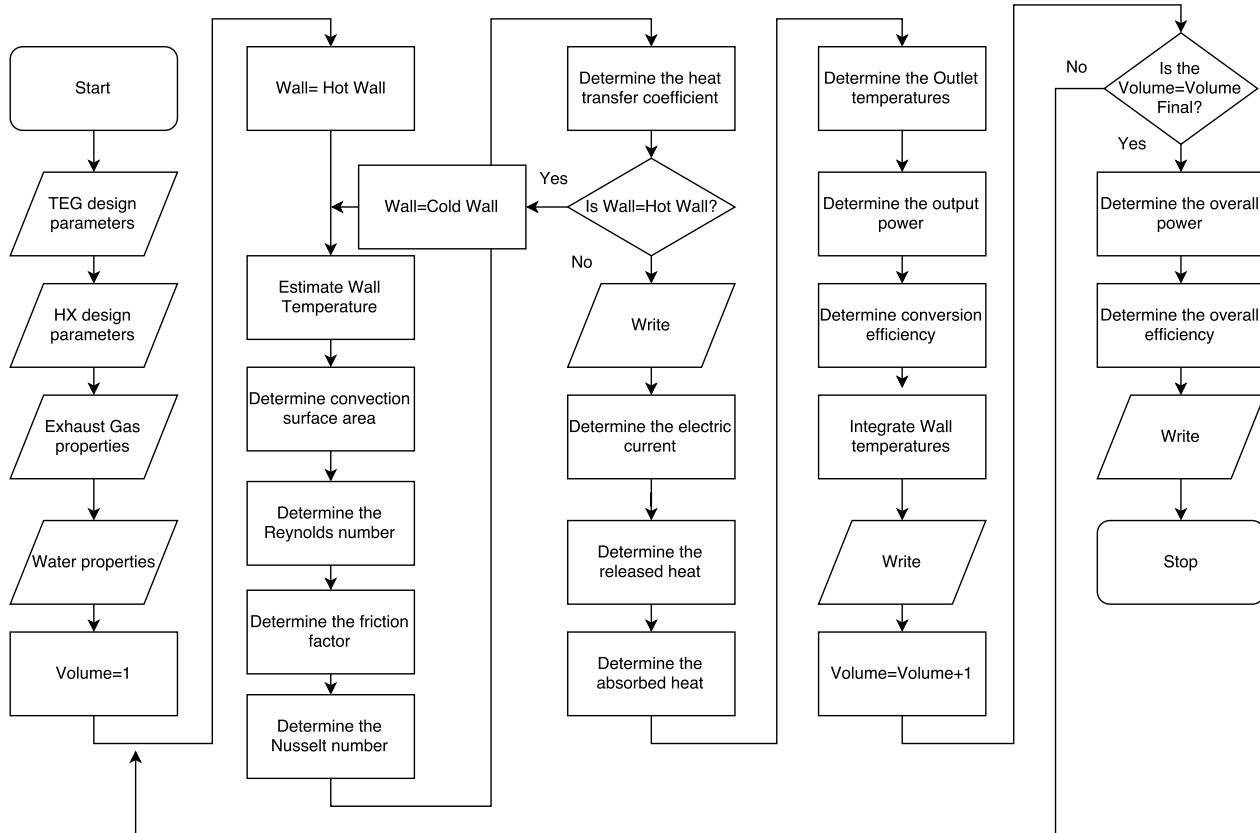
Then, the power per unit of TEG area is defined:

$$\Psi = \frac{P}{A_p + A_n}. \tag{4.18}$$

As demonstrated by Rowe [22], the optimum power per unit area Ψ is given by:

$$\Psi = \frac{(\Delta\varphi)^2}{4l \left[(\rho_n)^{1/2} + (\rho_p)^{1/2}\right]^2}, \tag{4.19}$$

where l is the length of the conductor, ρ_n and ρ_p are the electrical resistivity of the n and p junction.

4.1.3.2 Thermoelectric Efficiency

The thermoelectric conversion efficiency is provided by the ratio of the generated power output and the absorbed heat from the hot side of the heat exchanger:

$$\eta_{TE} = \frac{P}{\sum_1^{N_{TE}} \dot{Q}_{h,w,i}}. \tag{4.20}$$

As a design constraint, a minimum thermoelectric conversion efficiency η_{TE} of 2 % was adopted here. This is based on the TEG state-of-the-art improvements that have been achieved for high power generation, as shown in Table 2.1.

4.1.3.3 Effectiveness

During design of a TEG system, one possible objective might be to maximize the power output that could be generated by the HE/TEG system. As a design constraint, a minimum power of 800 W was considered here. This limit is based on the high power generation for thermoelectric applications, as described in Table 2.1.

Since the thermoelectric conversion efficiency is given by:

$$\eta_{TE} = \frac{P}{\dot{Q}_{h,w}}, \tag{4.21}$$

By setting a minimum thermoelectric efficiency and output power, the minimum absorbed heat from the hot side of the heat exchanger is

achieved.

In respect to the maximum heat transfer rate that could be exchanged from the hot to the cold stream in the hot heat exchanger, the design constrain is defined in terms of effectiveness ε:

$$\varepsilon = \frac{\dot{Q}_{h,w}}{\dot{Q}_{max}}, \tag{4.22}$$

where $\dot{Q}_{max} = \dot{C}_{min}(T_{h,i} - T_{c,i})$ is the maximum heat transfer rate that could be exchanged between fixed $T_{h,i}$ and $T_{c,i}$ and, $\dot{C}_{min} = (\dot{M}c_p)_{min}$.

Therefore, for $T_{h,i}$ and $T_{c,i}$ shown in Table 4.1, minimum output power of 800 W and thermoelectric conversion efficiency of 2 %, the minimum heat exchanger effectiveness is equal to 0.14.

The effectiveness is evaluated as function of the capacitance ratio, the number of transfer units, and the flow arrangement,

$$\varepsilon = \varepsilon(\dot{C}_R, NTU, \text{flow arrangement}), \tag{4.23}$$

where the capacitance ratio is given by:

$$\dot{C}_R = \frac{\dot{C}_{min}}{\dot{C}_{max}}, \tag{4.24}$$

and NTU is the number of transfer units. For a parallel flow regime, Nellis and Klein [59] provided an expression for effectiveness.

The number of transfer units represents the dimensionless size of the heat exchanger and is given by the ratio of heat exchanger conductance (UA) and the minimum capacitance ($\dot{C}_{min} = \dot{m}\,c_p$):

$$NTU = \frac{UA}{\dot{C}_{min}}. \tag{4.25}$$

The heat exchanger conductance UA gives an estimate of the HE area. This parameter provides a characteristic heat exchanger size parameter, useful for comparing different solutions. A small area is desired, since it does not greatly affect the pressure loss. An overall characteristic thermal conductance is determined via a thermal resistance network representing the heat exchanger module, shown in Figure 4.1. The inverse of total thermal resistance (R_t) provides the heat

exchanger conductance (UA) and is given by:

$$R_t = \frac{1}{UA} = R_{ku,c} + R_{TEG} + R_{ku,exh},$$ (4.26)

where $R_{ku,c}$ is the convection resistance between the water and the outer module surface, $R_{ku,exh}$ is the convection resistance between the exhaust gas and the inner module surface, and R_{TEG} to conduction through the module, which encompasses the resistance to conduction through the tubes thickness and through the thermocouples.

The convection resistance between the module surfaces and the stream is given by:

$$R_{ku} = \frac{1}{\bar{h}A},$$ (4.27)

where $\bar{h}$ is the average heat transfer coefficient, defined previously.

The conduction resistance, through the module is approximated as the thermal resistance to radial conduction through a cylinder, given by [59]:

$$R_{TEG} = \frac{ln\left(\frac{D}{D_{out}}\right)}{2k_s \pi L},$$ (4.28)

where k_s is the conductivity on the HE/TEG module, defined as the weighted arithmetic mean of the conductivity of the stainless steel (used in the HE) and the silicon germanium alloy (used in the TEG).

4.1.3.4 Pressure Loss

The pressure loss (or, head loss) analysis aims at optimizing the heat exchanger design based on the hydraulic diameter for the hot stream pipe and the number of modules. As a design constraint, a maximum allowable pressure loss of 2 % of the ambient pressure (abs.) was selected. This limit is based on engine operation constraints used in the design of muffler system [66, 67] and on the fuel increase consumption due to the increase on the backpressure [68]. The analysis followed the procedure described by Fox and McDonald [69] in which the Colebrook (1939 apud Fox and McDonald [69], 1985) correlation for the friction factor is employed:

$$\frac{1}{f_{fd}^{0.5}} = -2.0 log \left[log \left(\frac{e/D}{3.7} + \frac{5.74}{Re^{0.9}} \right) \right]^{-2}.$$ (4.29)

In order to determine the design constraints due the head loss, the most critical condition is tested, which occurs at the highest ratio of fluid gas mass flow to density.

4.1.4 Optimization

The optimization procedure aimed at obtaining the hot-side surface area of the heat exchanger. Here we consider that the upper limit of the HE area is obtained when the maximum pressure loss (2 % of the ambient pressure) is reached, and the lower limit is given by the minimum area required to reach 0.14 heat exchanger effectiveness.

The first parameter optimization performed achieved maximum hot-side HE surface area based on the pressure loss criteria. We used two methods. For both methods, the HE/TEG model was solved in the EES software using the effectiveness-NTU method. Furthermore, we assumed averaged exhaust and cold flow properties, and constant wall temperatures ($T_{h,w} = 808$ K and $T_{c,w} = 367$ K).

The first method considered only a single tube and implemented the method of quadratic approximations in EES software to find the tube diameter and length required to meet the pressure loss with maximum hot-side HE surface area. The first method left the HE tube length as the independent variable, which ranged from 1 mm to 1 m, and the tube diameter was the value required to keep the pressure loss at 2 % for each length.

The second method included the number of tubes as independent variable and implemented a genetic algorithm routine in EES software to find the number of tubes, their length and diameter to achieve the maximum hot-side HE surface area. The second method left the HE tube length, which ranged from 1 mm to 0.5 m, and the number of tubes, which ranged from 1 to 25, as independent variables. The genetic algorithm routine derived from the public domain Pikaia optimization program. More information concerning the two optimization methods can be found in Klein and Nellis [71].

The second parameter optimization performed achieved minimum hot-side HE surface area based on the minimum heat exchanger effectiveness and pressure loss criteria. Similarly to the first parameter optimization, the quadratic approximations and the genetic algorithms were employed to achieve an optimized arrangement that met these two criteria. Moreover, we used the same constant parameters. However, here, the first method left the HE tube diameter as independent

variable, which ranged from 1 mm to 0.1 m, while the length and the number of tubes were those required to meet the constraints. Analogously, in the second method both the tube diameter, which ranged from 1 mm to 0.1 m, and the number of tubes, which ranged from 1 to 9, 16, or 25, were used as independent variables.

4.2   Results

This section is divided in three analysis. First, the TEG input data and geometries described in this study are applied to other methods, available in the literature, as a way of assessing that there have been no gross mistakes in the model or programing. Subsequently, a thermoelectric generator is designed, the model is applied to this configuration and an optimized layout is presented. Lastly, the model is used to explore the transient phenomena and the energy gains during transient regime.

4.2.1 Testing of Model and Numerical Implementation

This section aims at testing the model, the solution algorithm, and the programing. The strategy used consists in programing several models available in the literature in the same routines developed here and comparing these results when applied to the data utilized in this study, shown in Table 4.1.

Figure 4.4 presents the generated power predicted from each model using the same mathematical routines. It can be noted that the results are consistent with previous studies. The difference between this model and those proposed in the literature are mostly due to the inclusion of temperature dependent properties and the transient considered in this study. The difference between each method is discussed below.

Karri, Thacher and Helenbrook [29] divided the system in a series of finite volume and considered a counterflow heat exchanger. Wang, Wang and Dai [34] also divided the system into a series of finite volume, although a parallel flow heat exchanger was considered. Rowe [22] presented a method whose input parameter was the temperature of the wall of the TEG, unlike the other methods which have the temperature of the streams as input parameter. The major difference between the models came from the one proposed by Hsu et al. [4, 28], which

Figure 4.4 – Predicted TEG power output from: this study;
Karri, Thacher and Helenbrook [29]; Wang, Wang and Dai [34];
Rowe [22]; Hsu et al. [4, 28]; Crane and Jackson [27]; Hendricks
and Lustbader [30, 31].
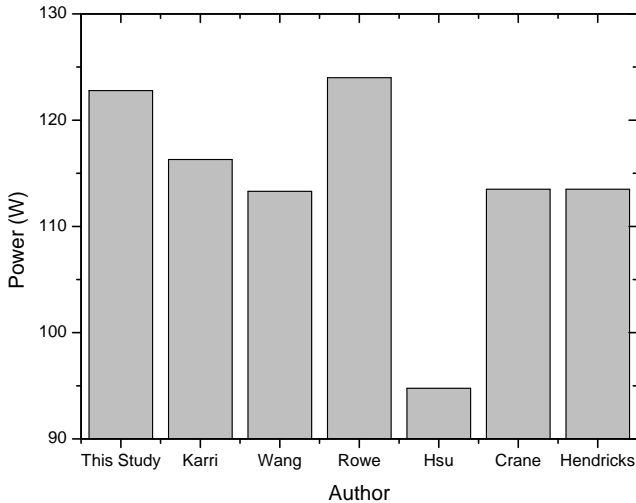
computed the contact resistance by an experimental approach. Lastly,
Crane and Jackson [27] and Hendricks and Lustbader [30, 31] showed
the same output; this similarity could be caused by the common source
used: Angrist [63].

Excluding the results obtained with the model by Hsu et al.
[4,28], despite the minor disagreements between the methodologies, the
results can be considered in agreement with the literature. Therefore,
the model can be employed in the thermoelectric generator optimiza-
tion analysis.

4.2.2 Design of Basic Configuration

The design of the thermoelectric generator involves simultaneous
design of the heat exchanger and the TEG, since the thermoelements
are embedded in the wall separating the hot and cold stream and there

is simultaneous heat absorption and release in this region.

In this study, four aspects regarding the TEG optimization are explored: (1) the thermoelements' material, (2) the cold fluid employed in the heat exchanger, (3) the effect of transient regime on the heat exchanger hot wall temperature, and (4) the maximum power per unit of TEG area.

4.2.2.1 Effect of Thermoelectric Material

The non-dimensional figure-of-merit (ZT) associates the material employed in the thermoelements to the thermoelectric generator's performance. Therefore, the focus of this analysis was to achieve the highest average ZT over the entire operating temperature range of the exhaust pipe. In addition, as mentioned in Section 2.2.4, there are ideal group alloys to convert heat into electricity in three specific temperature ranges: bismuth-telluride for $T < 770$ K, lead telluride for $T < 900$ K, and silicon-germanium alloys for $T < 1300$ K. These temperature ranges encompass the temperature variation found along the exhaust pipe, which could reach high temperatures (T>800 K).

The electric power provided by each material as a function of the hot side temperature is shown in Figure 4.5. The vertical dashed lines identify the maximum operating temperature for each material. Time-averaged characteristics for the exhaust flow were considered and water at T=351 K was selected as cold fluid. The results indicated that bismuth telluride would be the best choice for the low temperature range, while lead telluride would work best for the medium range. Although the lead telluride would be the best option for high temperature range also, the material deteriorates at T=900 K. Considering the entire temperature range encompassed by the TEG operation, since cold start up until steady-state operation at high load, the silicon-germanium alloy would be the best choice. Therefore, since power is influenced by the figure of merit (Z) and the temperature gradient, this choice of silicon-germanium alloy material is mainly due the temperature gradient and not due to the maximum figure of merit for that region. Still, by employing this composition, the thermoelectric generator would be able to provide 228 W at the maximum operating temperature.

Figure 4.5 – Predicted generated power as a function of hot wall heat exchanger's temperature for different thermoelectric materials using engine coolant as cold fluid. (T_c= 351 K)
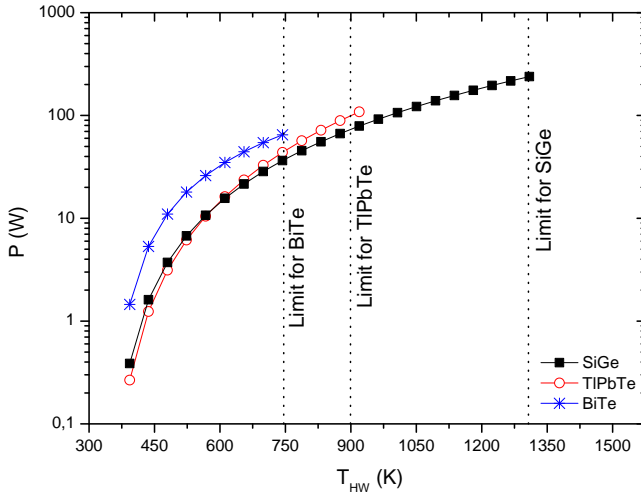
4.2.2.2 Effect of Choice of Cold Fluid

The cold side plays an important role in the design of a thermoelectric generator. The choice of cold fluid and material must guarantee a high rate of heat transfer. However when, compared to the hot side, the cold side presents less operation problems, since the operation at lower temperatures results in a reduced degradation of the material and ensures that a greater variety of materials can be employed. For example, cooling media based on water (e.g., cooling fluid) or ethylene glycol is mildly corrosive, has a sufficiently high boiling point, thermal conductivity, and heat capacity, and is usually compatible with appropriate heat transfer materials [18].

In this study, two choices of cold fluid were tested. The first arrangement used external air as the cold fluid and required a blower to blower the cooling air through the heat exchanger. The second arrangement used the diesel engine's cooling water as the cold fluid. It is also worth mentioning that Organic Rankine Cycle (ORC) systems

could be combined with a TEG to increase thermal energy recovery as presented in Section 1. However ORC fluids were not tested at this point.

The predicted power generation using air at 298 K as cold fluid is presented in Figure 4.6. At their highest operational temperatures, lead telluride provides 75 W, while silicon-germanium alloy provides 86 W. Compared with Figure 4.5, the arrangement operating with water as cold fluid is the best option. Although, the system with external air employed the cold fluid at lower temperature, 298 K versus 351 K, the higher specific heat capacity for water compensated the smaller temperature difference. In addition, due the air lower density, the fan would require extra power to operate and hence would reduce the overall fuel savings.

Figure 4.6 – Predicted generated power as a function of hot wall heat exchanger's temperature for different thermoelectric materials using external air (T_c= 298 K) or water (T_c= 351 K) as cold fluid.
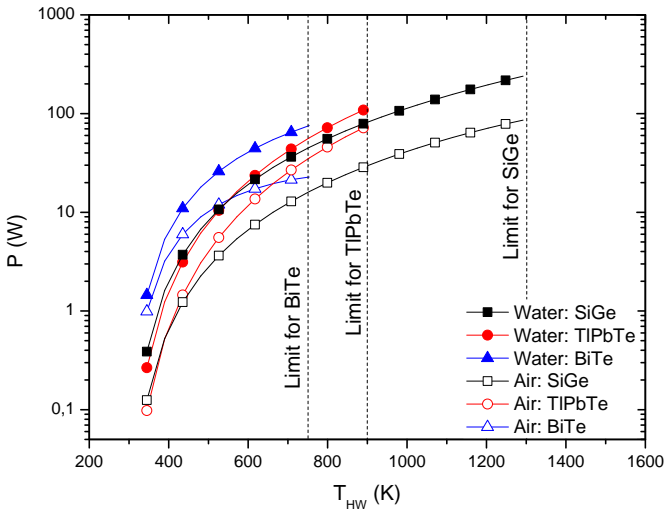

Table 4.2 summarizes the analysis performed at Sections 4.2.2.1 and 4.2.2.2. The table presents the predicted power generated at the maximum temperature for different thermoelectric materials operating

with water or air as cold fluid. From the table, it can be noted the most appropriate design choices are: silicon-germanium alloy as thermoelectric material and water as cold fluid.

Table 4.2 – Power generated at the maximum temperature for different thermoelectric materials operating with air and water.

Cold Fluid	Thermoelectric Material	Maximum temperature of operation, T_{max}	Power generated at T_{max}, W
Water at T_c=351 K	Bi_2Te_3	750	65
	TlPbTe	900	103
	SiGe	1300	228
Air at T_c=298 K	Bi_2Te_3	750	22
	TlPbTe	900	75
	SiGe	1300	85

Once the diesel engine's cooling water was selected as cold fluid, the pinch point analysis could be performed. The heat exchanger position where the temperature difference between the fluid streams is minimum is called pinch point. The objective of this analysis is to verify the change in water temperature as the load in the heat exchanger is increased. The results of the analysis can detect the possibility of phase change, which should be avoided. Figure 4.7 shows the temperatures of the two streams as a function of the duty (the rate of heat transfer between the streams, $\dot{q}_{CV}$). According to the figure, the temperature difference is greater than zero throughout the heat exchanger, so there is no second law violation due to the pinch point. Also the water temperature remains safely well below the boiling temperature.

4.2.2.3 Effect of Transient Hot Wall Temperature

Although the material analysis (performed at Section 4.2.2.1) indicated the silicon-germanium alloy at the maximum workable temperature as the most appropriate option, the position closest to the exhaust manifold may exceed the maximum temperature even for this alloy. This analysis aimed at verifying the compatibility of the SiGe alloy when the HE/TEG is close coupled to the engine, using the system described in Tables 3.1 and 4.1.

Figure 4.8 indicates TEG hot wall temperature when the generator is placed near the exhaust manifold. The maximum working

Figure 4.7 – Average temperature of the exhaust gas and temperature of the diesel engine's cooling water in the thermoelectric generator as a function of the duty.
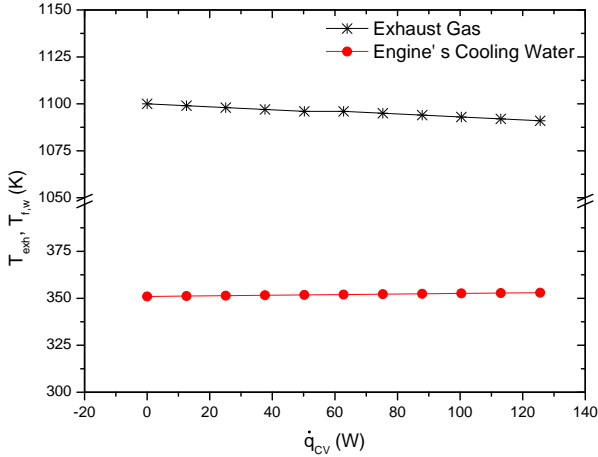
temperature is indicated as a dashed horizontal line. The TEG hot wall temperature is expressed as a function of the crank angle, which can be obtained by the product between engine speed in rpm and the elapsed time:

$$\frac{d\theta}{dt} = N \times \frac{360 \ (\text{degrees/rotation})}{60 \ \text{s/min}}, \tag{4.30}$$

where N is the angular crank shaft speed. In this analysis N=1600 rpm. Therefore,

$$\frac{d\theta}{dt} = 9600. \tag{4.31}$$

In order to achieve a faster convergence to steady state operation, the thermal mass of the TEG was divided by 9600, increasing its time response by the scaling factor of 9600. It can be noted that the silicon-germanium alloy can operate under the maximum allowable temperature. Furthermore, from the figure, the time averaged hot wall temperature is lower than the best arrangement exposed on the Section 4.2.2.1: 849 K versus 1300 K. Figure 4.9 presents the output power as a function of crank angle for the TEG near the exhaust manifold. The

results indicated that the predicted power oscillates around the time average of 144 W.

Figure 4.8 – Thermoelectric generator hot wall temperature as a function of crank angle close coupled to the exhaust manifold.
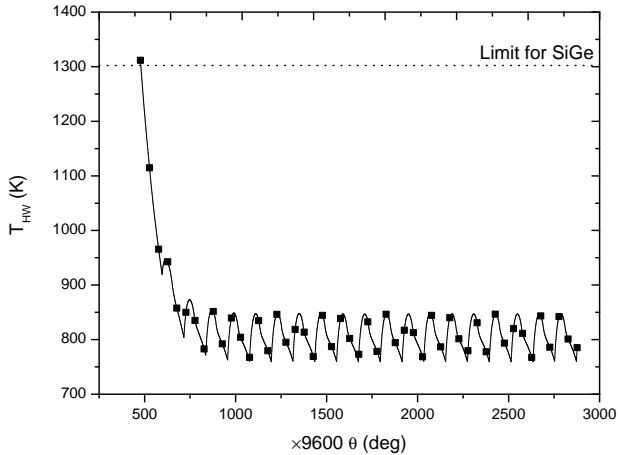
The predicted power fluctuates, since it includes changes in the temperature and in the flow of exhaust gases during the cycle (0-720), as shown in Figure 3.10. Even though the diesel engine is in steady state (periodic steady-state under constant load). Figure 4.9 also indicates that there is an opportunity to harvest a larger power during cold start-up, reaching values above 500 W.

4.2.2.4 Maximum Power Per Unit of TEG Area

Table 4.3 presents the optimum power per unit area supplied by the generator when it is coupled in different positions along the exhaust system. Figure 4.10 presents a typical temperature distribution of the exhaust gas system, which is composed of the exhaust manifold, exhaust pipe, catalytic converter, center muffler, and rear muffler. Moreover, Table 4.3 gives an estimate of what is the exchange area required for the power recovered at the position chosen.

Figure 4.9 – Predicted generated power as a function of crank angle close to the exhaust manifold.

P (W)

350
300
250
200
150
100
50

500   1000   1500   2000   2500

×9600 θ (deg)
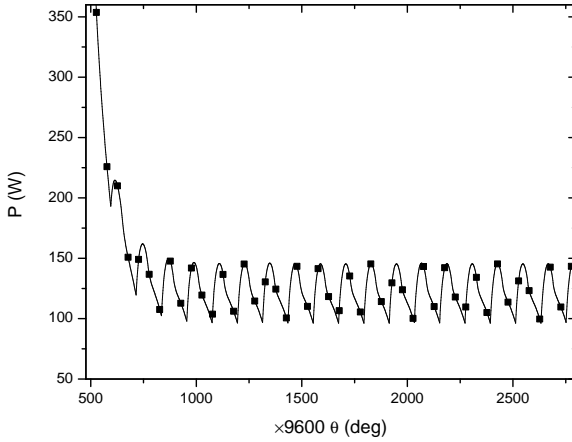
Figure 4.10 – Temperature distribution of exhaust gas.

Center Muffler 240
– 480 °C

Exhaust Manifold
550 – 790 °C

Catalytic Converter
320 – 560 °C

Rear Muffler
190 – 430 °C

Exhaust Pipe

Diesel
Engine

Heat
Exchanger

TEG
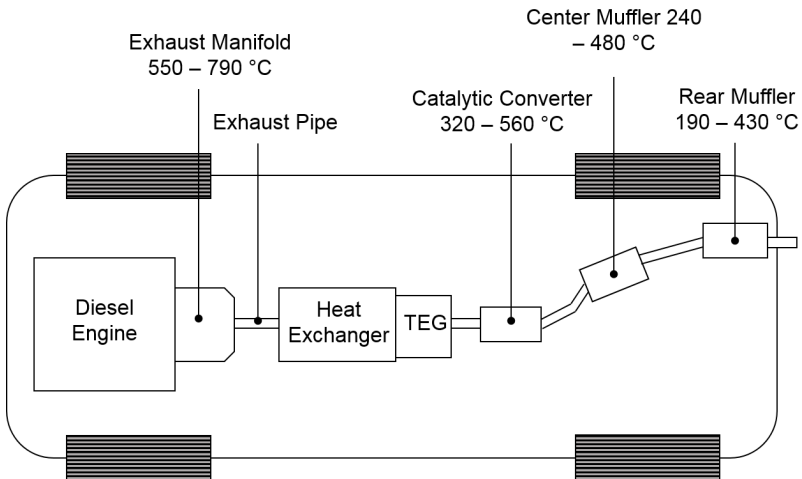
Source: adapted from Zhang, Chau and Chan [3].

Table 4.3 – Maximum power per unit area.

Hot Wall Temperature T_{exh}, K	Power per unit Area Ψ, W/m^2
1118	3639
1000	2748
900	1657
800	1086
650	461

4.2.3 Parameter Optimization

4.2.3.1 Maximum Heat Transfer Area Restricted by Pressure Loss

The pressure loss (or, head loss) analysis aims at optimizing the heat exchanger design based on the hydraulic diameter for the hot stream pipe and the number of modules. As a design constraint, a maximum allowable pressure loss of 2 % of the ambient pressure (abs.) was selected.

The analysis of the preliminary configuration, $D = 0.05$ m, $L = 0.1$ m and $N = 25$ tubes, showed that the restriction imposed by the pressure loss was satisfied. This results indicated that the diameter could be reduced or the length of the heat exchanger could be increased and the design criteria would still be met. Thus, it was possible to improve the exchanger design in order to increase the TEG efficiency.

Table 4.4 presents the results for each method. For a larger number of pipes the mass flow rate per pipe is smaller, as well as the pressure loss, since it always decreases with the flow rate. Therefore, by increasing the number of tubes, it is possible to reduce the tube diameter (obtaining a compact heat exchanger).

4.2.3.2 Minimum Heat Transfer Area Restricted by Thermoelectric Efficiency and Pressure Loss

The analysis evaluated the minimum hot-side surface area of the heat exchanger that would still meet the minimum heat exchanger effectiveness($\varepsilon = 0.14$), while keeping the pressure drop below 2 % of the ambient pressure. Table 4.5 presents the results for a single tube

Table 4.4 – Optimization keeping the overall pressure loss under
2 % of atmospheric pressure.

	Quadratic Approximations	Genetic Algorithm
Number of tubes, N	1	25
Tube length, L, m	1	0.5
Tube diameter, D, m	0.078	0.032
Area, A, m^2	0.246	1.248
Pressure loss, Δp, kPa	2.027	2.027
Effectiveness, ε, kPa	0.089	0.120
Thermoelectric efficiency, η_{TE}, %	3.792	3.792

heat exchanger, and for a set of N pipes. The analysis indicated that
all configurations were useful, although due to the TEG volume and
the placement along the exhaust pipe, the arrangement with 9 tubes
was adopted. When compared to the preliminary configuration, the
efficiency was close to 4.23 %. However, the output power was 123 W
and the effectiveness 0.009, which evidences the gains by optimizing
the TEG system.

Table 4.5 – Optimization to reach a desired thermal efficiency.

	Quadratic Ap proximations	Genetic Algorithm		
Maximum number of tubes, N	1	9	16	25
Number of tubes,N	1	9	14	25
Tube length, L, m	1.667	0.414	0.319	0.214
Tube diameter, D, m	0.063	0.022	0.019	0.014
Area, A, m^2	0.291	0.286	0.266	0.235
Volume, m^3	0.007	0.017	0.019	0.019
Pressure loss, Δp, kPa	2.027	1.944	1.443	1.658
Effectiveness, ε, kPa	0.141	0.141	0.141	0.141
Thermoelectric efficiency, η_{TE}, %	3.792	3.792	3.792	3.792

Table 4.6 – Performance parameters as a function of the design parameters.

	Optimized Power	Optimized Conversion Efficiency
Number of tubes, N		9
Tube length, L,m		0.414
Inner tube diameter, D, m		0.022
Outer tube diameter, D_{out}, m		0.068
Conductor material		SiGe
Conductor length, m		0.006
Conductor diameter, m		0.003
Inner tube pressure loss, kPa		1.006
Annular tube pressure loss, kPa		0.182
Number of TE couples, N_{TE}	562	150
Effectiveness, ε	0.09	0.04
Power, P, W	811	550
Thermoelectric efficiency, η_{TE}, %	4.27	10.4

4.2.3.3 Optimized Arrangement

Based on the analysis conducted, this section presents the thermoelectric generator obtained from the optimization. The arrangement proposed uses the silicon-germanium alloy as the material employed in the thermoelements, it is coupled close to the exhaust manifold and, uses the diesel engine's cooling water as the cold fluid. The heat exchanger consists of 9 tubes with a length of 0.414 m and a diameter of 0.022 m. After the optimization process in EES, we tested the configuration in the model written in Fortran language. Here, we simulated the transient regime and adopted temperature dependent properties. Table 4.6 presents the performance parameters for two configuration varying the number of thermocouples. Here, we noticed that the heat exchanger effectiveness is less than 0.14. This occurs due to the complexity of the model written in Fortran language which considers the effect of transient regime, temperature dependent properties, and the energy generation by Joule and Seebeck effect. Therefore, the interface between the optimization model written in EES and the more complex model written in Fortran needs to be improved.

Figure 4.11 exhibits the output power as a function of crank angle for the TEG closed-coupled to the exhaust manifold for each configuration. Here we noticed the differences between the proposed configurations when simulated in the program written in Fortran language. Since in the routine developed in the EES, the internal resistance of the generator was approximated as a thermal resistance to radial conduction through a cylinder, it was not encompassed the energy generation terms because of Joule and Peltier effect. Furthermore, in the EES model, we assumed that a layer of the thermoelectric material enveloped the inner tube (hot side). Therefore, there was no distinction of the number of cells. In the model written in Fortran language, we presented two configurations: one aimed at the maximum power and another at the maximum conversion efficiency. The arrangement with 562 thermoelectric couples provides higher power and meets the minimum power criterion. However, the arrangement with 150 thermoelectric couples ensures higher average power per unit of thermoelectric couple and has lower cost.

Figure 4.11 – Predicted generated power as a function of crank angle for the TEG with 150 or 562 thermoelectric couples.
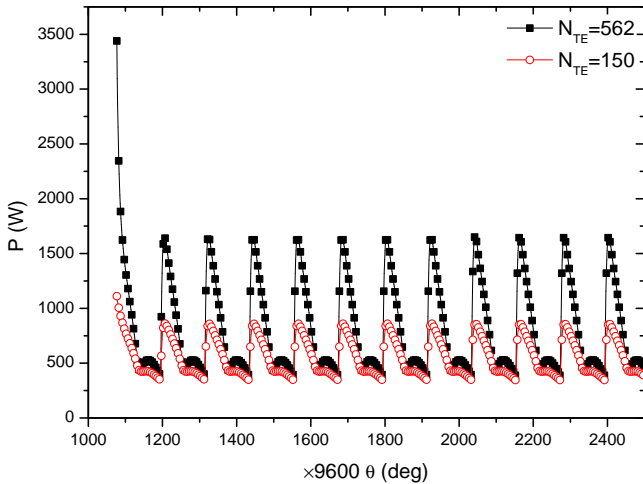
Figure 4.11 exhibits the output power as a function of crank angle for the TEG closed-coupled to the exhaust manifold for each con-

figuration. Moreover, Figure 4.12 presents the electric current and the potential difference generated for TEG with 562 thermoelectric couples per tube. The transient simulation indicated that there is a peak power of 3500 W during start-up and peak power at periodic steady-state of 1100 W could be reached in the configuration of maximum power. The current and voltage at start-up would reach 5 A and 80 V, respectively, and the peak values at periodic steady-state would reach 3.7 A and 65 V, respectively.

Figure 4.12 – TEG electric current and potential difference generated with 562 thermocouples per tube.
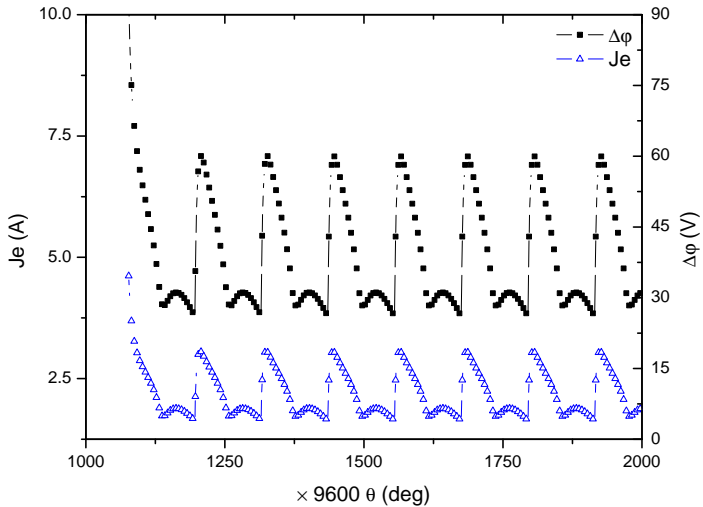
4.2.4 Analysis of Optimized Design

This section intends to investigate the transient behavior of the thermoelectric generator and possible energy recovery (or increased power output). As shown in Figure 4.13, for the previous TEG configuration, there was an increase in the power provided by the equipment when operating in transient condition.

As the preliminary configuration, the optimized generator also

provides an energy boost during the beginning of its operation, as shown in Figure 4.9. However, the optimized generator reaches steady state faster when compared to the previous. It is also worth mentioning that the thermal inertia of the generator was greater than that of the engine; then, it reacted slowly to changes in the exhaust stream. Figure 4.14 zooms at the operation for short time. This figure was generated using the real thermal mass of the TEG, without using the scaling factor of 9600.

Figure 4.13 – Predicted generated power as a function of crank angle.
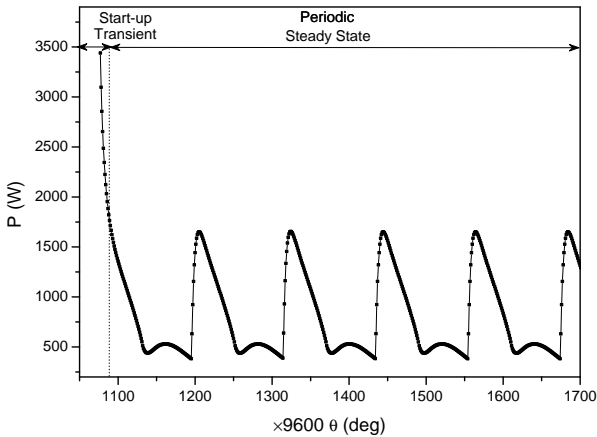
Figure 4.14 indicates that there is an opportunity to explore the equipment's start up, because of the high power obtained. In order to evaluate the energy gains, Figure 4.15 presents the energy recovery (by integrating the output power) as a function of crank angle, E. In the figure, the square indicates the beginning of the steady state. The transient period provides about 27 kJ in 14s seconds (about 2 kW), which is higher than the 1 kW (approximately) provided during steady-state operation. The fast start up of the thermoelectric generator combined with the high power obtained during this period indicates opportunities to investigate the behavior of TEG in a drive cycle in an urban cycle with stops and starts.

Figure 4.14 – Predicted generated power as a function of crank
angle during the TEG start operation.
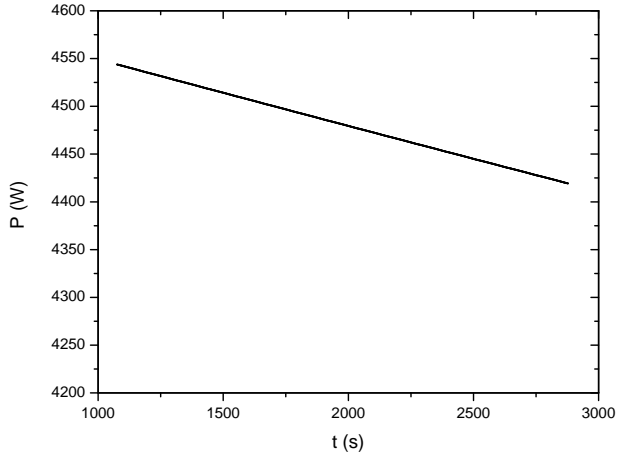
Figure 4.15 – Predicted energy recovered as a function of crank
angle.
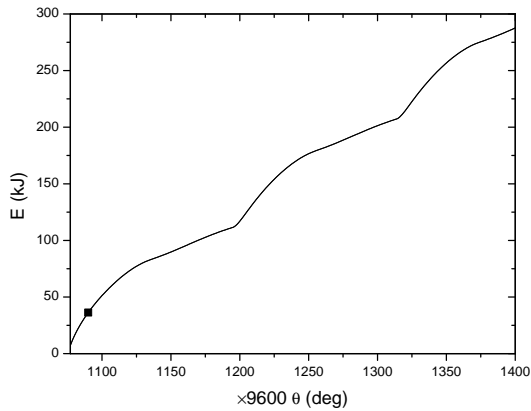
4.3   Summary

In this chapter, the heat exchanger and thermoelectric generator
were analyzed in detail. The heat exchanger design used the Newton's

law of cooling, whereas the thermoelectric generator used a methodology mostly based on Wang, Wang and Dai; Park and Kaviany [34, 37]. However, differently from previous approaches, the Thomson effect were coupled to the TEG model and the transient operation was analyzed. In addition, the model was tested by comparison with models by other authors presented in the literature.

Subsequently, a basic generator was built. This configuration provided the guidance for the system's optimization. The following aspects were covered: the thermoelectric material, the cold fluid, the effect of the transient regime on the TEG hot wall temperature, the pressure loss, and the performance parameters. As a result, it was obtained a TEG with thermoelectric efficiency around 10.4 % and another capable of recovering 811 W on average.

Finally, an analysis of transient behavior during the start of the generator's operation was developed. This analysis explored possible energy gains during start up. The TEG system provided energy recovery, during start up, of 2 kW (approximately) compared to 1 kW obtained in steady state operation.

5 CONCLUSIONS, MAIN CONTRIBUTIONS, AND FUTURE WORKS

This chapter presents the conclusions, main contributions of this Master Thesis, and future work recommendations regarding the use of thermoelectric generators for wasted energy recovery in diesel engines.

5.1 Conclusions

Chapter 2

Regarding the thermoelectric generation, after analyzing the most commonly used materials, the advantages, and major drawbacks, it was possible to recognize some key points for the improvement of this technology, such as: new materials development, heat exchanger optimization, and control unit design. Furthermore, through the study of state-of-the-art, it was found that it is possible to recover up to 25 % energy [37] and generate up to 6000 W [31], which suggests a potential for application in heavy-duty engines.

Chapter 3

Here, a transient model for the diesel engine was developed and implemented in FORTRAN. The results were contrasted with those provided by the literature. The power per cycle was slightly lower: 38 kW versus 41.5 kW reported by reference [42], which could be a consequence of the constants used to evaluate the Nusselt number and the value of stagnation pressure at the start of exhaust process. Furthermore, the dimensionless cylinder-space volume, fluid pressure, and temperature curve profiles were in agreement with those presented in previous studies [42, 43]. Then, the last result compared was exhaust mass flow, here it was found the greatest differences concerning the profile curves, however both have two peaks in the flow and their maximum values were close to 0.5 kg/s. As a conclusion, the results were considered adequate and therefore, able to provide the input conditions for the TEG: temperature and mass flow of the hot stream (exhaust gas).

Chapter 4

A simple configuration was used in the study: a parallel flow heat exchanger formed by a number of individual concentric tubes arranged in parallel. Each tube, by its turn, had a number of thermoelements embedded on its walls. From the aspects investigated, the following

guidelines have been found: the silicon-germanium alloy as a material for the thermocouple, the diesel engine's cooling water as the cold stream, the position close to the exhaust manifold to the site for the TEG installation, the maximum exchange area limited to 2 % pressure loss and the minimum area to achieve 2 % thermoelectric efficiency and 800 W output power. As a consequence, two configurations were derived: one optimized for conversion efficiency and the other for power. The second TEG exhibited an efficiency closed 4.27 % and generated 811 W on average, which was within the range covered by other studies available in the literature.

Furthermore, based on the slow thermal inertia of the TEG in comparison with the diesel engine, it was explored the effect of the transient to increase the energy recovery. It was noted that the TEG can recover on average 2 kW during start-up when compared to 1 kW in steady-state.

In conclusion the results indicated the importance of the project for optimization of thermoelectric generators and that low energy conversion efficiency greatly constrains the applicability of such equipment. Therefore, it is emphasized here that the development of new materials is essential to make this a more attractive technology. For instance, by testing the configuration for maximum power but using SnSe crystals as the material of the thermoelectric cells it would be possible to achieve efficiency close to 12 %.

5.2 Main Contributions

A computational model for the simulation of diesel engines
The diesel engine model provides outputs other than those used in the thermoelectric generator. Therefore, this tool can be adapted to the other projects in future. From the engine model, parameters can be obtained, for instance, the rate of burning and fuel injection, the average flue gas velocity, the heat transfer in the diesel engine combustion chamber surface (through the three transfer modes). Then, the computational tool can be used to study the engine's behavior under different operation and design characteristics.

A computational model for the simulation of thermoelectric generators
Following the arguments set out in the discussion relating to the contributions of the diesel engine model, the thermoelectric generator

also has a computer model that can be used in other projects. From this model, variables and design constraints on the TEG optimization can be identified.

A methodology for thermoelectric generator optimization

The methodology undertaken here identified some optimization parameters of the generator. Since the methodology is independent of the materials used, as new thermoelectric materials are introduced in the market, it is interesting to revisit this study due to the guidance provided herein. Furthermore, the methodology can be used in prototypes to demonstrate the concepts of wasted energy recovery, the effects of system degradation, and the thermal cycling.

5.3   Future Works

Perform CFD simulations of the diesel engine:

The diesel engine study employed the single cylinder model, i.e., the conservation equation were solved separately for each cylinder of an internal combustion engine. The integration between the exhaust flows from different cylinders occurs in the exhaust manifold, which was treated as a global open system. The analysis conducted did not consider the formation of vortices and assumed perfect mixing in the exhaust manifold. This does not reproduce with accuracy the manifold behavior, thus, it is expected that this should be accessed with CFD simulation, in order to analyze the interaction between the exhaust and the thermoelectric generator.

Design the electric circuit:

The typical automotive waste heat recovery system includes: an exhaust pipe, a heat exchanger, a thermoelectric device, a power conditioning unit, and the batteries. In this master thesis, only the first three equipments were modeled. Therefore, it is necessary to model the power conditioning unit and mainly analyze its integration with the generator.

From this, a feasibility study could be performed concerning the electrical circuit. Moreover, it would be possible to obtain the load resistance, since in this work, an optimum one was adopted. As a result, a more realistic TEG model would be available. Furthermore, with the power conditioning unit, there will be a basis for the study of the integration thereof with the existing vehicle power management.

Design and test a prototype

Through experiments, it is expected to evaluate the heat transfer between the TEG and the surroundings, since in this study, these losses are neglected. In addition, the model did not consider the temperature drop between the exhaust valve and the heat exchanger, something that could be evaluated with an experiment. In addition, through an experimental approach, it can be assessed the TEG behavior when exposed to engine's transient period and it would be possible to evaluate the TEG continuous exposure to a high temperature gradient.

REFERENCES

[1] SAIDUR, R. et al. Technologies to recover exhaust heat from internal combustion engines. **Renewable and Sustainable Energy Reviews**, v. 16, n. 8, p. 5649 – 5659, 2012.

[2] YU, C.; CHAU, K. Thermoelectric automotive waste heat energy recovery using maximum power point tracking. **Energy Conversion and Management**, Elsevier, v. 50, n. 6, p. 1506–1512, 2009.

[3] ZHANG, X.; CHAU, K.; CHAN, C. Overview of thermoelectric generation for hybrid vehicles. **Journal of Asian Electric Vehicles**, Asian Electric Vehicle Society, v. 6, n. 2, p. 1119–1124, 2008.

[4] HSU, C.-T.; HUANG, G.-Y.; CHU, H.-S.; YU, B.; YAO, D.-J. Experiments and simulations on low-temperature waste heat harvesting system by thermoelectric power generators. **Applied Energy**, v. 88, n. 4, p. 1291 – 1297, 2011.

[5] YANG, J. Potential applications of thermoelectric waste heat recovery in the automotive industry. In: INTERNATIONAL CONFERENCE ON THERMOELECTRICS, 24. **Thermoelectrics, 2005. ICT 2005. 24th International Conference on**. Clemson, US, 2005. p. 170–174.

[6] EPE, E. de P. E. . **Balanço Energético Nacional**. Rio de Janeiro, 2015.

[7] ENERGIA, M. de Minas e. **Energia no Mundo**. Brasilia, BR, 2015.

[8] KAVIANY, M. **Principles of heat transfer**. New York, US: John Wiley & Sons, 2002.

[9] MILLER, E. W.; HENDRICKS, T. J.; PETERSON, R. B. Modeling energy recovery using thermoelectric conversion integrated with an organic rankine bottoming cycle. **Journal of Electronic Materials**, Springer, v. 38, n. 7, p. 1206–1213, 2009.

[10] QIU, K.; HAYDEN, A. Integrated thermoelectric and organic rankine cycles for micro-chp systems. **Applied Energy**, Elsevier, v. 97, p. 667–672, 2012.

[11] WANG, E. et al. Study of working fluid selection of organic rankine cycle (orc) for engine waste heat recovery. **Energy**, Elsevier, v. 36, n. 5, p. 3406–3418, 2011.

[12] SOO, S. L. **Direct energy Conversion**. Englewood Cliffs, US: Prentice- Hall Inc., 1968.

[13] MATERIALS SCIENCE - DIVISION OF ENGINEERING & APPLIED SCIENCE - CALIFORNIA INSTITUTE OF TECHNOLOGY. **Brief History of Thermoelectrics**. Available from Internet: <http://thermoelectrics.caltech.edu/ thermoelectrics/history.html>. Accessed: 05/07/2016.

[14] SAIDUR, R.; RAHIM, N.; HASANUZZAMAN, M. A review on compressed-air energy use and energy savings. **Renewable and Sustainable Energy Reviews**, v. 14, n. 4, p. 1135 – 1153, 2010.

[15] FERNANDES, A. E. S. dos S. **Conversão de energia com Células de Peltier**. 119 p. MasterThesis (Master of Science in Aerospace Engineering) — Faculdade de ciências e Tecnologia Universidade Nova de Lisboa, Lisboa, PT, 2012.

[16] RIFFAT, S. B.; MA, X. Thermoelectrics: a review of present and potential applications. **Applied Thermal Engineering**, Elsevier, v. 23, n. 8, p. 913–935, 2003.

[17] JET PROPULSION LABORATORY - NATIONAL AERONAUTICS AND SPACE ADMINISTRATION. **Voyager Mission Status Bulletin**. Pasadena, US, 1978.

[18] HENDRICKS, T.; CHOATE, W. T. **Engineering Scoping Study of Thermoelectric Generator Systems for Industrial Waste Heat Recovery**. Richland, US, 2006.

[19] MAZAR, B. **State of the Art Prototype Vehicle with a Thermoelectric Generator**. Available from Internet: <energy.gov/sites/prod/files/2014/03/f10/mazar.pdf>. Accessed: 04/02/2016.

[20] CRANE, D. T. Potential thermoelectric applications in diesel vehicles. In: DIESEL ENGINE EMISSIONS REDUCTION (DEER) CONFERENCE, 9. Newport, US: United States. Department of Energy. Office of Energy Efficiency and Renewable Energy, 2003.

[21] HAIDAR, J.; GHOJEL, J. Waste heat recovery from the exhaust of low-power diesel engine using thermoelectric generators. In: INTERNATIONAL CONFERENCE ON THERMOELECTRICS, 20. **Thermoelectrics, 2001. Proceedings ICT 2001. XX International Conference on**. Beijing, CN, 2001. p. 413–418. ISSN 1094-2734.

[22] ROWE, D. (Ed.). **CRC Handbook of Thermoelectrics**. Boca Raton, US: CRC Press, 1995.

[23] BÖTTNER, H.; CHEN, G.; VENKATASUBRAMANIAN, R. Aspects of thin-film superlattice thermoelectric materials, devices, and applications. **MRS bulletin**, Cambridge Univ Press, v. 31, n. 03, p. 211–217, 2006.

[24] DUGHAISH, Z. Lead telluride as a thermoelectric material for thermoelectric power generation. **Physica B: Condensed Matter**, v. 322, n. 1, p. 205 – 223, 2002.

[25] HEREMANS, J. P. et al. Enhancement of thermoelectric efficiency in pbte by distortion of the electronic density of states. **Science**, American Association for the Advancement of Science, v. 321, n. 5888, p. 554–557, 2008.

[26] ZHAO, L.-D. et al. Ultralow thermal conductivity and high thermoelectric figure of merit in snse crystals. **Nature**, Nature Publishing Group, v. 508, n. 7496, p. 373–377, 2014.

[27] CRANE, D. T.; JACKSON, G. S. Optimization of cross flow heat exchangers for thermoelectric waste heat recovery. **Energy Conversion and Management**, v. 45, n. 9–10, p. 1565 – 1582, 2004.

[28] HSU, C.-T.; YAO, D.-J.; YE, K.-J.; YU, B. Renewable energy of waste heat recovery system for automobiles. **Journal of Renewable and Sustainable Energy**, AIP Publishing, v. 2, n. 1, p. 013105, 2010.

[29] KARRI, M.; THACHER, E.; HELENBROOK, B. Exhaust energy conversion by thermoelectric generator: Two case studies. **Energy Conversion and Management**, v. 52, n. 3, p. 1596 – 1611, 2011.

[30] HENDRICKS, T.; LUSTBADER, J. Advanced thermoelectric power system investigations for light-duty and heavy duty

applications. i. In: INTERNATIONAL CONFERENCE ON THERMOELECTRICS, 21. **Thermoelectrics, 2002. Proceedings ICT '02. Twenty-First International Conference on**. Long Beach, USA, 2002. p. 381–386.

[31] HENDRICKS, T.; LUSTBADER, J. Advanced thermoelectric power system investigations for light-duty and heavy duty applications. ii. In: INTERNATIONAL CONFERENCE ON THERMOELECTRICS, 21. **Thermoelectrics, 2002. Proceedings ICT '02. Twenty-First International Conference on**. Long Beach, US, 2002. p. 387–394.

[32] ZHANG, Y. et al. High-temperature and high-power-density nanostructured thermoelectric generator for automotive waste heat recovery. **Energy Conversion and Management**, Elsevier, v. 105, p. 946–950, 2015.

[33] ZHANG, X.; CHAU, K. An automotive thermoelec-tric–photovoltaic hybrid energy system using maximum power point tracking. **Energy Conversion and Management**, v. 52, n. 1, p. 641 – 647, 2011.

[34] WANG, Y.-C.; WANG, S.-X.; DAI, C. A theoretic model of thermoelectric device using automobile exhaust gas for power generation. In: POWER AND ENERGY ENGINEERING CONFERENCE (APPEEC), 1. **Power and Energy Engineering Conference (APPEEC), 2012 Asia-Pacific**. Shangai, CN, 2012. p. 1–4. ISSN 2157-4839.

[35] HE, W.; WANG, S.; ZHANG, X.; LI, Y.; LU, C. Optimization design method of thermoelectric generator based on exhaust gas parameters for recovery of engine waste heat. **Energy**, Elsevier, v. 91, p. 1–9, 2015.

[36] LIU, X.; DENG, Y.; LI, Z.; SU, C. Performance analysis of a waste heat recovery thermoelectric generation system for automotive application. **Energy Conversion and Management**, Elsevier, v. 90, p. 121–127, 2015.

[37] PARK, C.-W.; KAVIANY, M. Combustion-thermoelectric tube. **Journal of Heat Transfer**, ASME, v. 122, n. 4, p. 721–729, jun. 2000.

[38] HEYWOOD, J. **Internal Combustion Engine Fundamentals**. New York, US: McGraw-Hill Education, 1988.

[39] ALEGRE, J. A. A. V. **Simulação dos processos e análise exergética do motor de ciclo diesel**. 179 p. Thesis (Doctor in Mechanical Engineering) — Faculdade de Engenharia Mecânica Universidade Estadual de Campinas, São Paulo, 1993.

[40] RAKOPOULOS, C.; GIAKOUMIS, E. Simulation and analysis of a naturally aspirated {IDI} diesel engine under transient conditions comprising the effect of various dynamic and thermodynamic parameters. **Energy Conversion and Management**, v. 39, n. 5–6, p. 465 – 484, 1998.

[41] CHOW, A.; WYSZYNSKI, M. Thermodynamic modelling of complete engine systems—a review. **Proceedings of the Institution of Mechanical Engineers, Part D: Journal of Automobile Engineering**, Sage Publications, v. 213, n. 4, p. 403–415, 1999.

[42] PARK, C.-W.; KAVIANY, M. Evaporation-combustion affected by in-cylinder, reciprocating porous regenerator. **Journal of Heat Transfer**, ASME, v. 124, n. 1, p. 184–194, maio 2001.

[43] PEREIRA, F. M.; OLIVEIRA, A. A. M. Analysis of the performance of a porous foam soot regenerative filter for diesel engines. In: INTERNATIONAL CONGRESS OF MECHANICAL ENGINEERING, 18. Ouro Preto, 2005.

[44] ROSA, O.; OLIVEIRA, A.; OLIVEIRA, R. Wasted thermal energy recovery in heavy duty diesel vehicles using a thermoelectric/heat exchanger device. In: INTERNATIONAL CONFERENCE ON EFFICIENCY, COST, OPTIMIZATION, SIMULATION AND ENVIRONMENTAL IMPACT OF ENERGY SYSTEMS (ECOS), 28. Pau, FR, 2015.

[45] ASSANIS, D. N.; EKCHIAN, J. E.; FRANK, R. M.; HEYWOOD, J. B. **A Computer Simulation of the Turbocharged Turbocompounded Diesel Engine System: A Description of the Thermodynamic and Heat Transfer Models**. Cambrigde, US, 1985.

[46] OLIVEIRA, A. A. M. Modelo zero-dimensional. Notas de Aula, Disciplina Modelagem de Motores e Combustão Interna. 2014.

[47] WOSCHNI, G. **A universally applicable equation for the instantaneous heat transfer coefficient in the internal combustion engine**. [S.l.], 1967.

[48] BRUNETTI, F. **Motores de combustão Interna**. São Paulo: Edgard Blucher, 2012.

[49] CCACYA, A. O. R. **Estudo Experimental da Ignição por Compressão de Misturas Homogêneas em Motores a Combustão Interna**. 132 p. MasterThesis (Master of Science in Mechanical Engineering) — Pontífícia Universidade Católico do rio de Janeiro, Rio de Janeiro, 2010.

[50] ZHAO, H. (Ed.). **Hcci and Cai Engines for the Automotive Industry**. Cambridge, GB: Elsevier Science, 2007.

[51] WATSON, N.; PILLEY, A.; MARZOUK, M. **A combustion correlation for diesel engine simulation**. Warrendale, US, 1980.

[52] COONEY, C.; WORM, J.; MICHALEK, D.; NABER, J. et al. Wiebe function parameter determination for mass fraction burn calculation in an ethanol-gasoline fuelled si engine. **Journal of KONES**, v. 15, n. 3, p. 567–574, 2008.

[53] GHOJEL, J. Review of the development and applications of the wiebe function: a tribute to the contribution of ivan wiebe to engine research. **International Journal of Engine Research**, SAGE Publications, v. 11, n. 4, p. 297–312, 2010.

[54] FLYNN, P.; MIZUSAWA, M.; UYEHARA, O. A.; MYERS, P. S. **An experimental determination of the instantaneous potential radiant heat transfer within an operating diesel engine**. [S.l.], 1972.

[55] ANNARATONE, D. **Handbook for Heat Exchangers and Tube Banks design**. 1. ed. Heidelberg, DE: Springer-Verlag Berlin Heidelberg, 2010.

[56] THULUKKANAM, K. **Heat Exchanger Design Handbook**. 2. ed. Boca Raton, US: CRC Press, 2013.

[57] KAKAÇ, S. **Boilers, Evaporators, and Condensers**. Boca Raton, US: Wiley, 1991.

[58] KAKAÇ, S.; LIU, H.; PRAMUANJAROENKIJ, A. **Heat Exchangers: Selection, Rating, and Thermal Design**. 3. ed. Boca Raton, US: Taylor & Francis, 2012.

[59] NELLIS, G.; KLEIN, S. **Heat Transfer**. Cambridge, GB: Cambridge University Press, 2009.

[60] GNIELINSKI, V. New equations for hat and mass transfer in turbulent pipe and channel flow. **International Chemical Engineering**, v. 16, p. 359 – 368, 1976.

[61] ZIGRANG, D.; SYLVESTER, N. Explicit approximations to the solution of colebrook's friction factor equation. **AIChE Journal**, Wiley Online Library, v. 28, n. 3, p. 514–515, 1982.

[62] ROHSENOW, W. M.; HARTNETT, J. P.; CHO, Y. I. et al. **Handbook of heat transfer**. NY, US: McGraw-Hill New York, 1998. v. 3.

[63] ANGRIST, S. **Direct energy conversion**. Boston, US: Allyn and Bacon, 1982.

[64] SANDOZ-ROSADO, E. J.; WEINSTEIN, S. J.; STEVENS, R. J. On the thomson effect in thermoelectric power devices. **International Journal of Thermal Sciences**, Elsevier, v. 66, p. 1–7, 2013.

[65] TANG, X. et al. Preparation and thermoelectric transport properties of high-performance p-type bi2te3 with layered nanostructure. **Applied Physics Letters**, v. 90, n. 1, 2007.

[66] MAYER, A. **Particle filter retrofit for all diesel engines**. DE: expert verlag, 2008. v. 97.

[67] MUNJAL, M. L. **Acoustics of ducts and mufflers with application to exhaust and ventilation system design**. Calgary, CA: John Wiley & Sons, 1987.

[68] THIRUVENGADAM, A.; PRADHAN, S.; THIRUVENGADAM, P.; BESCH, M.; CARDER, D. **Heavy-Duty Vehicle Diesel Engine Efficiency Evaluation and Energy Audit**. Morgantown, US, 2014.

[69] FOX, R.; MCDONALD, A. **Introduction to fluid mechanics**. Hoboken, US: Wiley, 1985.

[70] COLEBROOK, C. F. Turbulent flow in pipes, with particular reference to the transition region between the smooth and rough pipe laws. **Journal of the Institution of Civil Engineers**, v. 11, n. 4, p. 133–156, 1939.

[71] KLEIN, S. A.; NELLIS, G. **Mastering EES**. [S.l.]: F-Chart Software, 2013.

APPENDIX A – Heat Transfer Rate through P and N-type Thermoelements

The thermoelectric efficiency for the thermocouple depends on the amount of conduction heat transfer rate along the elements. For the hot side ($x = 0$), the heat transfer rate, in the x direction, through the p and n-type thermoelements is given by:

$$Q_{p,h,w} = \alpha_{S,p} J_e T_{h,w} - k_p A_p \frac{dT}{dx}\bigg|_{x=0}, \qquad (A.1)$$

$$Q_{n,h,w} = -\alpha_{S,n} J_e T_{h,w} - k_n A_n \frac{dT}{dx}\bigg|_{x=0}. \qquad (A.2)$$

where k is the thermal conductivity and dT/dx is the temperature gradient. Note that the negative sign for $\alpha_{S,n}$ applies when electrons move from the p-type material to the n-type material (and the current is from the n-type material to the p-type material) [8, 22]. Also, the p and n elements act as thermal resistances arranged in parallel.

Similarly, for the cold side ($x = L_p$ or L_n) , the heat transfer, in the x direction, through the p and n-type thermoelement are given by:

$$Q_{p,c,w} = \alpha_{S,p} J_e T_{c,w} - k_p A_p \frac{dT}{dx}\bigg|_{x=L_p}, \qquad (A.3)$$

$$Q_{n,c,w} = -\alpha_{S,n} J_e T_{c,w} - k_n A_n \frac{dT}{dx}\bigg|_{x=L_n}. \qquad (A.4)$$

Assuming that $L = L_p = L_n$, Equations A.1 and A.2 and Equations A.3 and A.4 are coupled into an expression for the heat transfer rate to the hot and cold sides ($x = L$):

$$Q_{h,w} = (\alpha_{S,p} - \alpha_{S,n}) J_e T_{h,w} - (k_p A_p + k_n A_n) \frac{dT}{dx}\bigg|_{x=0}, \qquad (A.5)$$

$$Q_{c,w} = (\alpha_{S,p} - \alpha_{S,n}) J_e T_{c,w} - (k_p A_p + k_n A_n) \frac{dT}{dx}\bigg|_{x=L}. \qquad (A.6)$$

In order to evaluate dT/dx, the temperature distribution must be determined. The rate of heat generation per unit length in the thermoele-

ments, due to Joule effect, is associated to temperature gradient by the conservation of energy as:

$$-k_p A_p \frac{d^2 T}{dx^2} = \frac{J_e^2 \rho_{e,p}}{A_p}, \tag{A.7}$$

$$-k_n A_n \frac{d^2 T}{dx^2} = \frac{J_e^2 \rho_{e,n}}{A_n}. \tag{A.8}$$

Setting the boundary conditions that $T = T_{h,w}$ at $x = 0$ and $T = T_{c,w}$ at $x = L_n$ or L_p, Equations A.7 and A.8 can be integrated to provide:

$$k_p A_p \frac{dT}{dx} = \frac{J_e^2 \rho_p (x - L_p/2)}{A_p} + \frac{k_p A_p (T_{c,w} - T_{h,w})}{L_p}, \tag{A.9}$$

$$k_n A_n \frac{dT}{dx} = \frac{J_e^2 \rho_n (x - L_n/2)}{A_n} + \frac{k_n A_n (T_{c,w} - T_{h,w})}{L_n}. \tag{A.10}$$

Substituting the Equations A.9 and A.10 in the Equation A.5, the expression for the absorbed heat ($x = 0$) is given by:

$$Q_{h,w} = (\alpha_{S,p} - \alpha_{S,n}) J_e T_{h,w} + R_k^{-1}(T_{h,w} - T_{c,w}) - J_e^2 R_e/2. \tag{A.11}$$

Similarly, for the released heat ($x = L$):

$$Q_{c,w} = (\alpha_{S,p} - \alpha_{S,n}) J_e T_{c,w} + R_k^{-1}(T_{h,w} - T_{c,w}) + J_e^2 R_e/2, \tag{A.12}$$

where R_k is the overall thermal resistance of the thermocouple, given by:

$$\frac{1}{R_k} = \left(\frac{Ak}{L}\right)_p + \left(\frac{Ak}{L}\right)_n. \tag{A.13}$$

Note that the energy converted by joule heating arrives at the heat sink while, presumably, the other half turns up at the heat source.

To conclude, using Equations 2.8 and A.11, the thermoelectric (conversion) efficiency can be given by the ratio of the electric power and the heat transfer rate from the hot side,

$$\eta_{TE} = \frac{P}{Q_{h,w}}. \tag{A.14}$$

APPENDIX B – Curve Fitted Functions for Thermoelectric Material Properties

Microsoft Excel® software was used to obtain the curve fitted functions.

BiTe

The bismuth telluride curve fitted functions were based on the properties measured by Tang et al. [65]. (280 K≤ T ≤ 440 K)

Thermal Conductivity (W/m-K):

$$k = 0.39732 \cdot exp(0.00361 \cdot T). \tag{B.1}$$

Seebeck Coefficient (V/K):

$$\alpha_S = -0.0000903 \ ln(T) + 0.0006997. \tag{B.2}$$

Electrical Resistivity (Ωm):

$$\rho_e = 0.0000149 \ ln(T) - 0.0000757. \tag{B.3}$$

TlPbTe

The lead telluride curve fitted functions were based on the properties measured by Heremans et al. [25]. (300 K≤ T ≤ 800 K)

Thermal Conductivity (W/m-K):

$$k = -1.19810 \ ln(T) + 8.86162. \tag{B.4}$$

Seebeck Coefficient (V/K):

$$\alpha_S = 0.00024 \ ln(T) - 0.00130. \tag{B.5}$$

Electrical Resistivity (Ωm):

$$\rho_e = 0.0000417 \ ln(T) - 0.0002195. \tag{B.6}$$

SiGe

The silicon-germanium alloy curve fitted functions were based on the properties measured by Rowe [22]. (300 K≤ T ≤ 1300 K)

Thermal Conductivity (W/m-K):

$$k = -0.3302408 \ ln(T) + 6.6344085. \tag{B.7}$$

Seebeck Coefficient (V/K):

$$\alpha_S = 0.0000852 \, ln(T) - 0.0003661. \tag{B.8}$$

Electrical Resistivity (Ωm):

$$\rho_e = 0.0000154 \, ln(T) - 0.0000796. \tag{B.9}$$